IISC - 21

Donostia-San Sebastián 2015 Spain

21st International Workshop on *Inelastic Ion-Surface Collisions*

Book of Abstracts

18-23 October 2015

Donostia-San Sebastián, Spain

Institutional support and funding

DONOSTIA INTERNATIONAL PHYSICS CENTER

Committees

Conference Chair

Iñaki Juaristi (University of Basque Country, Spain)

International Scientific Committee

G. Andersson (Australia)
F. Aumayr (Austria)
R. Hoekstra (The Netherlands)
S. Facsko (Germany)
I. Juaristi (Spain)
K. Kimura (Japan)
T. Koshikawa (Japan)
H. Lebius (France)
Ch. Linsmeier (Germany)
F. Meyer (USA)
J . Pomeroy (USA)
P. Roncin (France)
M. Schleberger (Germany)

Local Organizing Committee

Maite Alducin (CFM-CSIC)
Andrés Arnau (UPV/EHU)
María Blanco Rey (UPV/EHU)
Ricardo Díez Muiño (CFM-CSIC)
Ivor Lončaric (CFM)
Dino Novko (DIPC)

History of the IISC Workshop

IISC	Year	Location	Country	Organizer
1	1976	Bell Labs, Murray Hill NJ	USA	N. Tolk
2	1978	McMaster University, Hamilton	Canada	R. Kelly
3	1980	Feldkirchen-Westerham	Germany	E. Taglauer, W. Heiland
4	1982	Hindsgavl Manor, Middelfart	Denmark	P. Sigmund
5	1984	Gold Canyon Ranch, AZ	USA	P. Williams
6	1986	Argonne National Lab, IL	USA	D. Gruen
7	1988	Jagellonian University, Krakow	Poland	M. Szymonski
8	1990	Wiener Neustadt	Austria	G. Betz, P. Varga
9	1992	Aussois	France	M. Bernheim, J. P. Gauyacq
10	1994	Grand Targhee, WY	USA	N. Tolk
11	1996	Island Wangerooge	Germany	W. Heiland
12	1999	South Padre Island, TX	USA	J. W. Rabalais, P. Nordlander
13	2000	San Carlos de Bariloche	Argentina	M. Martiarena
14	2002	Island of Ameland	The Netherlands	R. Hoekstra, P. Zeijlmans van Emmichoven
15	2004	Ise-Shima	Japan	K. Morita, T. Koshikawa
16	2006	Hernstein	Austria	F. Aumayr
17	2008	Porquerolles	France	H. Lebius, B. Ban d'Etat
18	2010	Gatlinburg, TN	USA	C. O. Reinhold, P. S. Krstic, F. W. Meyer
19	2012	Frauenchiemsee	Germany	Ch. Linsmeier
20	2014	Wirrina Cove	Australia	G. Andersson
21	2015	Donostia-San Sebastián	Spain	I. Juaristi

IISC-21 SCHEDULE

Sunday 18th October 2015

17:30 **Registration Open**

19:30 **Reception**

20:00 **Dinner**

Monday 19th October 2015

09:00 **Opening**

Session Chair: J. Iñaki Juaristi (Spain)

09:10 **Gunther Andersson (Australia) Pl**

High Resolution Concentration Depth Profiles for analysing Soft Matter Surfaces with NICISS

09:55 **Kaoru Nakajima (Japan) I**

Transmission Secondary Ion Mass Spectrometry of Organic Molecules using 5 Mev C_{60}^{+} Ions

10:25 **Anders J. Barlow (UK) O**

Argon Gas Cluster Ion Sources in Surface Chemical Analysis: Measurements of Total Sputter Yields and a Semi-Empirical Predictive Model

10:45 **Coffee Break**

Session Chair: Henning Lebius (France)

11:15 **Brigitte Ban-d'Etat (France) I**

Nano-Structuring by Swift Heavy Ions at Grazing Incidence: Different Track Types with Different Targets

11:45 **Clara Grygiel (France) I**

From Surface to Bulk Modifications under Swift Heavy Ion Irradiation of Insulating Materials

12:15 **Kenji Kimura (Japan) O**

Temperature Measurement of Thermal Spike Using Desorption of Nanoparticles

12:35 **William Terry (UK) O**

Cluster Production and Ion-Induced Luminescence in the Matrix Assembly Cluster Source (MACS)

13:00 **Lunch**

Session Chair: Gunther Andersson (Australia)

15:00 **Roman Böttger (Germany) I**

Extremely High Energy Density Deposition by Heavy Polyatomic Ion Impacts–Surface Nanopatterning and Order Enhancement

15:30 **Charlotte Herbig (Germany) I**

Ion Irradiation of Graphene/Ir(111): Amorphization, Thermal Recovery, and Noble Gas Trapping

16:00 **Stefan Facsko (Germany) O**

Transition from Pits to Mounds in Ion Induced Patterning of Germanium

16:20 **Hubert Gnaser (Germany) O**

Self-Organized Nanocone Formation on Ion-Bombarded InP Surfaces

16:40 **Coffee Break**

Session Chair: Stefan Facsko (Germany)

17:10 **E. Harriet Ahlgren (Finland) I**

Creating Nanoporous Graphene with Swift Heavy Ions

17:40 **Roland Kozubek (Germany) I**

Highly Charged Ion Induced Modifications of Graphene on Different Substrates

18:10 **Martin Engler (Germany) O**

Reverse Epitaxy on Elemental Semiconductor

18:30 **Charles Bourin (France) O**

Platform for the Nanoscale Study and Characterization of Ion Implantation

20:00 **Dinner**

21:00 **Committee Meeting**

Tuesday 20th October 2015

Session Chair: Philippe Roncin (France)

09:00 **Hermann Nienhaus (Germany) Pl**

Non-Adiabatic Effects in Low-Energy Gas-Surface Interactions

09:45 **Richard A. Wilhelm (Germany) I**

Charge Exchange and Energy Loss of Slow Highly Charged Ions in Graphene

10:15 **Dino Novko (Spain) O**

Energy Loss in Gas-Surface Dynamics: Electron-Hole Pair and Phonon Excitations upon Adsorbate Relaxation

10:35 **Coffee Break**

Session Chair: Kenji Kimura (Japan)

11:05 **Peter Bauer (Austria) I**

Inelastic Losses in Low Energy Ion Scattering

11:35 **Peter Sigmund (Denmark) I**

Progress in Heavy-ion Stopping

12:05 **Pierfrancesco Riccardi (Italy) O**

Electron Promotion Effects in the Interaction of Slow Ions with Al Surface

12:25 **Daniel Sanchez Portal (Spain) O**

Electronic Stopping Power of H and He in a Narrow Band Gap Semiconductor

13:00 **Lunch**

Session Chair: Takanori Koshikawa (Japan)

15:00 **Taku Suzuki (Japan) I**

Low-Energy He+ Ion Scattering Spectroscopy; Recent Topics in Fundamentals and Applications

15:30 **R. Carmina Monreal (Spain) I**

Surface Scattering in the Plasmonic Resonances of Ultralow Electron Density Nanospheres

16:00 **Bo Hellsing (Sweden) O**

Plasmaron Footprints in Photoemission

16:20 **Sachiko T. Nakagawa (Japan) O**

What Promotes the Desired Self Assembly (DSA)?

16:40 **Coffee Break**

Session Chair: Peter Bauer (Austria)

17:10 **Poster Introduction Section**

Oral introductions for each poster. A time limit of 2 minutes for each poster is strictly enforced by the session chairperson!

María José Aliaga (Spain)

Molecular Dynamics simulations of ion implantation in Fe thin films

Barbara Bruckner (Austria)

Influence of Oxygen in the charge exchange process of He backscattered from Ta in LEIS

Sophie Cervera (France)

Towards the Understanding of Mecanisms Responsible of the Thermal Hysteresis Suppression by Higly Charged Ions Collisions in Thin Films

Ayman Sherif El-Said (Saudi Arabia)

Modifications of Gallium Phosphide Single Crystals using Swift Heavy Ions and Slow Highly Charged Ions

Alexander Fuchs-Fuchs (Austria)

Electron Emission Induced by Highly Charged Ion Impact on Single Layer Graphene

Elisabeth Gruber (Austria)

Interaction of Multiply Charged Ions with Single Layer Graphene: Charge Exchange and Energy Loss Studies

Rene Heller (Germany)

Time of Flight Backscattering and Secondary Ion Mass Spectrometry in a Helium Ion Microscope

Karima Khalal-Kouache (Algeria)

Monte Carlo Simulation of Charge Exchange Processes in He^+/Cu Scattering

Karima Khalal-Kouache (Algeria)

Multiple Scattering of Low Energy H^+ Ions in Matter: Mean Energy Approximation with the Sigmund and Winterbon Model

Takanori Koshikawa (Japan)

Magnetic Property of Ferromagnetic Material multi-layer with High Brightness and Highly Spin-polarized LEEM

Henning Lebius (France)

Nanostripes and nanoripples: surface modifications by swift heavy ions

Tomoya Marumo (Japan)

Transmission Secondary Ion Mass Spectroscopy of a Peptide using 5MeV C_{60}^+ Ions

Jiro Matsuo (Japan)

Secondary Molecular Ion Emission from Liquids under Ambient Pressure

Philippe Roncin (France)

Qualitative and Quantitative Description of SiC grown Graphene Corrugation by Grazing Incidence Fast Atom Diffraction

Philippe Roncin (France)

A Compact, Large Area, Time and Position Sensitive Detector for Time of Flight Measurements

Philippe Roncin (France)

Active Correction of the Tilt Angle of the Surface Plane with respect to the Rotation Axis during Azimuthal Scan

Rafael Saavedra (Spain)

Ionoluminescence and Microstructural Changes of Fused Silica under Swift Ion Irradiation

Chad E. Sosolik (USA)

Recent Results from the Ion Beam Laboratories at Clemson University

John A. Tanis (USA)

Transmission of Electrons through Insulating PET Foils: Charge Deposition, Angular and Energy Dependence

John A. Tanis (USA)

Incident Energy and Charge Deposition Dependences of Electron Transmission through a Microsized Tapered Glass Capillary

YuYu Wang (China)

Nanostructure Formation on CaF_2, Al_2O_3, c-SiO_2 and MgO Single Crystal Surfaces by Highly Charged Ions and Swift Heavy Ions Impact

YuYu Wang (China)

Effects of Swift Heavy Ion Irradiation in a FeSiNbZrB Amorphous Alloy

Boris Weidtmann (Germany)

A Ballistic Transport Model for Electron Excitation Energy Induced by Particle Impact

Asier Zugarramurdi (Finland)

Helium Atom Scattering from Graphene: Testing the Pairwise Potential Ansatz

18:10 Poster Session

20:00 Dinner

Wednesday 21st October 2015

Special Session in Honor of Professor Helmut Winter

Session Chair: Ricardo Díez Muiño (Spain)

09:00 **Pedro Miguel Echenique (Spain)**
LAUDATIO FOR PROFESSOR HELMUT WINTER

09:30 **Andrei Borisov (France) I**
Tunneling at Surfaces: Atomic Projectiles and Localized Plasmons

10:00 **Helmut Winter (Germany) Pl**
IISC, Ions, and Surfaces – The First Four Decades

10:45 **Coffee Break**

Session Chair: Ronnie Hoekstra (The Netherlands)

11:15 **Maarten van Kampen (The Netherlands) I**
Ions in Extreme UltraViolet lithography tools

11:45 **Catia Costa (UK) I**
Imaging Mass Spectrometry in Forensic Science – New Tools, New Applications

12:15 **Norman H. Tolk (USA) O**
Dynamical Studies of Optoelectronic Modification arising from Heavy Ion Induced Point Defects using Coherent Acoustic Phonons

12:35 **Marco Trassinelli (France) O**
Highly Charged Ions Impact, a Promising Route to Exploit the Refrigeration Power of Giant Magnetocaloric Thin Films

13:00 **Lunch**

14:00 **EXCURSION**

20:00 **Dinner**

Thursday 22nd October 2015

Session Chair: Christian Linsmeier (Germany)

09:00 **Thomas Schwarz-Selinger (Germany) Pl**

Tungsten as Plasma Facing Material: Hydrogen Transport Studies and Defect Creation

09:45 **Mark E. Bannister (USA) I**

Surface Morphologies of He-Implanted Tungsten

10:15 **Evgeny Marenkov (Russia) O**

The Role of the Adatoms Diffusion in the Tungsten Fuzz Growth

10:35 **Coffee Break**

Session Chair: Fritz Aumayr (Austria)

11:05 **Bernhard Berger (Austria) I**

Erosion of Fusion-Relevant Wall Materials under Ion Bombardment studied with a Quartz Crystal Microbalance Technique

11:35 **Frederic Allegrini (USA) I**

Carbon Foils for Space Plasma Instrumentation

12:05 **Alvaro García Carrasco (Sweden) O**

The Impact of Helium Irradiation on Reflectivity of Self-Damaged Molybdenum Mirrors at High DPA Values

12:25 **Sergey Ryabtsev (Russia) O**

Deuterium Thermal Desorption from Vacancies in Tungsten

13:00 **Lunch**

Session Chair: Andrei Borisov (France)

15:00 **Philippe Roncin (France) I**

High Resolution Surface Topography with Grazing Incidence Fast Atom Diffraction.

15:30 **Paola Atkinson (France) I**

Dynamic Grazing Incidence Fast Atom Diffraction: in-situ monitoring of layer-by-layer growth oscillations and surface reconstructions during molecular beam epitaxys

16:00 **María Silvia Gravielle (Argentina) O**

Influence of the lighting on Fast Atom Diffraction studied via a Semi-Quantum Approach

16:20 **Cristina Díaz (Spain) O**

The Role of the Internal Degrees of Freedom in Molecular Diffractive Scattering under Fast Grazing Incidence

16:40 **Coffee Break**

Session Chair: Evgeny Marenkov (Russia)

17:10 **Hussein Hijazi (USA) I**

Solar Wind Sputtering of Lunar Soil Analogs: Charge State and Mass Effects

17:40 **Rafael Martinez (Brazil) I**

Astrophysical Material Analogs Irradiated by Swift Heavy Ions

18:10 **Eli Kolodney (Israel) O**

Velocity Correlated Cluster Emission in Surface Sputtering by a Large Polyatomic Projectile

18:30 **Carsten Bundesmann (Germany) O**

Secondary Particle Properties of the Ion Beam Sputter Process of Ag, Ge and Ti

20:00 **Refreshments**

20:30 **Conference Dinner**

Friday 23rd October 2015

Session Chair: María Silvia Gravielle (Argentina)

09:00 **Torgny Gustafsson (USA) Pl**

Studying Solids using the Helium Ion Microscope

09:45 **Yasushi Yamauchi (Japan) I**

Surface Microscopy using Spin-Polarized Metastable Helium Atom Beams

10:15 **Andrew Pratt (UK) O**

Laser Manipulation of Metastable Helium Atoms: Applications to Surface Analysis

10:35 **Coffee Break**

Session Chair: Maite Alducin (Spain)

11:05 **Ivor Loncaric (Spain) O**

Femtosecond Laser Pulse Induced Desorption: a Molecular Dynamics Simulation

11:25 **Dietmar Roth (Austria) O**

Electronic Stopping of Slow Light Ions in Vanadium Dioxide

11:45 **Natalia Koval (Spain) O**

TDDFT Calculations of the Vicinage Effect in the Energy Loss of a Hydrogen Dimer

12:05 **Karima Khalal-Kouache (Algeria) O**

Influence of the Interaction Potential on the Scattering Cross Section and the Energy Spectra in LEIS

12:25 **CLOSING REMARKS**

13:00 **Lunch**

ABSTRACTS

Monday 19th October 2015

High Resolution Concentration Depth Profiles forAnalysing Soft Matter Surfaces with NICISS

Gunther Andersson[1]

[1] Flinders Centre for NanoScale Science and Technology, Flinders University, GPO Box 2100, Adelaide SA 5001, Australia

1. INTRODUCTION

Soft matter surfaces play a vital role in many areas: polymers and dyes in organic electronics, surfactant solutions, foam films, functionalization of surfaces and biological membranes to name only a few examples. Often it is of interest to know how the various components are distributed along the depth scale. In the case of soft matter the depth resolution required is in the order of the size of the molecules forming the sample, i.e a depth resolution of less than 1 nm. The depth range required is in the order of a few 10 nm. The requirements on the concentration depth profiles can be met with neutral impact collision ion scattering spectroscopy (NICISS).

2. REQIREMENTS ON NICISS

In a NICISS experiment rare gas ions with a kinetic energy of a few keV are used. The mechanism on which deriving concentration depth profiles from NICISS measurements are based on are similar to those for Rutherford backscattering (RBS). The energy loss during backscattering including inelastic energy losses needs to be known as well as the stopping power of the projectiles, energy loss straggling, and the contribution of multiple scattering. If possible, the respective quantities have been measured experimentally. [1]

3. RESULTS

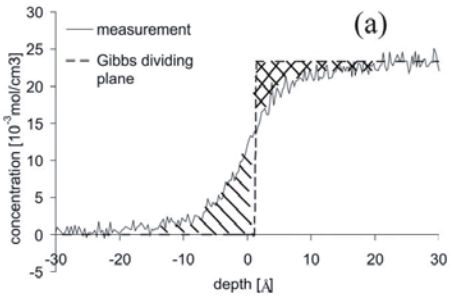

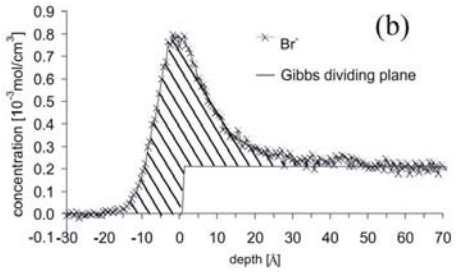

Figure 1: Concentration depth profiles of the solvent (a) and the solute (b) of a 0.2 molal.solution of tetrabutylphosphonium bromide (Bu_4PBr) in formamide. [2]

In Figure 1 concentration depth profiles of solute and solvent of a surfactant solution are shown. The shaded area shows for both components the experimentally determined surface excess.

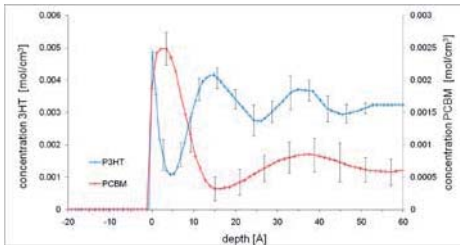

Figure 2: Concentration depth profiles of the polymer mixture poly (3-hexylthiophene) (P3HT) and [6,6]-phenyl-C61-butyric acid methyl ester (PCBM). [3]

In Figure 2 the layered structure of the polymer mixture formed by P3HT and PCBM is shown. The examples in both figures illustrate the information that can be gained through applying NICISS on soft matter surfaces.

4. REFERENCES

[1] G. Andersson, Ch. Ridings, Chem. Rev., **114**, 8361 (2014)

[2] G. Andersson, T. Krebs, H. Morgner, PCCP, **7**, 136 (2005).

[3] Natalya Schmerl, G.G. Andersson, PCCP .**13**, 14993 (2011).

TRANSMISSION SECONDARY ION MASS SPECTROMETRY OF ORGANIC MOLECULES USING 5 MeV C_{60}^+ IONS

K. Nakajima[1,*], *K. Nagano*[1], *T. Marumo*[1], *K. Narumi*[2], *Y. Saitoh*[2], *K. Hirata*[3], *and K. Kimura*[1]

[1] Department of Micro Engineering, Kyoto University, 615-8540 Kyoto, Japan
[2] Takasaki Advanced Radiation Research Institute, JAEA, Takasaki, Gumma 370-1292, Japan
[3] National Metrology Institute of Japan, AIST, Tsukuba, Ibaraki 305-8565, Japan

1. INTRODUCTION

Secondary ion mass spectrometry (SIMS) has recently extended its application field to organic material, biological and biomedical science. The use of various large cluster ions, such as C_{60} ions, argon gas cluster ions, water cluster ions, and metal cluster ions as primary ions provides a satisfactory yield of intact large molecular ions up to ~1000 Da. There is, however, still a strong demand for further improvement in sensitivity of SIMS to larger molecules for molecular imaging. Boussofiance-Baudin et al. have reported that a significant enhancement of intact molecular ions was achieved by detecting the secondary ions emitted in the forward direction compared to the backward direction, when a thin phenylalanine film on a carbon foil was penetrated by MeV Au_n^+ (n = 1–3) primary ions [1]. The origin of the enhancement was suggested to be larger stopping power due to higher charge states of the primary ions after their passage through the specimen. So far, however, there have been only few studies on SIMS in such a transmission geometry. In this work, we have combined MeV C_{60} primary ions with transmission SIMS for organic molecules [2]. It was found that a remarkable enhancement of intact molecular ions as well as significant suppression of fragment ions can be achieved by detecting secondary ions emitted in the forward direction.

2. EXPERIMENT

Phenylalanine (M.W. 165.2) was used as a target amino acid. The samples were ex-situ prepared by vacuum-evaporating phenylalanine on self-supporting amorphous silicon nitride (a-SiN) membranes (20–50 nm thick). The thickness of the phenylalanine film was ranging from ~20 nm to ~100 nm. In the SIMS measurements, the samples were irradiated from the a-SiN side with 5 MeV C_{60}^+, as well as with 6 MeV Cu^{4+}. Positive secondary ions emitted in the forward direction were mass-analyzed with time-of-flight techniques under transmission of primary ions through the samples. Secondary ions emitted in the backward direction from the same samples irradiated from the phenylalanine side were also measured for comparison.

3. RESULTS

Figure 1 shows typical mass-to-charge ratio (m/z) spectra of positive secondary ions emitted in the forward and backward directions, respectively. A peak at m/z 166 correspond to the protonated molecular ions, $[Phe+H]^+$. A number of peaks in lower m/z region are assigned as various fragment ions originating from a phenylalanine molecule. Remarkable enhancement of the molecular ions along with suppression of the fragment ions for the forward emission, as seen in Fig. 1 will be discussed in terms of the lateral distribution of energy deposition on the surface to be analyzed.

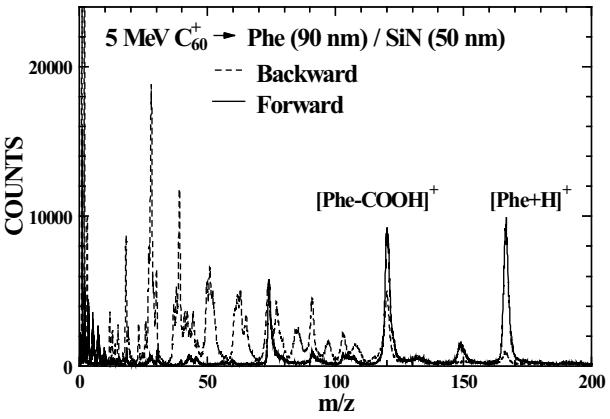

Figure 1: mass-to-charge ratio spectra of positive secondary ions from a phenylalanine film on an a-SiN membrane using 5 MeV C_{60}^+.

REFERENCES

[1] K. Boussofiance-Baudin, A. Brunelle, P. Chaurand, S. Della-Negra, J. Depauw, P. Hakansson and Y. Le Beyec, Nucl. Instr. Meth. B **88**, 61 (1994).
[2] K. Nakajima, K. Nagano, M. Suzuki, K. Narumi, Y. Saitoh, K. Hirata and K. Kimura, Appl. Phys. Lett. **104**, 114103 (2014).

* Corresponding author e-mail address: nakajima.kaoru.4a@kyoto-u.ac.jp

Argon Gas Cluster Ion Sources in Surface Chemical Analysis: Measurements of Total Sputter Yields and a Semi-Empirical Predictive Model

A.J. Barlow[*], *N. Sano, J.F. Portoles, and P.J. Cumpson*

National EPSRC XPS Users' Service (NEXUS), School of Mechanical and Systems Engineering, Newcastle University, Newcastle Upon Tyne, NE1 7RU, UK

1. INTRODUCTION

Argon clusters are increasingly important in the surface analysis of soft materials, polymer, organic coatings, biomaterials and bio-related surfaces [1]. Further to this, they have become crucial for the in-situ cleaning of organic/inorganic contaminants from surfaces under study in our laboratory [2].

There is however a pressing need for reference data to allow sputter depth profiling using clusters and the quantification of depth in Secondary Ion Mass Spectrometry (SIMS) and X-ray Photoelectron Spectroscopy (XPS). In our laboratory we have two argon gas cluster ion sources installed on XPS instruments, and a third on a Time-of-Flight SIMS (ToF-SIMS). Thus, an understanding of the ion-surface collision mechanism becomes paramount.

2. RESULTS

We have used a quartz crystal microbalance (QCM) to measure the total sputter yield for argon cluster ions in a number of materials important in studies of biomaterials and diagnostic devices, including polymethyl methacrylate, collagen, hydroxyapatite, borosilicate glass, soda lime glass, silicon dioxide and the native oxides on titanium and stainless steel [3]. This device is installed within one of our XPS spectrometers, and allows for a direct, in-situ measurement of sputter ion rates during a depth profile analysis (Figure 1). The data collected from numerous materials fit a simple semi-empirical equation [4] very well, so that the total sputter yield can now be estimated for any of them for the entire range of cluster ion energy typical in XPS or SIMS.

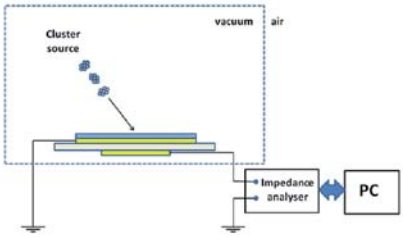

Figure 1: Schematic representation of QCM within our XPS instrument.

Very recently, for sputter measurements on soft materials we have developed a new low-frequency resonator mass sensor that extends our measurement capability to a wide range of polymeric and organic materials. Our QCM device is most suited to the lower energy-per-atom range, from 1-10 eV, which is also the accessible energy range for the source installed on our XPS instruments. On the basis of our total sputter yield measurements, we discuss useful 'figures-of-merit' for choosing the optimum cluster ion energy to use in depth profiling or cleaning organic/inorganic samples in both XPS and ToF-SIMS.

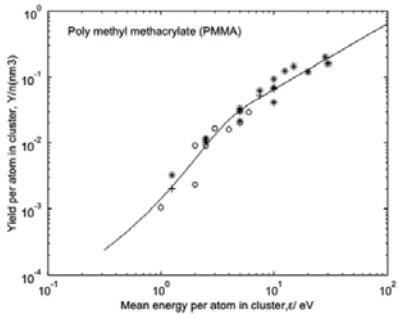

Figure 2: Measurements of total argon cluster-ion sputter yield from PMMA. The continuous line is a fit to the developed model, while data points are yields from laboratory measurements (from [4]).

3. REFERENCES

[1] TOF-SIMS with Argon Gas Cluster Ion Beams: A Comparison with C60+, S Rabbani, A M Barber, J S Fletcher, N P Lockyer, and J C Vickerman, Anal. Chem. 83 (2011) 3793–3800.

[2] Stability of reference masses: VI. Mercury and carbonaceous contamination on platinum weights manufactured at a similar time as the international and national prototype kilograms, P J Cumpson, J F Portoles, N Sano, A J Barlow, Metrologia 50 518 (2013).

[3] Depth profiling organic/inorganic interfaces by argon gas cluster ion beams: sputter yield data for biomaterials, *in vitro* diagnostic and implant applications, P J Cumpson, J F Portoles, A J Barlow, N Sano, M Birch, Surf. and Interface Anal. 45 (2013) 1859-1868.

[4] Accurate argon cluster-ion sputter yields: Measured yields and effect of the sputter threshold in practical depth-profiling by x-ray photoelectron spectroscopy and secondary ion mass spectrometry, P J Cumpson, J F Portoles, A J Barlow, N Sano, J. Appl. Phys 114 (2013) 124313

[*] Corresponding author e-mail address: anders.barlow@newcastle.ac.uk

NANO-STRUCTURING BY SWIFT HEAVY IONS AT GRAZING INCIDENCE: DIFFERENT TRACK TYPES WITH DIFFERENT TARGETS

B. Ban-d'Etat[1,*], *E. Gruber*[2], *F. Meinerzhagen*[3], *M. Karlušić*[4], *F. Aumayr*[2], *L. Bergen*[2], *C. Grygiel*[1], *A. Benyagoub*[1], *E. Lattouf*[1], *H. Lebius*[1], *D. Marie*[1], *O. Ochedowski*[3], *J. Rangama*[1], *P. Salou*[1], *Y. Wang*[2], *M. Schleberger*[3]

[1] CIMAP (CEA-CNRS-ENSICAEN-UCN), bld Henri Becquerel, 14070 Caen, France
[2] Institute of Applied Physics, TU Wien, 1040 Vienna, Austria
[3] Fakultät für Physik, Universität Duisburg-Essen and CENIDE, 47057 Duisburg,
[4] Ruđer Bošković Institute, Bijenička cesta 54, 10000 Zagreb, Croatia

Swift heavy ion (SHI) irradiation of solid targets can lead to permanent structural modifications at their surface. In the case of normal incidence, the surface modification is relatively small. However, by inclining the ion beam direction to a grazing angle with regards to the target's surface, the track which was before hidden deep in the bulk, is now projected along the surface allowing larger structures. All the topological structures discussed here are studied by atomic force microscopy. Under this geometry, typically the impact of an individual ion is producing a long surface track. The goal of this presentation is to show the different surface structures, which can be produced by varying the target material and the kinetic energy of the projectile.

Besides the classical line of hillocks (e.g. in $SrTiO_3$ [1]), we can observe characteristic double structures (e.g. in muscovite mica, see figure 1, and GaN, see figure 2 [2]). Other examples are SiC, where grooves with single-layer depth are created [3], and also very shallow grooves in front of the above-mentioned tracks in $SrTiO_3$. The different structures will be presented and interpreted.

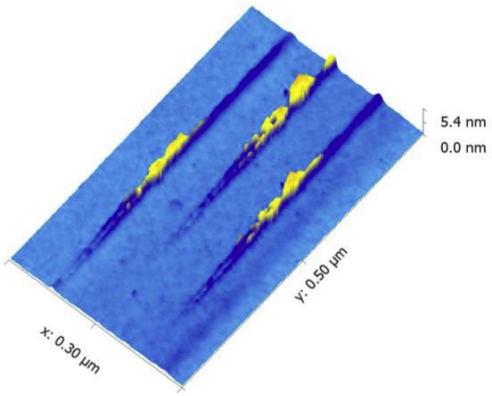

Figure 1: Surface tracks formed on a muscovite mica surface after 92 MeV Xe ion irradiation at 0.9°.

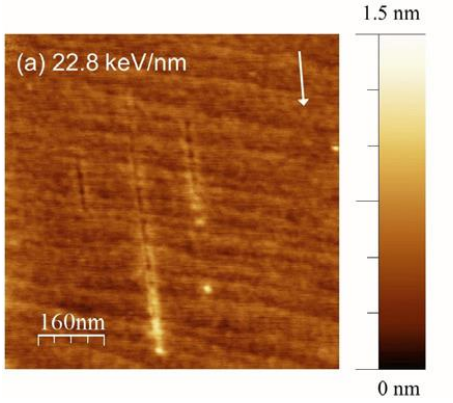

Figure 2: Nanostripes in GaN after 92 MeV Xe irradiation at 1° of incidence.

This work has been partly supported by the French-Austrian collaboration SIISU, financed by ANR (France, ANR-12-IS04-0005-01) and FWF (Austria, I 1114-N20).

1. REFERENCES

[1] E. Akcöltekin et al., Nature Nanotechnology 2 (2007) 290
[2] M. Karlušić et al., J. Phys. D: Appl. Phys., in print (2015)
[3] O. Ochedowski et al., Nature Communications 5 (2014) 3913

* Corresponding author e-mail address: bandetat@ganil.fr

FROM SURFACE TO BULK MODIFICATIONS UNDER SWIFT HEAVY ION IRRADIATION OF INSULATING MATERIALS

C. Grygiel[1*], *H. Lebius*[1], *B. Ban-d'Etat*[1], *E. Gardes*[1] *and I. Monnet*[1]

[1] *CIMAP, CEA-CNRS-ENSICAEN-UCN, BP5133 F-14070 Caen cedex 5 France*

1. INTRODUCTION

Swift heavy ions have the specificity to mainly lead to the deposition of high energy density of electronic excitations, opposite to low energy ions leading either to nuclear energy deposition or, in the case of highly charged ions, to potential energy deposition. Swift heavy ions are known to entail modifications at the surface of insulating material and in the bulk. The nanostructures created at the surface are commonly characterized by atomic force microscopy (AFM) in terms of numbers, dimensional sizes (lateral size, height, length) and shape (pit or hillock or chains of these previous). These surface effects are linked to the material characteristics which are also strongly affected by irradiation in the bulk where defect formation, phase transitions and microstructure evolutions might be observed. These bulk effects are commonly studied by optical absorption for the colour centre formation, by transmission electron microscopy (TEM) for the individual latent track formation and X-Ray diffraction (XRD) for structural and microstructural evolutions.

In our study, we try to bridge the gap between surface modifications, near surface and bulk modifications due to swift heavy ions by using two methods making sensitivity to the surface: normal irradiation with in-situ analysis in grazing geometry, and grazing irradiation with ex-situ analysis in normal geometry.

The first method used bulk technique when used in grazing geometry (around 1° of incidence) is well suitable for the characterization of irradiated materials where the upper irradiated part of samples might be strongly and non-homogeneously modified in depth. The given example is the in-situ Grazing X-Ray diffraction [1] developed by CIMAP since few years to probe with a good resolution the modifications in the near-surface region (depth chosen with the incidence angle of the X-ray beam).

The second method is the grazing irradiation of surfaces with ex-situ analysis in normal geometry. The grazing irradiation studies are a strong activity of CIMAP laboratory [2]. A complementary tool for this characterization is also a bulk technique made sensitive to the surface: it is the Focused Ion Beam (FIB) technique associated to TEM which allow to pick-up and to observe a nano-size area of sample, for example a hillock chain just beneath the surface produced by grazing SHI irradiation (see Fig 1).

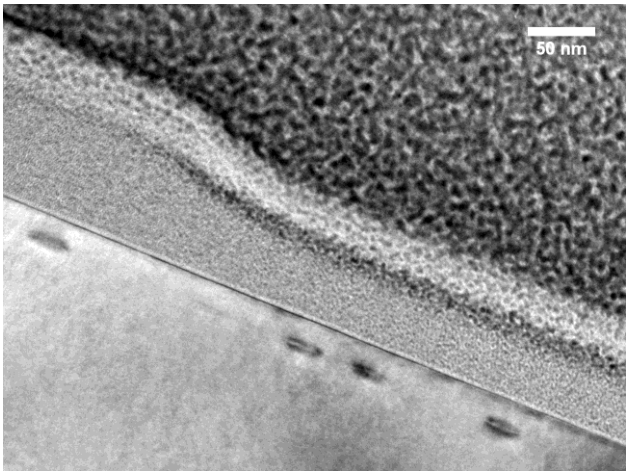

Figure 1: Observation of a chain of hillocks induced by grazing irradiation at 0.5° by Xe ions at 7.6MeV/A and observed by TEM after a selective sample preparation by FIB.

2. EXPERIMENTS AND RESULTS

In the presentation, studies of material modifications induced by swift heavy ions and observed from the surface to the bulk will be presented. Results obtained with the two previously detailed methods will be shown. The cases of model insulating materials, especially oxides like $SrTiO_3$ perovskite will be taken to highlight the modification profile along the ion trajectory. The irradiation experiments have been performed at the IRRSUD beamline and the SME beamline of the GANIL facility (Caen, France) where the energy is ranging from 0.3 up to 13 MeV/A.

3. REFERENCES

[1] C. Grygiel et al, Rev. Sci. Instrum. Volume **83**, Issue 1, 013902 (2012).

[2] E. Akcöltekin et al, Nature Nanotechnology **2**, 290 (2007).

[*] Corresponding author e-mail address: grygiel@ganil.fr

TEMPERATURE MEASUREMENT OF THERMAL SPIKE USING DESORPTION OF NANOPARTICLES

*T. Kitayama[1], H. Hayashi[1], K. Nakajima[1], K. Narumi[2], Y. Saitoh[2], M. Matsuda[3], M. Sataka[3], M. Tsujimoto[4], M. Toulemonde[5], S. Bouffard[5] and K. Kimura[1]**

[1] Department of Micro Engineering, Kyoto University, Kyoto, Japan
[2] Takasaki Advanced Radiation Research Institute, JAEA, Takasaki, Japan
[3] Nuclear Science Research Institute, JAEA, Tokai, Japan
[4] Institute for Integrated Cell-Material Sciences,, Kyoto University, Kyoto, Japan
[5] CIMAP-GANIL (CEA-CNRS-ENSICAEN-Université de Caen Basse Normandie), Bd. H. Becquerel, 14070 Caen, France

1. INTRODUCTION

When swift heavy ions penetrate solids the ions excite solid electrons. The energy of the excited electrons is gradually transferred to the lattice and eventually cylindrical damage regions, so-called ion tracks, may be created when the electronic energy loss is larger than a material dependent threshold value. There are several models proposed for the mechanism of the track formation. Among these models, only the inelastic thermal spike (i-TS) model explains the observed track radius quantitatively [1]. In the thermal spike model, ion tracks are assumed to be formed if the atomic temperature rises beyond the melting or boiling temperatures. There has been, however, no measurement of the temperature during the track formation. Because the thermal spike is formed in a localized region of nanometer scale and continues only on a picosecond time scale. Such ultrafast local heating cannot be measured conventional techniques. In this presentation, we demonstrate that the temperature of the thermal spike can be traced by observing desorption of metal nanoparticles upon impact of swift heavy ions.

2. EXPERIMENT

Gold and platinum nanoparticles (diameter a few nm) were deposited on self-supporting amorphous silicon oxide (a-SiO_2, thickness 20 nm) and amorphous silicon nitride (a-SiN, thickness 30 nm) films. These films were irradiated with 420 MeV Au ions at normal incidence to a fluence of ~ 5×10^{10} ions/cm^2. In the irradiation, a carbon foil (20 μg/cm^2) was placed in front of the samples to acquire an equilibrium charge state. This carbon foil was also used as a collector foil, i.e. used to capture particles emitted from the target during irradiation. The irradiation was performed either on the nanoparticle-deposited surface (will be referred to as a "front surface irradiation") or on the rear surface ("rear surface irradiation") at normal incidence. In the rear surface irradiation, a self-supporting a-SiO_2 film was placed just behind the sample (facing to the gold-deposited surface) to collect gold nanoparticles emitted from the film during the irradiation. Both the irradiated samples and the collector foils were observed using TEM (JEOL JEM-2200FS) equipped with a field emission gun operating at 200 kV. An example of the observed TEM images is shown in Fig. 1. This TEM image shows that gold nanoparticles disappear from the vicinity of the ion track. Based on the MD simulation [2], which showed that the desorption of gold nanoparticles occurs when the temperature surpasses the melting point of gold, the present result indicates that the observed nanoparticle-cleared region was heated beyond the melting point of gold upon the impact of Au ions. The results of a-SiN films together with the results of the desorption of platinum nanoparticles will be presented in the conference and these results will be compared with the i-TS calculations.

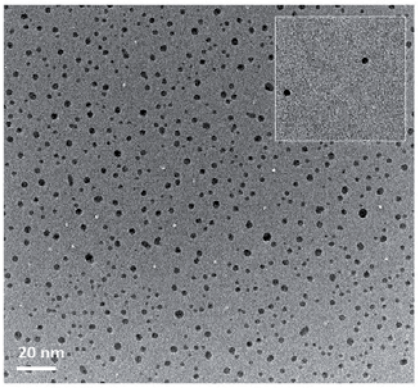

Figure 1: TEM bright field images of gold-nanoparticle-deposited a-SiO_2 films irradiated with 420 MeV Au ions on the rear surface. The gold nanoparticles and the ion tracks are seen as dark and bright spots. The gold nanoparticles disappeared from the vicinity of the ion track. The inset shows a TEM image of a collector foil.

3. REFERENCES

[1] M. Toulemonde et al, Mat. Fys. Medd. **52**, 263 (2006).
[2] C. Anders et al, NIMB **267**, 2503 (2009).

* Corresponding author e-mail address: kimura@kues.kyoto-u.ac.jp

Cluster production and ion-induced luminescence in the Matrix Assembly Cluster Source (MACS)

*W. Terry, L. Cao, J. Liu, F. Yin, and R. E. Palmer**

Nanoscale Physics Research Laboratory, School of Physics and Astronomy, University of Birmingham, UK

1. INTRODUCTION

Cluster ion beam technology has been widely used over the last 20 years to investigate size-selected clusters. The study of size-selected clusters is of interest both to improve our fundamental understanding of nano systems on the sub-10nm scale and due to their potential applications [1, 2]. However there is a significant barrier to harnessing this potential: state of the art cluster sources can produce ~1nA (~µg/h) of size-selected clusters [3], which is not sufficient for test-tube science let alone industrial scale applications.

Here we demonstrate a novel instrument for cluster production, the Matrix Assembly Cluster Source (MACS), which could increase production by seven orders of magnitude or more. This works by co-condensing rare gas and metal atoms (e.g. Ar & Ag) onto a cryogenically cooled plate (<15K) and then sputtering it with rare gas ions (e.g. Ar^+ ~1kV). This sputtering causes clusters to be produced in the thermal spike regime, which are collected on TEM grids for analysis by HAADF (High Angular Annual Dark Field) STEM (Scanning Transmission Electron Microscopy). The cluster flux depends on the incident ion beam current and the cluster conversion yield.

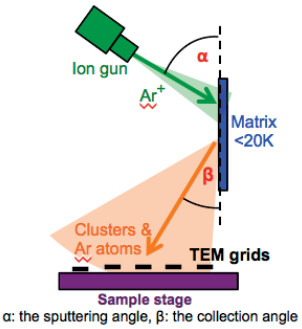

Figure 1: Schematic diagrams showing principle of cluster production and collection via matrix assembly.

2. RESULTS

2.1. Cluster Production

We have demonstrated that Matrix Assembly (MA) can produce clusters at several incident sputtering angles (10°-45° with respect to the surface). For each sputtering angle (α), clusters have been collected at several collection angles (β), between parallel to the surface and normal. Integration of the cluster flux over this arc gives a cluster to Ar^+ yield of ~1% (~3µA to 28nA equivalent calculated current). For each sputtering angle the integrated cluster flux was found to be similar. However, the peak cluster flux collection angle shifted, the greatest cluster flux was always observed when the sum of the incident and collection angles were ~110°.

2.2. Ion-Induced Luminescence

While under ion bombardment the matrix emits light visible to the eye. This light emission has been studied with a view to provide real time condition and composition monitoring of the matrix. The Spectrum in Figure 2 demonstrates the ability to detect vacuum impurities within the argon matrix, in this case O_2 (similar studies have been carried out with N_2). Well known features allow conclusive identification of these impurities e.g. ArO excimer and Vegard Kaplan lines in N_2 [4, 5]. We also observe quenching of the ion-induced luminescence by the addition of Ag in the matrix. The quenching is enhanced by higher concentrations of Ag.

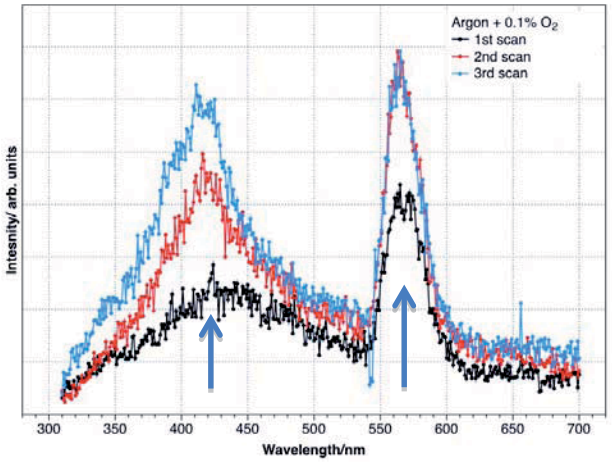

Figure 2: Spectra of ion induced light emission from an argon matrix doped with 0.1% O_2, showing intensity increase over repeated scans.

3. REFERENCES

[1] K. P. Arkill, J. M. Mantell, S. R. Plant, P. V. Verkade, R. E. Palmer, *Sci. Rep*, 5, 9234 (2015)
[2] V. Habibpour, et al, *J. Phys. Chem. C*, **116**, 50, 26295 - 26299, (2012)
[3] S. Pratontep, et al, *Rev. Sci. Instrum,* **76**, 045103 (2005)
[4] A.G. Belov, I.Y. Fugol, E.M. Yurtaeva, and O.V. Bazhan, *Journal of Luminescence,* **91**, 107 (2000).
[5] R. Friedl and U. Fantz, *New J Phys,* **14**, 043016 (2012).

* Corresponding author e-mail address: wdt287@bham.ac.uk

Extremely High Energy Density Deposition by Heavy Polyatomic Ion Impacts – Surface Nanopatterning and Order Enhancement

R. Böttger[1,*], *K.-H.Heinig*[2], *L. Bischoff*[1], *B. Liedke*[1], *C. Anders*[2], *H. M. Urbassek*[2]

[1] Helmholtz-Zentrum Dresden-Rossendorf, Institute of Ion Beam Physics and Materials Research, Dresden, Germany
[2] University Kaiserslautern, Physics Department and Research Center OPTIMAS, Kaiserslautern, Germany

1. INTRODUCTION

Heavy ions like Bi or Au of a few tens of keV deposit a high energy density into the collision cascade volume of due to (i) their high mass and (ii) their low projected range. At higher energies, this density becomes diluted as the cascade volume increases super-linearly with ion energy.

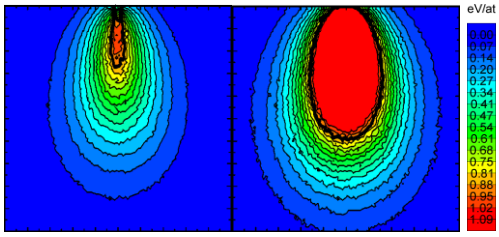

Figure 1: 20x20 nm² cross-sections of the energy per Ge target atom as deposited by 20 keV/at Bi_1 (left) and 20 keV/at Bi_3 ion impact.

Compared to monatomic ions, heavy polyatomic ions deposit an even higher energy density (Figure 1). This is sufficient to form a pool of a localized, almost classical melt in a semiconductor surface lasting up to half of a nanosecond.

2. RESULTS

Local melting and re-solidification by single polyatomic ion impacts is proven by molecular dynamics calculations.

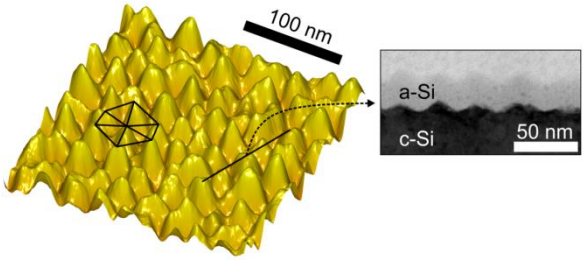

Figure 2: 3D representation of SEM image of Si nanodots (250x250 nm²) formed by heavy Bi_3 ion irradiation

Well-ordered, self-organized dot patterns on Si, Ge and GaAs surfaces have been found after heavy polyatomic ion irradiation, which can be attributed to the impact-induced local transient melting (Figure 2). Similar patterns were found with monoatomic ions at elevated substrate temperatures, where the energy per substrate atom exceeds a critical value within a larger volume.

The kinetics of localized melt pools leads to a generic, Kuramoto-Sivashinsky-type (KS) partial differential equation for the surface evolution. Whereas so far the mechanisms of ion-induced surface pattern evolution are assumed to be surface-curvature-dependent ion erosion or ion-momentum-induced mass drift of surface atoms, for heavy polyatomic ions we have identified a completely different mechanism.

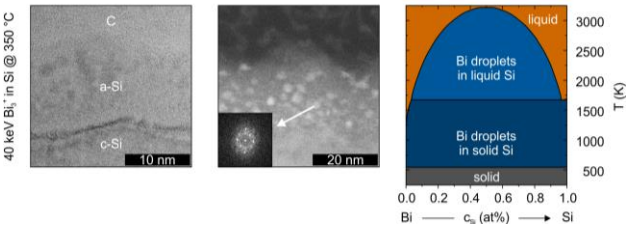

Figure 3: Cross-sectional TEM study of Bi precipitates in a-Si surface layer after Bi_3 ion irradiation. Precipitation results from the pathway of heating/quenching shown in the Bi–Si phase diagram.

The local melting and quenching process is so far from equilibrium that particularities of phase diagrams like the Bi state in Si or Ge are frozen into the nanostructure of the re-solidified volume. This opens the possibility to study extremely fast solid-liquid phase transitions (Figure 3).

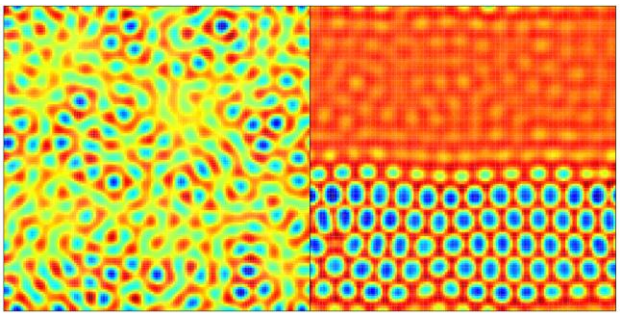

Figure 4: Integrated KS-type PDE. Left: starting from an initially flat surface. Right: starting from an additionally perturbed (surface).

Finally, a possibility of enhancing the regularity of such self-organized surface patterns will be demonstrated based on geometrical constraints (Figure 4).

The authors thank the German Research Foundation for funding projects Bi508/14-1, He2137/4-2 and Ur32/23-1.

* Corresponding author e-mail address: r.boettger@hzdr.de

ION IRRADIATION OF GRAPHENE/IR(111):AMORPHIZATION, THERMAL RECOVERY, AND NOBLE GAS TRAPPING

C. Herbig[1,*], *E. H. Åhlgren*[2], *U. A. Schröder*[1], *A. J. Martínez-Galera*[1], *M. A. Arman*[3], *J. Kotakoski*[4], *J. Knudsen*[3,5], *A. V. Krasheninnikov*[6], *and T. Michely*[1]

[1] II. Physikalisches Institut, Universität zu Köln, Zülpicher Str. 77, 50937 Köln, Germany
[2] Department of Physics, University of Helsinki, P.O. Box 64, FI-00014 Helsinki, Finland
[3] Division of Synchrotron Radiation Research, Lund University, Box 118, 22100 Lund, Sweden
[4] Faculty of Physics, University of Vienna, Boltzmanngasse 5, 1090 Vienna, Austria
[5] MAX IV Laboratory, Lund University, Box 118, 22100 Lund, Sweden
[6] Department of Applied Physics, Aalto University, P.O. Box 11100, FI-00076 Aalto, Finland

Ion irradiation of 2D-materials is a new field of ion-matter interaction research that offers rich and unique opportunities. Though still in its infancy, whenever careful analysis follows the application of ion beams to a 2D-material under controlled conditions, new phenomena are discovered: interface channeling of ions in between Gr and its substrate was experimentally discovered and simulated [1]; a regular nanomesh of vacancy clusters self-organized due to the periodic modulation of the Gr-substrate interaction [1], nanotents above implanted ions [2], and sputter protection was theoretically predicted [3].

In this study we employ noble gas ion irradiation on epitaxially grown Gr/Ir(111) and follow the decisive steps during annealing using STM, LEED, XPS, and TDS. Our experiments are corroborated by MD Simulations and DFT calculations.

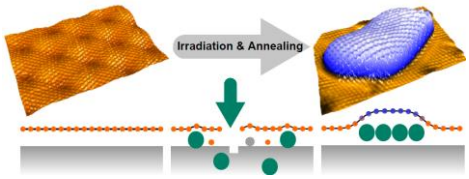

Figure 1: STM image Gr/Ir(111) before (upper left) and after ion irradiation and annealing to 1000K (upper right). Schematics of the as grown Gr film (lower left), after irradiation (middle), and annealing (lower right).

Upon room temperature ion irradiation, Gr on Ir(111) amorphizes. It recovers its crystalline structure during annealing. We follow this process by STM, LEED, and XPS and track the onset temperatures for recrystallization. Additionally, we observe bulge formation in the Gr sheet that can be traced back to noble gas trapping in between the Gr layer and the substrate [4, 5].

After 3keV Xe^+ ion irradiation of bare Ir(111) at room temperature noble gas is implanted into the bulk, as visible from the Xe core level peaks in the XPS spectra in Fig. 2 (a) (bottom). Upon annealing to 1000K and subsequently to 1300K the Xe signal diminishes [middle and top spectra of Fig. 2 (a)]. We explain these changes to be due to thermal excitation that leads to a partial release from its trapping sites in the crystal and enables diffusion and subsequent desorption to the vacuum.

Conducting the same experiment for a Gr covered Ir(111) surface leads to a higher Xe intensity already at room temperature, followed by a substantial increase upon annealing to 1000K and 1300K, respectively. The interpretation is straightforward: Instead of being released to vacuum, the Xe diffusing out from the Ir bulk becomes trapped under the Gr cover forming bulge structures (compare Fig. 1).

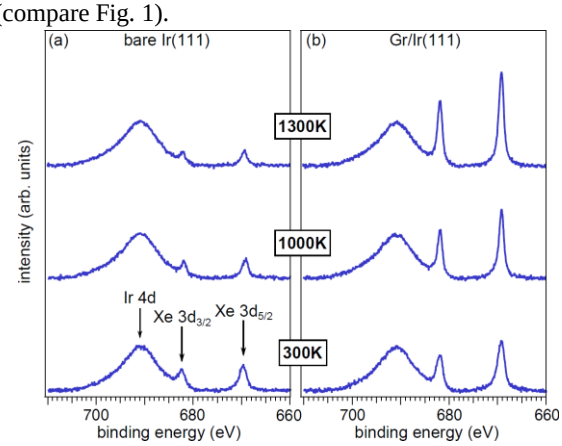

Figure 2: XPS of the Ir 4d, Xe $3d_{3/2}$, and Xe $3d_{5/2}$ core levels for (a) bare Ir(111) and (b) Gr covered Ir(111) after exposure to 0.1MLE of 3keV Xe^+ at 300K and stepwise annealing to 1000K and 1300K.

In the presentation the energy, angle, and ion species dependence of noble gas trapping as well as the processes involved will be discussed. Moreover we will provide experimental insight for sputter protection of the substrate.

REFERENCES

[1] S. Standop, O. Lehtinen, C. Herbig, G. Lewes-Malandrakis, F. Craes, J. Kotakoski, T. Michely, A.V. Krasheninnikov, C. Busse, Nano Lett. **13**, 1948 (2013).
[2] H. Cun, M. Iannuzzi, A. Hemmi, S. Roth, J. Osterwalder, T. Greber, Nano Lett., **13**, 2098 (2013).
[3] E. H. Åhlgren, S. K. Hämäläinen, O. Lehtinen, P. Liljeroth, J. Kotakoski, Phys. Rev. B **88**, 155419 (2013).
[4] C. Herbig, E. H. Åhlgren, W. Jolie, C. Busse, J. Kotakoski, A. V. Krasheninnikov, T. Michely, ACS Nano **8**, 12208 (2014).
[5] C. Herbig, E. H. Åhlgren, U. A. Schröder, A. J. Martínez-Galera, M. A. Arman, W. Jolie, C. Busse, J. Kotakoski, Jan Knudsen, A. V. Krasheninnikov, T. Michely, ACS Nano **9**, 4664 (2015).

* Corresponding author e-mail address: herbig@ph2.uni-koeln.de

TRANSITION FROM PITS TO MOUNDS IN ION INDUCED PATTERNING OF GERMANIUM

S. Facsko[1,*], and X. Ou[2]

[1] Helmholtz-Zentrum Dresden-Rossendorf, Institute of Ion Beam Physics and Materials Research, Bautzner Landstr. 400, 01328 Dresden, Germany

[2] State Key Laboratory of Functional Material for Informatics, Shanghai Institute of Microsystem and Information Technology, Chinese Academy of Sciences, Shanghai 200050, China

1. INTRODUCTION

Low energy ion irradiation drives surfaces out of equilibrium by continuous creation of displacements in the sub-surface region. At room temperature the accumulation of displacements leads to the amorphization of the irradiated surfaces and self-organized ripple pattern perpendicular to the ion beam direction are formed for incidence angles higher than 50° [1]. At normal incidence irradiation smoothing dominates and no pattern are observed for low energy ion irradiation. At higher temperatures, point defects created by the displacements in the ion collision cascade can diffuse longer distances, thus vacancies and interstitial recombine more effectively or diffuse to the surface. Finally, at temperatures higher than the recrystallization temperature, all defects in the sub-surface region are annealed before an ion creates new defects and the surface remains crystalline. The average density of surface vacancies and ad-atoms on the surface is, however, much higher than the corresponding densities in thermal equilibrium resulting in a much higher entropy.

2. PATTERN FORMATION

In this regime, ion irradiation creates an excess of vacancies on the crystalline surface due to sputtering and the surfaces morphology is determined primarily by their kinetics. The diffusion of vacancies is biased by the Ehrlich-Schwoebel barrier, i.e. an additional barrier for crossing terrace steps, similar to the diffusion barrier of ad-atoms known from growth by molecular beam epitaxy. Consequently, ion sputtering leads to the erosion of 3D structures in a "reverse epitaxy" process. The resulting patterns are arrays of inverse pyramids growing into the Ge surface [1,2]. The morphology of these patterns is given by the crystal symmetry of the surface. Hence, checkerboard patterns appear on the Ge (001) surface (Figure 1a).

Here, we show that the inverse pyramid pattern on Ge(001) surface, which is observed for normal incidence ion irradiation at higher temperatures, turns into a pyramidal mound pattern (Figure 1b-c) at incidence angles between 50° and 70° with respect to the surface normal, and finally, into ripple patterns above 80° incidence (Figure 1d). All irradiations were performed at 350° C with 1 keV Ar^+ at a fluence of $1x10^{18}$ cm^{-2} from a Kaufman ion source.

The observed transition from pit to mound patterns in reverse epitaxy can be understood by assuming a transition from vacancy dominated pattern formation to ad-atom dominated pattern formation. Therefore, at incidence angles above 50° the pattern resemble mound patterns observed in growth. Furthermore, the transition to ripples patterns at higher incidence angles is ascribed to a shadowing instability at these grazing incidence angles.

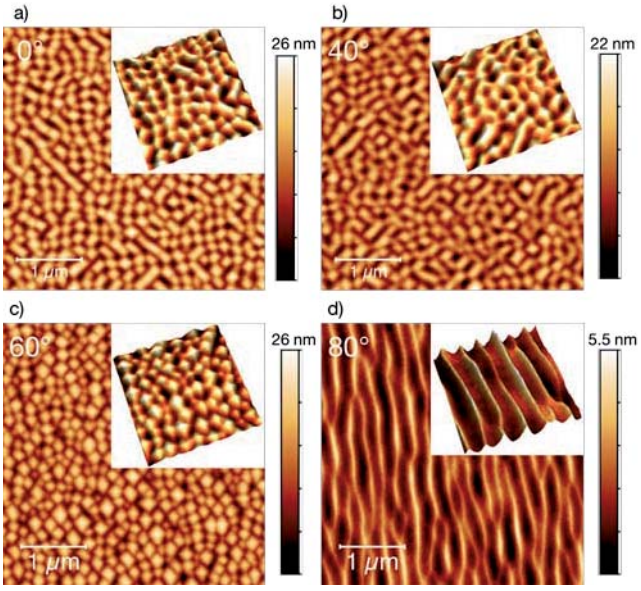

Figure 1: Atomic force microscopy (AFM) images of crystalline patterns on Ge(001) surface induced by 1 keV Ar^+ irradiation with a fluence of $1x10^{18}$ cm^{-2} at 350°C and incidence angles of a) 0°, b) 40°, c) 60°, and d) 80°, respectively. The insets show 3D zooms of the AFM images. A transition from pit to mound and finally to ripple patterns with incidence angles is observed.

3. REFERENCES

[1] A. Keller and S. Facsko, Materials 2010, Vol. 3, Pages 4811-4841 **3**, 4811 (2010).

[2] X. Ou, A. Keller, M. Helm, J. Fassbender, and S. Facsko, Phys. Rev. Lett. **111**, 016101 (2013).

[3] X. Ou and S. Facsko, Nucl. Instr. Meth. B **341**, 13 (2014).

* Corresponding author e-mail address: s.facsko@hzdr.de

SELF-ORGANIZED NANOCONE FORMATION ON ION-BOMBARDED InP SURFACES

Hubert Gnaser[1,2,*], *Detlef Kramczynski*[1], *and Tobias Radny*[1]

[1] Fachbereich Physik and Landesforschungszentrum OPTIMAS, Technische Universität Kaiserslautern, 67663 Kaiserslautern, Germany
[2] Institut für Oberflächen- und Schichtanalytik GmbH (IFOS), Trippstadter Str. 120, 67663 Kaiserslautern, Germany

Surfaces of InP(100) were bombarded by Ar^+ ions with energies of 1.5–3 keV under normal incidence. The total accumulated ion fluence Φ the samples were exposed to was varied from 1×10^{17} cm^{-2} to 3×10^{18} cm^{-2} while ion fluxes f of roughly $(0.1–2)\times10^{14}$ cm^{-2} s^{-1} were used. The surface morphology resulting from these ion irradiations was examined by atomic force microscopy (AFM) and scanning electron microscopy (SEM). For a specific range of ion fluxes and fluences, regular closely-spaced nanocone arrays are found to form, with typical heights and diameters of some 10 nm (Fig. 1).

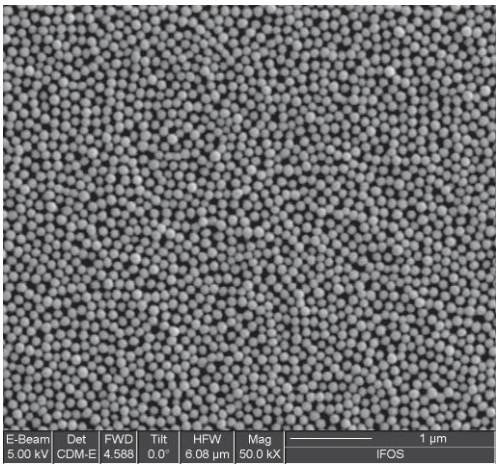

Figure 1. SEM image of an InP surface bombarded by 2.1 keV Ar^+ ions. Ion fluence $\Phi = 1\times10^{18}$ ions cm^{-2} and ion flux $f = 1.5\times10^{14}$ cm^{-2} s^{-1}.

These nanocones exhibit no long-range ordering but their feature sizes such as height, diameter, and spacing show a distinct dependence on the fluence and the flux of the bombarding ions. As a function of the ion fluence, the mean radius r, height h, and spacing l of the cones can be fitted by power-law dependences: $r \propto \Phi^{0.40}$, $h \propto \Phi^{0.48}$, and $l \propto \Phi^{0.19}$ [1]. In terms of the ion flux, there appears to exist a distinct threshold: below $f \sim 1.1\times10^{14}$ cm^{-2} s^{-1} no regular arrays of nanocones evolve; rather, singular cones are observed which show a considerable variation in size.

Around their outer peripheries, individual nanocones commonly exhibit rather distinct protrusions (Fig. 2). The inspection of the initial stages of their formation indicates that the growth of adatom islands, first on the pristine surface and later on previously form islands, may lead to these 3D nanostructures. This finding implies that surface diffusion processes of adatoms might constitute an important mechanism in the evolution of the observed surface topography.

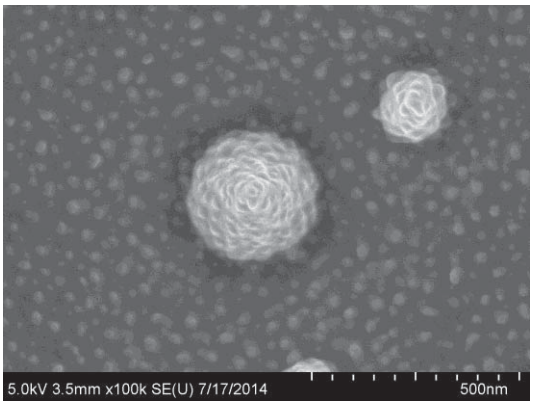

Figure 2. SEM image of individual nanocones on an InP surface bombarded by 2.1 keV Ar^+ ions. The ion flux was $f \sim 1.0\times10^{14}$ cm^{-2} s^{-1} and the fluence $\Phi \sim 1.0\times10^{18}$ cm^{-2}.

In order to determine possible local compositional changes in these nanostructures induced by ion impact, selected samples were prepared for atom probe tomography (APT) [2]. The results indicate that APT can provide analytical information on the composition of *individual* InP nanocones evolving under ion bombardment. By means of 3D APT data their surface regions could be examined with atomic spatial resolution. At the InP surface, the values of the In/P concentration ratio are distinctly higher over a distance of ~1 nm and amount to 1.3–1.8.

Acknowledgments

The authors are grateful to S. Wolff for recording the SEM images. Financial support from the Deutsche Forschungsgemeinschaft (DFG Grant GN18/25-1) is acknowledged.

References

[1] T. Radny, H. Gnaser, Nanoscale Res. Lett. **9**, 403 (2014).
[2] B. Gault, M.P. Moody, J.M. Cairney, S.P. Ringer, *Atom Probe Microscopy,* Springer, New York, 2012.

* Corresponding author e-mail address: gnaser@rhrk.uni-kl.de

CREATING NANOPOROUS GRAPHENE WITH SWIFT HEAVY IONS

E. H. Åhlgren[1,*], *A. A. Leino*[1], *O. Ochedowski*[2], *A. V. Krasheninnikov*[3], *F. Djurabekova*[1], *K. Nordlund*[1], *J. Kotakoski*[4], *M. Schleberger*[2]

[1] Department of Physics, University of Helsinki, P.O. Box 43, 00014 Helsinki, Finland
[2] Fakultät für Physik, Universität Duisburg-Essen, 47048 Duisburg, Germany
[3] Department of Applied Physics, Aalto University, P.O. Box 1100, 00076 Espoo, Finland
[4] Department of Physics, University of Vienna, Boltzmanngasse 5, 1090 Vienna, Austria

1. INTRODUCTION

Controllable modification of nanoscale materials can be achieved by irradiating the sample with energetic ions. Swift heavy ions (energy in the MeV range) on graphene have been studied only for a short time in a few experimental studies [1, 2]. We present results on highly controllable defect production in suspended single layer graphene samples with swift heavy ions. The study comprises of an experimental ion irradiation study with Raman spectroscopy analysis, as well as simulation results with two temperature molecular dynamics model, including coupled subsystems for the ions and the electrons. We also present density functional theory calculations of the specific electronic heat capacity for graphene with different chemical potentials.

Controllable modification of the atomic structure of graphene opens a way for patterning suspended samples for application purposes, such as creating porous graphene membranes for highly sensitive sensors and filters.

2. RESULTS

Raman mapping of freestanding graphene after irradiation with swift heavy ions with different ion types and energies shows an increase in the defect size for increasing stopping power of the ion. The stopping power depends on the ion and its energy, describing the amount of energy deposited to the target. The same trend is also seen in the simulations, where the high energy irradiation creates cylindrical defects in the membrane, see Figure 1. The diameter of the pore vary from few nm's up to hundreds of nm's. The diameter of the defects can be controlled precisely with the stopping power of the ion. By comparing the experimental and simulation results we also discuss the electronic thermal conductivity of graphene, suggesting a value in the range of 450 $\mathrm{Wm^{-1}K^{-1}}$.

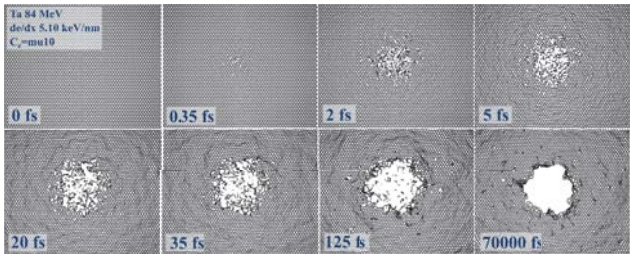

Figure 1: Visualization of a pore evolution simulated with two temperature molecular dynamics. The energy is deposited to graphene at the beginning of the simulation. Top view is presented after irradiation with 84 MeV Ta, corresponding to a stopping power of 5.10 keV/layer, at different simulation times. The final diameter of the pore is about 60 Å corresponding to about 4 000 missing carbon atoms.

3. REFERENCES

[1] S. Akcöltekin , H. Bukowska , T. Peters, O. Osmani, I. Monnet, I. Alzaher, B. Ban d'Etat, H. Lebius, M. Schleberger, Appl. Phys. Lett. **98**, 103103 (2011).

[2] O. Ochedowski, S. Akcltekin, B. Ban d'Etat, H. Lebius, M. Schleberger, Nucl. Inst. and Meth. in Phys. Res. B **314**, 18 (2013).

*Corresponding author e-mail address: ahlgren.harriet@gmail.com

HIGHLY CHARGED ION INDUCED MODIFICATIONS OF GRAPHENE ON DIFFERENT SUBSTRATES

R. Kozubek[1,*], *J. Hopster*[1], *P. Ernst*[1], *and M. Schleberger*[1]

[1] Fakultät für Physik and CENIDE, Universität Duisburg-Essen, D-47048 Duisburg, Germany

1. INTRODUCTION

Slow highly charged ions (HCI) have proven to be a powerful tool for surface modification on the nanoscale. The potential energy of such a HCI, i.e. the sum of the ionisation energies of all stripped electrons, is deposited in a very localized and limited volume of only a few nm^3 via electronic transitions, which leads to a strong excitation of the electronic system. As a result, the surface of solids as well as two dimensional materials experience drastic topographical changes, e.g. structural or chemical modifications. In the case of graphene, ion beam irradiation has been limited either to singly charged ions with kinetic energies in the keV regime[1] or to swift heavy ions in the MeV - GeV regime[2]. Recently, we reported about damage in single layer graphene created by HCI irradiation, which was investigated as function of E_{pot} and E_{kin} of the ions[3]. One fingerprintöf HCI induced defects is the regions of enhanced friction without topographical changes, which could be attributed to a chemical modification. This could present a promising candidate to modify the electronic properties for further applications.

2. IRRADIATION OF GRAPHENE

In this contribution we present experimental results of the interaction of HCI with graphene. To investigate a possible influence of the underlying material on the defect formation, monolayers graphene were exfoliated on four different substrates. Because different substrates lead to different doping of the graphene, TiO_2 was used for comparison with most widely used SiO_2. As the defects in graphene could arise from mechanisms in the substrate, we choose CaF_2, which is a well known system, that shows hillocks after HCI impact. Furthermore, we have used a prepatterned SiO_2 substrate, which allows us to investigate suspended graphene. The samples were irradiated with Xe ions with charge states up to $q = 40+$ at a kinetic energy of 260 keV under perpendicular incidence with respect to the graphene. The surface was investigated afterwards using an atomic force microscope in friction force mode under ambient conditions. The obtained results will be presented and discussed at the conference.

3. REFERENCES

[1] S. Standop, O. Lehtinen, C. Herbig, G. Lewes-Malandrakis, F. Craes, J. Kotakoski, T. Michely, A. V. Krasheninnikov and C. Busse, Nano Letters **13**, 1948 (2013).

[2] O. Ochedowski, B. Kleine Bussmann, B. Ban D'Etat, H. Lebius and M. Schleberger, Appl. Phys. Lett. **102**, 152103 (2013).

[3] J. Hopster, R. Kozubek, B. Ban-d'Etat, S. Guillous, H. Lebius and M. Schleberger , 2D Materials **1**, 011011 (2014).

*Corresponding author e-mail address: roland.kozubek@uni-due.de

Reverse Epitaxy on Elemental Semiconductors

M. Engler[1,2*], *T. Michely*[2], *and S. Facsko*[1]

[1] Institute for Ion Beam Physics and Materials Research, Helmholtz-Zentrum Dresden-Rossendorf, Dresden, Germany
[2] II. Physikalisches Institut, Universität zu Köln, Cologne, Germany

1. INTRODUCTION

Self-organized pattern formation during ion beam erosion can produce a variety of periodic patterns. Depending on the substrate and the irradiation conditions ripples, dots, holes or checkerboard patterns have been observed [1]. Pattern formation by low energy ion beam irradiation at low temperature, where the semiconductor surface is amorphized has been studied in detail in the last decades.

Low energy ion beam irradiation performed above the dynamic recrystallization temperature prevents the amorphization of the semiconductor surface. Above this transition temperature, the diffusion of adatoms and vacancies across step edges is hindered by an additional potential barrier, the Ehrlich-Schwoebel barrier. This barrier induces an effective destabilizing surface current during ion beam irradiation. This instability induces pattern formation even at conditions leading to a smooth surface below the transition temperature.

This mechanism, termed reverse epitaxy [2], allows the creation of novel types of surface patterns aligned to certain crystallographic directions of the irradiated surface.

2. PATTERNS FORMED

In this contribution we will present different types of patterns on elemental semiconductor surfaces and how it can be changeds by choosing the surface orientation and the irradiation conditions. For example, the pattern changes qualitatively on Si(100) under 2 keV Kr ion irradiation (Figures 1 and 2) with the ion fluence. Furthermore the pattern symmetry is determined by the symmetry of the irradiated surface. For Si(100) the ridges in the high fluence case are aligned to the [010] and [001] directions, whereas on Si(110) (Figure 3) the pattern is symmetric to the $[1\bar{1}0]$ and [001] directions.

3. REFERENCES

[1] Chan, Wai Lun, and Eric Chason. J. Appl. Phys. 101 (2007): 121301
[2] Ou, Xin, Adrian Keller, Manfred Helm, Jürgen Fassbender, and Stefan Facsko. Phys. Rev. Lett. 111 (2013): 016101

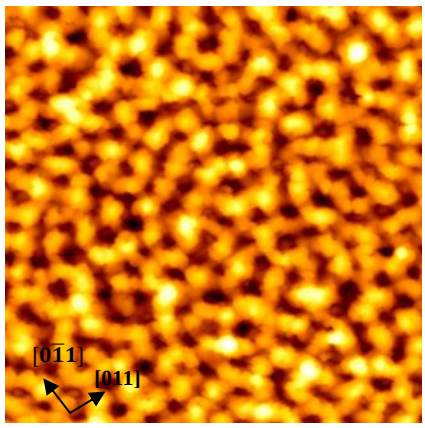

Figure 1 1.4µm STM image of Si(100) after 2keV Kr irradiation at 430°C, fluence 4.7×10^{17} ions/cm^2, z-scale 16nm

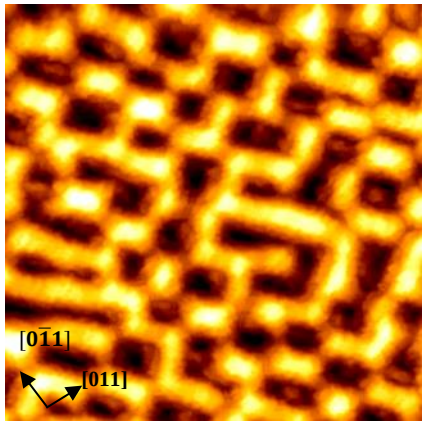

Figure 2 1.4µm STM image of Si(100) after 2keV Kr irradiation at 430°C, fluence 2.5×10^{18} ions/cm^2, z-scale 24nm

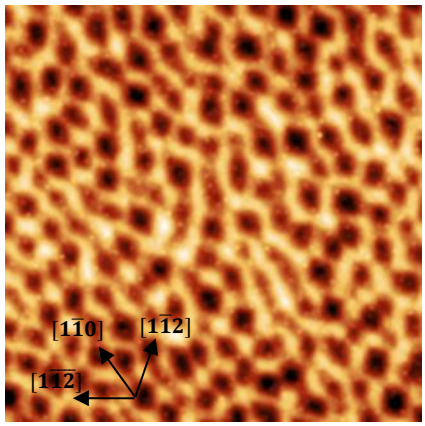

Figure 3 5µm AFM image of Si(110) after 500eV Ar irradiation at 460°C, fluence 5×10^{18} ions/cm^2, z-scale 40nm

* Corresponding author e-mail address: m.engler@hzdr.de

Platform for the nanoscale study and characterization of ion implantation

C. Bourin[1,*], B. Ban D'Etat[1], A. Benyagoub[1], A. Cassimi[1], A. Delobbe[2], C. Feierstein[1], E. Giglio[1], S. Girard[1], C. Grygiel[1], A. Houel[2], H. Lebius[1], A. Mery[1], I. Monnet[1], J.-M. Ramillon[1], J. Rangama[1], F. Ropars[1], E. Verzeroli[2], M. Vitteau[2], and S. Guillous[1]

[1] Centre de Recherche sur les Ions, les Matériaux et la Photonique, CIMAP (CEA /CNRS /ENSICAEN /Université de Caen Normandie)
[2] Orsay Physics (Tescan-Orsay Holding)

1. INTRODUCTION

Localized ion implantation is paramount for research and development in the fields of nanoscience and nanotechnologies. It is also widely used in microelectronics, nanophotonics, spintronics, and in the elaboration of nanomaterials by modifying the electrical, optical, magnetic and chemical properties of matter on the nanoscale. The most promising technique for localized ion implantation is the Focused Ion Beam (FIB) technology as it does not require time-consuming lithography techniques.
Recent developments in FIB technology aimed to improve performances by reducing the beam size or increasing the beam current. A lot of work has also been put into making more ions available, such as non-contaminating ion beams (noble gases) or reactive ions for analysis (Cs, O).

In the PELIICAEN project (Plateforme pour l'Etude de l'Implantation Ionique Caractérisée et Analysée à l'Echelle Nanométrique) we offer an original solution, by combining the known techniques of FIB and ECRIS sources, to generate localized multiply charged ion beams with a greater range of possible ions and implantation depths. This tool will open up new avenues for nanosciences and nanotechnologies by enabling doping / machining of surfaces up to depths of a few hundred nanometers according to a predefined nanostructure with multiply charged ions of varying types, as well as allow in-situ characterization of the sample surface.

2. EXPERIMENTAL SETUP

The experimental setup includes an e-Clipse SEM column, and a Cobra FIB column from Orsay-Physics. The Ga source originally present on the Cobra FIB column is replaced with one of the ARIBE (CIMAP-GANIL) beam lines to use multiply charged ions.
Imaging while using the FIB or SEM columns is done with an Orsay-Physics secondary electron detector. This enables real-time control of the surface machining.
Present in the same UHV chamber is a SPECS Curlew AFM/STM allowing in-situ analysis of the surface modifications.
All the equipment is located in an ultra-high vacuum chamber ($<10^{-9}$ mbar) and all experiments are performed at room temperature.

3. FUTUR DEVELOPMENTS

PELIICAEN was created to enable future evolution of the tool. For example, adding a mass spectrometer to the UHV chamber would allow SIMS measurements for a precise and localized chemical analysis of the surface as well as enabling us to study the sputtering yield of multiply charged ions.

4. PROJECT PARTNERS

The PELIICAEN project was financed by the French research agency (ANR) in the P2N 2012 program (ANR-12-NANO-008) and includes the CEA–CIMAP, who bring their expertise of ion-matter interactions, and Orsay-Physics, a world leader in development and sales of FIB and SEM columns.

5. COMMUNICATION

The communication will focus on the experimental setup and the available tools as well as the first results obtained.

6. ACCESS TO PELIICAEN

PELIICAEN is located in CAEN in CIMAP-GANIL and is open to the scientific community. Experiment proposals can be submitted through the i-Pac committee of the Ciril platform.

* bourin@ganil.fr

ABSTRACTS

Tuesday 20th October 2015

Non-adiabatic effects in low-energy gas-surface interactions

Hermann Nienhaus[1,*]

[1] Faculty of Physics, University of Duisburg-Essen and Center of Nanointegration Duisburg-Essen (Cenide), Lotharstr. 1, 47048 Duisburg, Germany

1. ABSTRACT

Chemical reactions as well as low-energy impact of gas particles on metal surfaces transfer energies of a few eV per particle to the metal substrate. Such events are regularly described within the Born-Oppenheimer approximation ignoring any electronic excitations. However, the pertubation of the electronic system during gas-metal interactions can cause significant electronic excitations with lifetimes on the femtosecond timescale and energies in the lower eV range. Experimental evidence of such non-adiabatic processes is gained by detecting exoelectron emission into the vacuum, surface chemiluminescence or internal detection of hot hole or hot electron generation [1]. Exoelectron emission and chemiluminescence are weak phenomena due to radiation quenching and work functions of a few eV on metal surfaces. But the internal detection scheme is able to measure short-living hot charge carriers with high sensitivity. The method uses thin-film electronic devices with internal potential barriers as high-pass energy filters. Metal-semiconductor (Schottky) diodes are the most prominent examples. The principle of hot electron detection is schematically depicted in the energy-space diagram of the left panel in figure 1. It shows the Schottky barrier Φ_B and the edges of the conduction (CBM) and the valence band (VBM) in the semiconductor. The metal film thickness is the nanometer range of the mean free path of the ballistic charge carriers. Excited electrons can travel ballistically to the interface and surmount the barrier if their kinetic energy is larger than the barrier height, typically 0.5 eV. Eventually, they are detected as a *chemicurrent* in the diode. The right panel in figure 1 illustrates exemplary current traces for various reactions on metal surfaces. The transients reflect the chemical kinetics which is monitored under live conditions.

The non-adiabatic energy transfer occurs when electronic states are injected below the Fermi level such rapidly that the occupation of the states by resonant charge transfer is delayed. According to Zener's criterion [2] this happens more likely in cases of fast nuclear motion and of low coupling between gas particle and metal states. An empty state below the Fermi level may inject a hot hole into the band of occupied electronic metal states or can be filled either after Auger relaxation leading to an excited electron or by photon emission. For the oxidation of metals, Auger relaxation and hot hole injection can be distinguished by independent measurements of chemicurrents in *p*–type devices and of exoelectron detection [3].

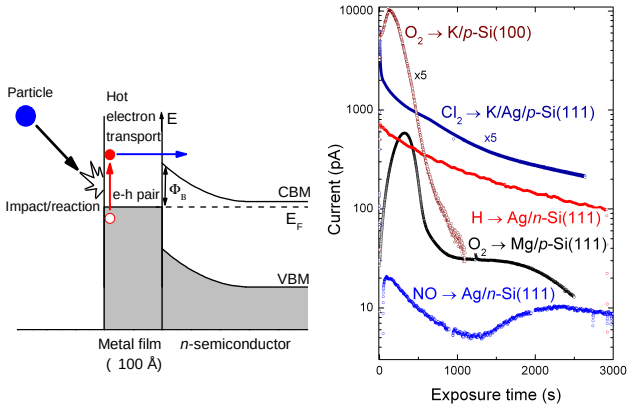

Figure 1: Left: principle of internal detection of impact or chemically induced hot electrons using a Schottky diode; right: collection of various chemicurrent traces showing the kinetics under live reaction conditions.

In addition, it is shown that rapid state injection does not necessarily imply the dissociation of the oxygen molecule as peroxide formation also leads to a significant excitation of the electronic system. The non-adiabatic process can be associated with a rapid intermolecular motion of the oxygen atoms during the reactive collision.

The presentation will further discuss the metal atom condensation on surfaces as an example for a non-adiabatic process which can be described in terms of electronic friction. The interaction of chlorine with potassium will be presented as a typical chemiluminescence reaction [4]. The Schottky diodes can be made insensitive to hot charge carriers by increasing the metal film thickness. Still, they work as efficient photodetectors. By use of K/Ag/Si-multilayer diodes the coupling between emitted photons and Ag surface plasmons leads to an enhanced photocurrent in the device at a typical Ag film thickness of around 50 nm. This is in excellent agreement with what is known from optical spectra recorded during the reaction.

2. REFERENCES

[1] H. Nienhaus, Surf. Sci. Rep. **45**, 3 (2002).

[2] C. Zener, Phys. Proc. R. Soc. Lond. A **137**, 696 (1932).

[3] D. Krix, H. Nienhaus, J. Chem. Phys. **141**, 074711 (2014); U. Hagemann, H. Nienhaus, New J. Phys. **16**, 113035 (2014).

[4] F. Becker, D. Krix, U. Hagemann, H. Nienhaus, J. Chem. Phys. **138**, 034710 (2013).

* Corresponding author e-mail address: hermann.nienhaus@uni-due.de

CHARGE EXCHANGE AND ENERGY LOSS OF SLOW HIGHLY CHARGED IONS IN GRAPHENE

R.A. Wilhelm[1,*], *E. Gruber*[2], *R. Kozubek*[3], *V. Smejkal*[2], *M. Schleberger*[3], *S. Facsko*[1], *and F. Aumayr*[2]

[1] Helmholtz-Zentrum Dresden-Rossendorf, Institute of Ion Beam Physics and Materials Research, Dresden, Germany, EU
[2] TU Wien, Institute of Applied Physics, Vienna, Austria, EU
[3] Universität Duisburg-Essen, Fakultät für Physik, Duisburg, Germany, EU

1. INTRODUCTION

Slow highly charged ion (HCI) interaction with surfaces was studied extensively in recent years and revealed many interesting aspects of the underlying processes [1]. Nanostructure formation by single HCI impact was successfully linked to defect mediated desorption or even surface melting due to HCI induced local electronic excitations. The neutralization dynamics of a slow ($v \ll v_0 = \alpha c$, α: fine structure constant, c: speed of light) HCI in front of a solid surface is well described by the classical-over-barrier model. However, not much is known about the neutralization below the surface, i.e. in the material. Below surface neutralization becomes important for normal incidence, because here the interaction time above the surface is not sufficient for neutralization and relaxation of the HCI.

2. RESULTS

We present results on charge exchange and energy loss measurements of slow highly charged Xe ions with charge states of $10 < Q < 35$ transmitted through freestanding single layer graphene as the thinnest and lightest solid target material there is. We find that the charge exchange is not bimodal as in case of transmission through 1 nm thick carbon nanomembranes [2], but only very large charge exchange is observed. We attribute this to (1) the availability of solely small impact parameters ($p < 1.5$ Å) in graphene as well as (2) very high mobilities of charge carriers and subsequently transfer of (at least) 20-30 electrons within less than 10 fs. Especially the second fact is surprising, because here the charge transfer is hardly conceivable as a sequential, but rather as a collective electron transfer process. For incident charge states $Q > 25$ we observe a saturation of charge exchange, i.e. the exit charge state distribution has a mean value $Q_{mean} \approx Q_{in} - 20$ (see fig. 1).
The contributions of above surface charge transfer and charge transfer during collision as well as energy loss and its dependence on the charge state and charge exchange will be discussed.

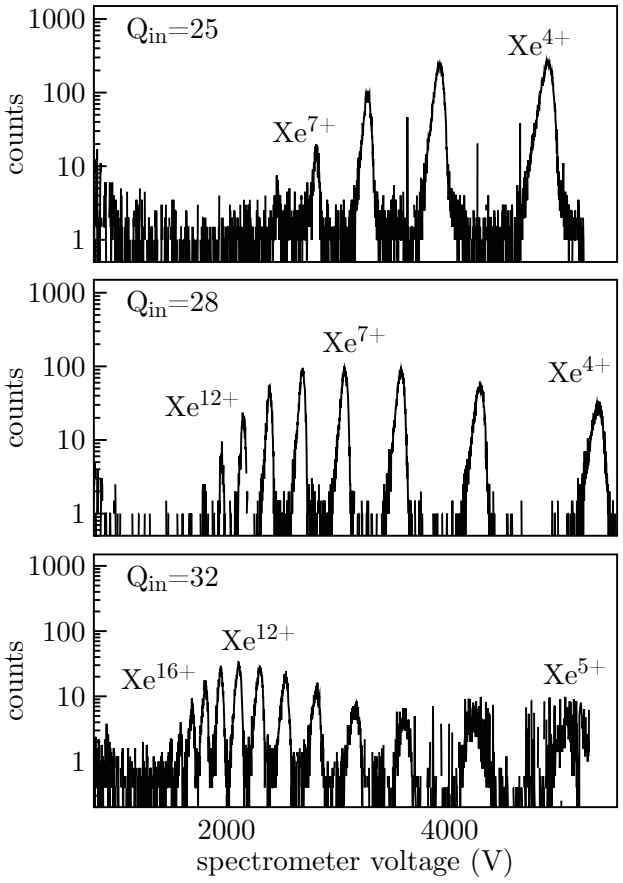

Figure 1: Charge state spectra of 4.4 keV$\times Q_{in}$ Xenon ions transmitted through a single layer of graphene.

3. REFERENCES

[1] Aumayr, F., Facsko, S., El-Said, A. S., Trautmann, C., Schleberger, M. Single ion induced surface nanostructures: a comparison between slow highly charged and swift heavy ions. *J. Phys. Condens. Matter* **23**, 393001 (2011).

[2] Wilhelm, R. A., Gruber, E., Ritter, R., Heller, R., Facsko, S., Aumayr, F. Charge Exchange and Energy Loss of Slow Highly Charged Ions in 1 nm Thick Carbon Nanomembranes. *Phys. Rev. Lett.* **112**, 153201 (2014).

*Corresponding author e-mail address: r.wilhelm@hzdr.de

ENERGY LOSS IN GAS-SURFACE DYNAMICS: ELECTRON-HOLE PAIR AND PHONON EXCITATIONS UPON ADSORBATE RELAXATION

D. Novko[1,*], *M. Blanco-Rey*[1,2], *J. I. Juaristi*[1,2,3], *and M. Alducin*[1,3]

[1] Donostia International Physics Center (DIPC), Paseo Manuel de Lardizabal 4, 20018 Donostia-San Sebastián, Spain
[2] Departamento de Física de Materiales, Facultad de Químicas UPV/EHU, Apartado 1072, 20080 Donostia-San Sebastián, Spain
[3] Centro de Física de Materiales CFM/MPC (CSIC-UPV/EHU), Paseo Manuel de Lardizabal 5, 20018 Donostia-San Sebastián, Spain

1. INTRODUCTION

To illustrate the importance of the energy transfer to electron-hole (e-h) pair and phonon excitations in the gas/surface reactions, we will discuss three distinct cases: (i) hot H atom relaxation on Pd(100), (ii) hot N atom on Ag(111) and (iii) the adsorption of N_2 on Fe(110). The accurate description of these two energy dissipation mechanisms constitutes an important challenge in present *ab initio* gas-surface dynamics simulations. This issue was reasonably tackled in a recent study on the relaxation of the transient hot H atoms formed from the dissociation of H_2 on Pd(100) [1]. In this study they used *ab initio* molecular dynamics that incorporates a friction force to account for the energy losses caused by excitations of e-h pairs (AIMDEF). This friction force is calculated on-the-fly within the local density friction approximation (LDFA) [2], which requires the knowledge at each integration step of the *bare surface* electron density. The latter becomes a complicated task when one is interested in allowing the surface atoms to move. Thus, to overcome this problem, we have developed a new method, based on LDFA, that accounts for the changes in the density caused by surface atom displacements on-the-fly.

2. RESULTS

The results of our simulations show the mutual game of the e-h pair and phonon excitations for the mentioned systems and the importance of going beyond the frozen surface density for the systems with large surface atom displacement, i.e. the N/Ag(111) and N_2/Fe(110) cases. For the case of H/Pd(111) the excitation of e-h pairs is the main channel for energy dissipation (see Fig.1), while for the other two cases, it is shown that the e-h pair excitation are still important although the phonon excitations are the dominant loss mechanism (for the N/Ag(111) case see Fig.2).

3. ACKNOWLEDGMENT

This work has been supported in part by the Basque Departamento de Educación, Universidades e Investigación, the University of the Basque Country UPV/EHU (Grant No. IT-756-13) and the Spanish Ministerio de Economía y Competitividad (Grant No. FIS2013-48286-C02-02-P). The authors thankfully acknowledge the computer resources, technical expertise and assistance provided by the Red Española de Supercomputación and by the DIPC computing center.

4. REFERENCES

[1] M. Blanco-Rey *et al.*, Phys. Rev. Lett. **112**, 103203 (2014).

[2] J. I. Juaristi *et al.*, Phys. Rev. Lett. **100**, 116102 (2008).

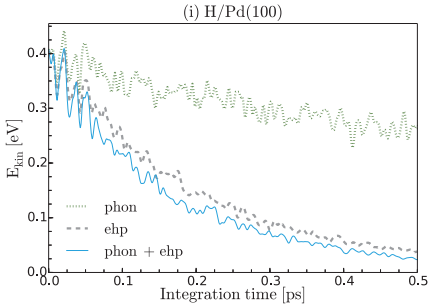

Figure 1: Kinetic energy of the H atom on Pd(100) as a function of integration time. The green dotted (grey dashed) line represents the simulation where only phonons (e-h pairs) are included, while the blue line represents the data where both loss channels are included.

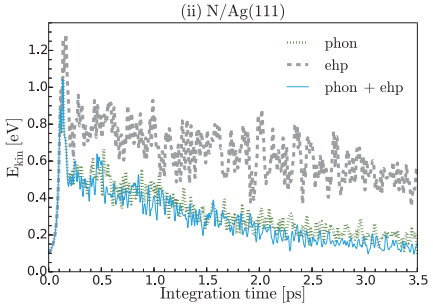

Figure 2: Kinetic energy of the N atom on Ag(111) as a function of integration time. Line colors same as in Fig. 1.

Inelastic Losses in Low Energy Ion Scattering

Barbara Bruckner, Dietmar Roth, Stefan Gruber, and Peter Bauer

JKU Linz, Dept. Experimental Physics, Atomic Physics and Surface Science, Linz, Austria.

1. LOW ENERGY ION SCATTERING

In a typical low energy ion scattering (LEIS) experiment, a target is bombarded with noble gas ions (He) with a primary energy E_0 of ~ 1–10 keV, at perpendicular incidence. Backscattered projectiles are detected at a scattering angle ϑ. The spectrum of positively charged ions exhibits a surface peak due to backscattering from a surface atom in a single binary collision [1]. Therefore, these projectiles have transferred energy $\Delta E_{elast} = [1- k(M_1/M_2,\vartheta]\cdot E_0$, to the collision partner and ΔE_{inel} due to inelastic losses. In the following we will further explore these inelastic losses.

2. INELASTIC LOSSES

2.1. Electronic stopping

In the LEIS regime, the stopping power $S = dE/dx$ in a free electron gas (FEG) is expected to be velocity proportional. For noble metals, band structure effects have been observed [2]; similar features were discovered for He even in materials, where for protons $S \propto v$, e.g., in Al or Ta [3].

2.2. Surface Peaks

While ΔE_{elast} is easy to evaluate quantitatively, ΔE_{inel} depends very much on the electronic properties of the collision partners and on their minimum distance in the backscattering collision (see Fig.1). Since for He, typical stopping power values are 3-15 eV/Å, ΔE_{inel} cannot be attributed only to dE/dx, but either to enhanced excitation of electron-hole pairs or to electronic excitations in the close collisions.

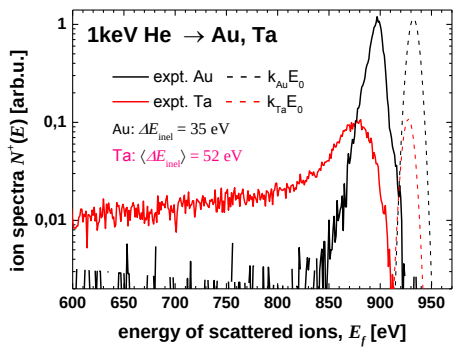

Figure 1: energy spectra of 1 keV He^+ ions, scattered from Au and from Ta by $\vartheta = 135°$ and detected as He^+. Both spectra were obtained for the same primary charge.

2.3. Reionization

One specific energy dissipation channel is reionization: there, the He ground state is promoted due to interaction with bound levels at the scattering partner such that it becomes resonant with the valence/conduction band. In such a collision, He^0 can be (re)ionized and He^+ neutralized in the backscattering collision. These processes require a minimum distance in the close collision, r_{min}, smaller than a critical distance $R_{crit}(E,\vartheta)$ and therefore require a certain threshold energy E_{th} for a given ϑ [1]. For He – Ta and He – Au, $E_{th} \approx$ 350eV and 1200eV, respectively. This is why in Fig. 1 the N^+ spectrum He - Au only consists of "survivals" (i.e., no charge exchange), leading to a surface peak corresponding to backscattering from the outer surface. It is shifted with respect to $k_{Au}\cdot E_0$ (due to excitation of electron hole pairs). Due to the low threshold for He – Ta, the corresponding ion spectrum in Fig. 1 exhibits a much lower ion yield in the surface peak (due to RN) and a considerably higher mean energy loss and a larger peak width (due to RI). Also the Ta 4f electrons that are close to being resonant with the He 1s level, may play an important role in the interaction He – Ta.

2.4. Electronic stopping in solids

At energies close to E_{th}, resonant processes are always related to large angle scattering. At much higher energies, however, they are possible at much smaller scattering angles and consequently occur along the projectile's path. In this contribution we discuss the possible contribution of charge exchange in atomic collisions to electronic stopping of H and He in metals, semiconductors and insulators at very low velocities.

3. REFERENCES

[1] H.H. Brongersma, M. Draxler, M. de Ridder, P. Bauer, Surf. Sci. Rep. **62**, 63 (2007).

[2] J. E. Valdés, J. C. Eckardt, G. H. Lantschner, and N. R. Arista, Phys. Rev. A49, 1083 (1994); S. N. Markin, D. Primetzhofer, M. Spitz, and P. Bauer, Phys. Rev. **B80**, 205105 (2009).

[3] D. Primetzhofer, S. Rund, D. Roth, D. Goebl, and P. Bauer, Phys. Rev. Lett. 107, 163201 (2011); B. Bruckner, Master thesis, JKU University Linz, 2015.

* peter.bauer@jku.at

PROGRESS IN HEAVY-ION STOPPING

P. Sigmund

Department of Physics, Chemistry and Pharmacy, University of Southern Denmark, DK-5230 Odense M, Denmark

This contribution is a brief summary of some highlights in a rather extensive research program on charge states and energy loss of heavy ions ($Z_1 \gg 1$) interacting with bulk matter at projectile speeds around and above the Bohr velocity. Several coauthors have been involved over the years, in particular Andreas Schinner (Linz), as well as Nestor Arista (Bariloche), Lev Glazov (Tomsk), Valery Kuzmin (Dubna), Orkhan Osmani (Duisburg), Annu Sharma (Kurukshetra) and my students André Fettouhi and Mia Weng. With the exception of the most recent progress, many details may be found in two monographs [1, 2] as well as original references quoted there.

A most useful tool is binary stopping theory, developed with A. Schinner and implemented in the PASS code, which provides a reliable connection between the ion charge and the stopping cross section [3]. Combined with a relation for the mean equilibrium charge versus beam velocity we have found reliable estimates of the mean energy loss for a large number of ion-target combinations.

The so-called effective charge, still a popular tool in the analysis of experimental stopping data, has been shown to be related to the transition between Bethe and Bohr stopping theory and is only remotely related to the ion charge [4].

While there exist reliable tabulations and empirical interpolation formulae for equilibrium charges in gaseous and solid media, theoretical understanding of this aspect is still more qualitative than quantitative, except for a small number of specific systems [2]. We have revisited the wellknown models by N. Bohr and Lamb for estimating equilibrium charges in gases on the basis of Clementi wave functions and binding energies, respectively, as well as Thomas-Fermi-type electron densities. In this context we have concerns about the validity of the well-known Brandt-Kitagawa scheme [5]. Recent work [6, 7] has elucidated several reasons why the so-called velocity-proportional regime in the stopping cross section cannot be expected to extend up to $v \sim v_{\rm Bohr} Z_1^{2/3}$, as is well-known from numerous experiments. Conversely, a reciprocity rule for low-energy electronic stopping cross sections has been found to be a useful tool in estimating stopping cross sections for $Z_1 \rightarrow Z_2$ from known cross sections for $Z_2 \rightarrow Z_1$ [8].

Binary theory has also been applied to estimate fluctuations in energy loss (straggling). We distinguish between linear straggling, accounting for all effects entering stopping cross sections such as shell and Barkas-Andersen correction as well as projectile excitation and screening [9], and correlation effects [10] which are classified as bunching – accounting for the proximity of electrons in atoms – and packing – accounting for the proximity of atoms in a molecule or a solid.

A particularly intriguing topic is the quantification of charge-exchange straggling. While formalisms to estimate charge-exchange straggling have been available for a long time, obtaining quatitative estimates has been hampered by the absence of a complete set of pertinent cross sections for electron capture and loss for most ion-target combinations. A recently-developed scheme [11] provides an expression in terms of transients in the development of charge fractions, which we have extracted from the ETACHA code [12] but which also could be extracted from measured transients. Application of this scheme to straggling in gas targets [13] indicates strong variations in the significance of various contributions to straggling. Moreover, a pronounced double-peak structure has been predicted in charge-exchange straggling.

E-mail: sigmund@sdu.dk

1. REFERENCES

[1] P. Sigmund, *Particle Penetration and Radiation Effects*, Springer 2006.

[2] P. Sigmund, *Particle Penetration and Radiation Effects Volume 2*, Springer 2014.

[3] P. Sigmund and A. Schinner, EPJD **12**, 425 (2000).

[4] P. Sigmund and A. Schinner, NIMB **174**, 535 (2001).

[5] W. Brandt and M. Kitagawa, Phys. Rev. B **25**, 5631 (1982).

[6] A. F. Lifschitz and N. R. Arista, NIMB **316**, 245 (2013).

[7] P. . Sigmund and A. . Schinner, NIMB **342**, 292 (2015).

[8] P. Sigmund, EPJD **47**, 45 (2008).

[9] P. Sigmund and A. Schinner, NIMB **195**, 64 (2002).

[10] P. Sigmund and A. Schinner, EPJD **58**, 105 (2010).

[11] P. Sigmund, O. Osmani, and A. Schinner, NIMB **269**, 804 (2011).

[12] J. P. Rozet, C. Stephan, and D. Vernhet, NIMB **107**, 67 (1996).

[13] C. Vockenhuber, et al., EPJD **67**, 145 (2013).

Electron promotion effects in the interaction of slow ions with Al surfaces

P. Riccardi[1,*], *A. Sindona*[1] *R.A. Baragiola*[2], *and C.A. Dukes*[2]

[1] Dipartimento di Fisica, Università della Calabria and INFN – Gruppo collegato di Cosenza- Via P. Bucci cubo 33C, 87036 Rende, Cosenza, Italy

[2] Engineering Physics, University of Virginia, Charlottesville, Virginia 22904, USA

1. ABSTRACT

Electron promotion in binary atomic collisions is one of the main processes for electron excitation and electronic stopping for slow ions travelling in solids. Despite of decades of investigation, it is currently the matter of an interesting debate [1-3]. Electron emission is an outcome of the inelastic processes that can be studied in detail. Ion-induced electron emission processes are grouped into the two main categories of potential electron emission (PEE) and kinetic electron emission (KEE), due respectively to the transfer to the solid of the potential and the kinetic energy brought by the incoming particle. In many cases electronic energy loss and electron emission are strictly related and KEE yields γ (number of emitted electrons per incident ion) are found to be proportional to the electronic stopping power for slow light ions . Moreover, impact parameter dependent effects, such as electron promotion in close atomic encounters, occur at impact energies above a threshold that is peculiar to the collision system and often promote electrons above the vacuum level, resulting in electron emission that produces features in the energy distributions and in the yield curve of emitted electrons.

In this work, we present energy distribution and yields of electrons emitted in the interaction of slow singly charged ions (He, Ne, Na, Ar, Kr) with Al surfaces as a function of incident ion energy in the range 0.1-10 keV. For all these projectiles, electron promotion occurs in binary collisions with target atoms either of projectiles that have been neutralized in the interaction with the surface and of survived ions, as well as in binary collisions between recoiling target atoms. The role of each of these collisions in determining the behaviour of the total electron emission yields with incoming ion velocity will be discussed.

This work follows a recent paper [3]. The final processing of that paper and the preparation of this new one has been overshadowed by Raul Baragiolas's death on June 21st. In sorrow we dedicate this work to his memory.

REFERENCES

[1] D. Primetzhofer et al. Phys. Rev. Lett. 107 (2011) 163201

[2] M. Ahnsan Zeb et al. Nucl. Instr. Meth. Phys. Res. B 303 (2013) 59

[3] P. Riccardi, R.A. Baragiola, C.A. Dukes , Phys. Rev. B at press.

* Corresponding author e-mail address: pierfrancesco.riccardi@fis.unical.it

ELECTRONIC STOPPING POWER OF H AND HE IN A NARROW BAND GAP SEMICONDUCTOR

R. Ullah[1,*], *D. Roth*[2], *P. Bauer*[2], *D. Sánchez-Portal*[3,4], *and E. Artacho*[1,4,5,6]

[1] CIC nanoGUNE, Ave. Tolosa 76, 20018 Donostia-San Sebastián, Spain
[2] Institut für Experimentalphysik, Abteilung für Atom- und Oberflächenphysik, Johannes Kepler University Linz, Altenberger Straße 69, 4040 Linz, Austria
[3] Centro de Física de Materiales CSIC-UPV/EHU, Paseo Manuel de Lardizabal 5, 20018 Donostia-San Sebastián, Spain
[4] Donostia International Physics Center, Paseo Manuel de Lardizabal 4, 20018 Donostia-San Sebastián, Spain
[5] Theory of Condensed Matter, Cavendish Laboratory, University of Cambridge, Cambridge CB3 0HE, United Kingdom
[6] Basque Foundation for Science Ikerbasque, Bilbao, Spain

1. ABSTRACT

The electronic stopping power (ESP) is the energy lost per unit distance to electronic excitations by a charged projectile shooting through a material. The most successful quantitative approaches for the calculation of the ESP are limited to the homogeneous electron gas model of metals and do not take into account important features like core state excitations and band gaps in case of insulators and semiconductors. Relatively recently time-dependent density-functional theory (TD-DFT) based first-principles calculations [1, 2, 3, 4] have been performed for insulators and noble metals to explain the experimental observations [5, 6].

We investigate the ESP of H and He projectiles in Ge, a narrow band gap semiconductor with relatively low packing density. A systematic direction and impact parameter dependence of the electronic stopping power is studied along with its velocity threshold behavior, using time-evolving time-dependent density functional theory. The calculations are carried out in channeling conditions with different impact parameters and in different crystal directions, for projectile velocities ranging from 0.05 to 0.6 atomic units.

The ESP of He in Ge is measured in backscattering using a sputter cleaned Ge wafer relative to polycrystalline copper, by means of time-of-flight low-energy ion scattering (TOFLEIS) setup ACOLISSA. For Ge the information on the ESP for He ions was deduced from the corresponding information for Cu and evaluation of the heights of the backscattering spectra. In order to minimize the influence of systematic errors due to uncertainties in the scattering cross sections and of multiple scattering, the experimental spectra were compared to corresponding spectra obtained by Monte-Carlo simulations, analogously as described in Ref [7]. In these simulations the only adjustable parameter is the ESP in Ge, which is fixed such that the height ratios coincide.

A finite velocity threshold is observed both in the simulations and the experiment. The calculated ESP changes with crystal direction and impact parameter. The overall agreement between theory [8] and experiment [7] is reasonably satisfactory so as to allow us to use the simulations to learn more about the stopping process in this kind of systems

2. REFERENCES

[1] J. M. Pruneda, D. Sánchez-Portal, A. Arnau, J. I. Juaristi and E. Artacho, Phys. Rev. Lett. **99**, 235501 (2007).

[2] A. A. Correa, J. Kohanoff, E. Artacho, D. Sánchez-Portal and A. Caro, Phys. Rev. Lett. **108**, 213201 (2012).

[3] M. A. Zeb, J. Kohanoff, D. Sánchez-Portal, A. Arnau, J. I. Juaristi and E. Artacho, Phys. Rev. Lett. **108**, 225504 (2012).

[4] M. A. Zeb, J. Kohanoff, D. Sánchez-Portal and E. Artacho, Nucl. Instrum. Methods. B **303**, 59 (2013).

[5] S. N. Markin, D. Primetzhofer, and P. Bauer, Phys. Rev. Lett. **103**, 113201 (2009).

[6] S. N. Markin, D. Primetzhofer, M. Spitz, and P. Bauer, Phys. Rev. B **80**, 205105 (2009).

[7] D. Roth and D. Goebl and D. Primetzhofer and P. Bauer, Nucl. Instrum. Methods. B **317, Part A**, 61 (2013).

[8] R. Ullah, F. Corsetti, D. Sánchez-Portal, and E. Artacho, Phys. Rev. B **91**, 125203 (2015).

*Corresponding author e-mail address: r.ullah@nanogune.eu

Low-energy He^+ ion scattering spectroscopy; Recent topics in fundamentals and applications

T.T. Suzuki, O. Sakai, Y. Adachi, K. Watanabe, N. Saito, I. Sakaguchi, N. Ohashi, S. Hishita

National Institute for Materials Science, 1-1 Namiki, Tsukuba, Ibaraki 305-0044, JAPAN

1. Introduction

Low-energy He^+ ion scattering spectroscopy (He^+ LEIS) has been utilized for both analysis of the elemental composition and the atomic arrangement on various solid surfaces. In the present talk, I will present two topics from our recent studies on He^+ LEIS. The first topic is concerning fundamentals of He^+ LEIS, that is about the role of electron -spin in the He^+ ion-surface atom collision. More specifically, it is related to spin-orbit coupling in the collision. On the other hand, the second topic is related to application of He^+ LEIS, and it is about the surface analysis of ZnO doped with W for gas sensing applications. Both view points of fundamentals and applications are important to advance the understanding of He^+ LEIS.

2. Fundamentals; Spin-orbit coupling

We have demonstrated that spin-orbit coupling (SOC) plays an important role in He^+ ion-surface collisions. It is intuitively interpreted as the effect on the projectile electron spin of the magnetic field induced by the projectile angular motion around the target nucleus during the projectile–target binary collision (Biot-Savart law). In the present study, we further investigated SOC from both the experimental and theoretical approaches. In the experiment, electron-spin-polarized $^4He^+$ ion beam was projected onto the target surface, and the intensity of scattered He^+ ions was measured as a function of their kinetic energy. We found that the scattering angle θ dependence of the spin dependent scattering is remarkably different between the targets of the transition metal and the non-transition metal. This is explained from SOC in the collisional intermediate state, in which an electron of the target is transferred to the He^+ ion [1,2].

3. Applications; W-ZnO gas sensor

We have systematically investigated surface segregation of doped elements in metal oxides as a novel method to modify the surface of gas sensing materials. In the present talk, I will show our recent study on zinc oxide doped with tungsten.

We grew *c*-axis oriented ZnO films doped with W on α-Al_2O_3 substrates by pulsed laser deposition (PLD) [3]. The doping amounts of W in the targets were 0.05, 0.25, 1, and 4 mol%. We observed surface segregation of W by annealing at elevated temperature. We found that the W–ZnO surface terminates with an O-layer, and W is located in a substitutional site of Zn at the second surface layer as a consequence of segregation (Fig. 1) [3].

We further investigated gas sensing properties of W-ZnO (Fig .2). We observed that both sensitivity and response time of ZnO were improved by the W doping. Considering the structure analysis by He^+ LEIS, the W atom located at the ZnO surface may play a role in gas sensing by W-ZnO.

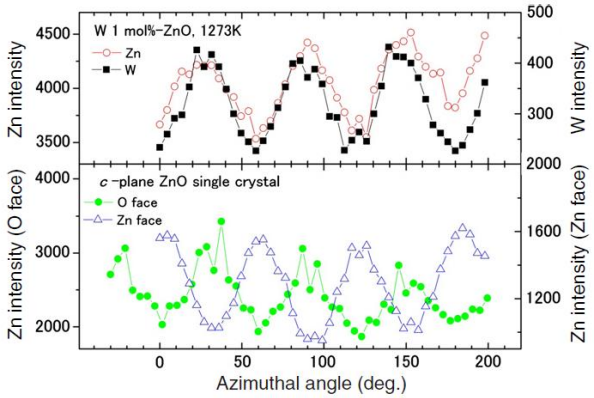

Fig. 1. Azimuthal angle dependence of the He^+ LEIS peak intensity of the W 1 mol%-ZnO and *c*-plane ZnO single crystal surfaces.

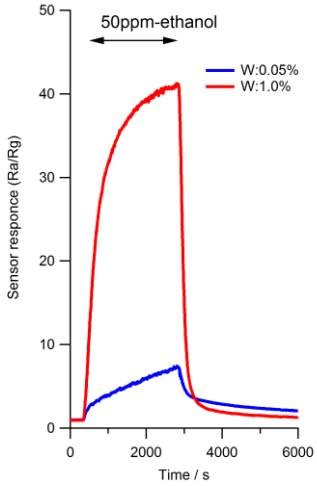

Fig. 2. Typical dynamic response of the W-ZnO film for 50-ppm C_2H_5OH in air.

[1] S. Ichinokura et al., Radiation Effects & Defects in Solids, 169 (2014) 1003.
[2] T.T. Suzuki et al., NIMB 354 (2015) 163.
[3] Y. Adachi et al., J. Ceram. Soc. Jpn. 122 (2014) 908.
[4] T.T. Suzuki et al., Surf. Sci. 625 (2014) 1.

* Corresponding author e-mail address: suzuki.taku@nims.go.jp

SURFACE SCATTERING IN THE PLASMONIC RESONANCES OF ULTRALOW ELECTRON DENSITY NANOSPHERES

R.Carmina Monreal

Departamento de Física Teórica de la Materia Condensada and Condensed Matter Physics Center (IFIMAC)
Universidad Autónoma de Madrid, E-28049 Madrid, Spain

Localized surface plasmon resonances (LSPRs) have recently been identified in extremely diluted electron systems obtained by doping semiconductor quantum dots. Here we investigate the role that different surface effects, namely electronic spill-out and diffuse surface scattering, play in the optical properties of these ultra-low electron density nanosystems. Diffuse scattering originates from imperfections or roughness at a microscopic scale on the surface. Using an electromagnetic theory that describes this mechanism in conjunction with a dielectric function including the quantum size effect, we find that the LSPRs show an oscillatory behavior both in position and width for large particles and a strong blueshift in energy and an increased width for smaller radii, consistent with recent experimental results for photodoped ZnO nanocrystals. We thus show that diffuse scattering at the particle surface can play an unexpectedly important role in determining the properties of the LSPRs in ultralow carrier density nanosystem.

* Corresponding author e-mail address: r.c.monreal@uam.es

PLASMARON FOOTPRINTS IN PHOTOEMISSION

*B. Hellsing**

Department of Physics, Gothenburg University, S-41296 Gothenburg, Sweden
Donostia International Physics Center, ES-20018 San Sebastián, Spain

In photoemission experiments, photo-electrons carry information of many-body interactions created by the photo-hole and by the escaping photo-electron itself. In the case of strong coupling between the photo-hole or induced density caused by the photo-electron, and plasmon excitations, the quasi particle picture breaks down and new loss peaks appear in the photoemission spectrum. The excitation formed by the photo-hole – plasmon interaction defines the *intrinsic plasmaron* and the photo-electron – plasmon interaction defines the *extrinsic plasmaron* [1].

For systems with a surface-state-band crossing the Fermi level, a plasmon localized at the surface and characterized by a sound-like dispersion, so-called Acoustic Surface Plasmon (ASP), has been predicted to exist [2, 3]. Later on Electron Energy Loss Spectroscopy experiments have confirmed the presence of the ASP mode at the Be(0001) surface in good agreement with calculations [4] and at noble metal surfaces [5] and graphene adsorbed on metal substrates [6].

In cases when surface localized quantum well states are formed, e.g. when atomic layers of alkali metals are adsorbed on a metal surface the possibility opens up to design ASP by varying the depth of the quantum well (type of alkali atoms) and the width of the quantum well (number of layers).

A challenge is to find out about the relative occurence of the *intrinsic* and *extrinsic* plasmarons from a photoemission experiment. I will show that for a surface system with ASP, the extrinsic plasmaron excitation channel can be traced by looking at the photon energy dependence of the photo-electron yield. Simple kinematics indicate an approximative inverse square root dependence, while the *intrinsic* plasmaron is not expected to depend on the photon energy. I will present results from an extension of a previous calculation on the system - a monolayer potassium adsorbed on graphite (p(2×2)-K/Graphite) [7].

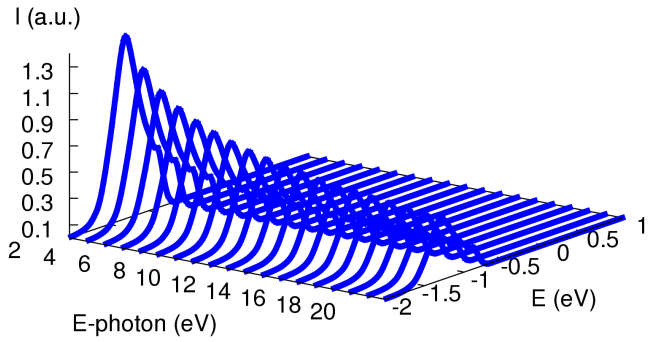

Figure 1: Photo-electron intensity in the $\bar{\Gamma}$-point as a function of photon energy and photo-electron energy vs Fermi level

1. REFERENCES

[1] B. Lundqvist, Phys. Kondens. Mat. **6**, 193 (1967); L. Hedin, B. I. Lundqvist, and S. Lundqvist, Solid State Commun. **5**, 237 (1967).

[2] V. M. Silkin, A. García-Lekue, J. M. Pitarke, E. V. Chulkov, E. Zaremba, and P. M. Echenique, Europhys. Lett. **66**, 260 (2004); V. M. Silkin, J. M. Pitarke, E. V. Chulkov, and P. M. Echenique, Phys. Rev. B **72**, 115435 (2005); J. M. Pitarke, V. M. Silkin, E. V. Chulkov, and P. M. Echenique, Rep. Prog. Phys. **70**, 1 (2007).

[3] V. M. Silkin, B. Hellsing, L. Walldén, P. M. Echenique, and E. V. Chulkov, Phys. Rev. B **81**, 113406 (2010).

[4] B. Diaconescu, K. Pohl, L. Vattuone, L. Savio, Ph. Hofmann, V. M. Silkin, J. M. Pitarke, E. V. Chulkov, P. M. Echenique, D. Farías, and M. Rocca, Nature (London) **448**, 57 (2007).

[5] S. J. Park and R. E. Palmer, Phys. Rev. Lett. **105**, 016801 (2010); K. Pohl, B. Diaconescu, G. Vercelli, L. Vattuone, V. M. Silkin, E. V. Chulkov, P. M. Echenique, and M. Rocca, EPL **90**, 57006 (2010); M. Jahn, M. Müller, M. Endlich, N. Neel, J. Kröger, V. Chis, and B. Hellsing, Phys. Rev. B **86**, 085453 (2012); L. Vattuone, M. Smerieri, T. Langer, C. Tegenkamp, H. Pfnür, V. M. Silkin, E. V. Chulkov, P. M. Echenique, and M. Rocca, Phys. Rev. Lett. **110**, 127405 (2013); J. Pischel et al., J. Phys. Chem. C **117**, 26964 (2013).

[6] T. Langer et al., New J. Phys. **13**, 053006 (2011); A. Politano et al., Phys. Rev. B **84**, 033401 (2011); A. Politano, et al., Phys. Rev. B **86**, 085420 (2012).

[7] V. Chis, V.M. Silkin, B. Hellsing, Phys. Rev. B **89**, 205429 (2014)

*Corresponding author e-mail address: hellsing@physics.gu.se

WHAT PROMOTES THE DESIRED SELF ASSEMBLY (DSA)?

S. T. Nakagawa and S. Sugita

Graduate School of Science, Okayama Univ. of Science, Japan.

1. OUTLINE

A low energy electron beam (EB) can let the self-interstitial atoms (SIA) cause the desired self-assembly (DSA) [1], *i.e.,* $\{311\}_{SIA}$ platelet in c-Si was produced. We have studied how an SIA migrates to form the platelet, making use of a molecular dynamic (MD) simulation to trace all the atoms and crystallographic analysis method (PM) method [2, 3] to analyze crystalline defects. In fact, we skipped the EB irradiation stage that produces SIAs. Instead, before MD some Frenkel pairs (FP) were randomly distributed in bulk, and reproduced the observed DSA [4]. Note that the total number of Si atoms was remained constant.

The PM segments the crystalline space into small cubic cells called pixel, to specify whether an atom locates at a stable, metastable, or unstable site. Note that the ratio of atoms located at stable sites (solid line in Fig.1) means the long-ranger-order (LRO) parameter. On the other hand, the platelet is made of SIAs located only at metastable sites, thus we focused the SIAs located at metastable sites (open c in Fig.1).

Because of the presence of FPs, the crystallinity of c-Si is once collapsed after the start of annealing. The crystalline to amorphous (CA) transition is shown as a solid line in Fig.1. In the mean time, atoms kicked out from original lattice sites migrate around. When the initial fraction of SIA is low, e.g. at 1 atomic %, cooperative and oscillatory movement was found in the ratio of metastable sites as shown in the open circles in Fig.1. However, no such global wavy motion was observed in cases including much higher FPs, as if a pinning effect occurred. Therefore, a proper concentration of SIAs would promote DSA due to more SIAs migrating toward metastable sites.

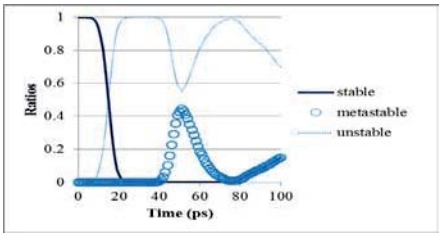

Figure 1 Time series of the atomic distribution at three kinds of sites, when the initial concentration of FP was 1 % and annealed at 1000 K.

2. DISCUSSIONS

2.1. Is the electron beam essential?

The irradiation of a target material causes many SIAs that play main role to promote self-ionization during annealing process. Takeda et al. first described the DSA procedure of the {311} platelet in a c-Si using 300 keV high Resolution Transmission Electron Microscopy when annealed at 723 K; DSA had two steps [1]; SI $\langle 2\bar{3}\bar{3} \rangle$ As agglomerated to form atomic rows along $\langle 0\bar{1}1 \rangle$ direction, then those rows aligned parallel along the direction of, which completed the $(311)_{SIA}$ platelet. Making use of MD for a case of low energy ion beam (IB), which was 1 keV self-irradiation [5], we proved that the same DSA was developed in c-Si. The orientation of atomic rows or the Miller indexes are identified by the PM method. The DSA process was the migration of SIAs to metastable sites expected by the PM. Whichever irradiation source of IB or EB was adopted, the DSA process could reach the same result. This was why we skipped the stage of SIA formation under EB irradiation.

2.2 Is there suitable concentration of SIAs for DSA?

In the first 100 ps since annealing started, SIA migrated toward metastable sites. However, the dependence of SIA concentration on DSA was surprising. There found a coherent wavy motion of target atoms (Fig.1) in the tail of CA transition clearly unless the initial SIA fraction exceeds 3 atomic %. We suppose the cooperative motion may promote DSA.

3. REFERENCES

[1] S. Takeda and T. Kamino: Phys. Rev. B **51**, 214 (1995).
[2] S. T. Nakagawa, Phys. Rev. B **75**, 205406 (2002).
[3] S. T. Nakagawa, in *Ion beams in Nanoscience and Technology (*Chap.9), Springer (2009).
[4] S. T. Nakagawa: Rad. Effect Defect Solids, (2014). doi**:** 10.10 80/10420150.2014.984613.
[5] S. T. Nakagawa, H. J. Whitlow, and G. Betz, *Surf. Coating Tech.,* **201**, 8393 (2007).

* Corresponding author e-mail address: stnak@dap.ous.ac.jp

POSTER ABSTRACTS

Molecular Dynamics simulations of ion implantation in Fe thin films

M. Aliaga[1,*], *M. J. Caturla*[1]

[1] Dept. Física Aplicada, Facultad de Ciencias, Fase II, Universidad de Alicante, Alicante, E-03690, Spain

Radiation damage in materials is a multiscale problem which, at the shortest timescale, that is, the picosecond timeframe, can only be addressed computationally. As an energetic ion travels through the lattice it transfers its energy both to the electrons and to the nucleus system, in an extend to each system that depends on the energy of the ion. For low energies (up to approximately 500 keV), most of the energy is transfered to the nucleus system. In the elastic collisions with the nuclei a collision cascade is produced. The energy deposited is dissipated through the electrons and lattice vibrations.

Molecular dynamics simulations is the perfect tool to study this kind of events. The recent growth in computational power has made it possible to improve the models used in the calculations, but there are still major challenges to face [1]. One of the most importants is the treatment of the ion-electron interaction. In classical molecular dynamics this interaction is often neglected or treated in a phenomenological manner [2].

We have used molecular dynamics simulations with recent interatomic potentials developed for Fe, to study the first stage of radiation damage in thin films of pure Fe under irradiation with Fe ions of energies between 50keV and 150keV. For every energy condition we have performed two sets of parallel simulations. In one set we have used the Lindhard model [3] to include a friction force proportional to the velocity for all atoms with a kinetic energy greater than 5 eV to mimic the inelastic energy losses produced by collisions with the electrons. Whereas in the second set we do not include any explicit inelastic damping force apart from the heating bath to control the temperature. In this work we compare how including this electronic energy loss affects the total number of defects produced for a given energy, as well as how these defects are arranged (clustering).

[1] Stoneham A M 1997 Finding the gaps: problems in radiation damage theory Radiat. Effects Defects Solids 142 191–203
[2] Stoneham A M 1990 Energy transfer between electrons and ions in collision cascades in solids Nucl. Instrum. Methods Phys. Res. B 48 389–98
[3] J. Lindhard, V. Nielsen, M. Scharff and P.V. Thomsen, K. Dan. Vidensk. Selsk. Mat. Fys. Medd. 33, no. 10 (1963) Notes on Atomic Collisions III.

* Corresponding author e-mail address: mj.aliaga@ua.es

Influence of Oxygen in the charge exchange process of He backscattered from Ta in LEIS

B. Bruckner[*], *D. Goebl, D. Roth, and P. Bauer*

Institut Experimentalphysik, Johannes Kepler Universität, Linz, Austria.

1. INTRODUCTION

Low energy ion scattering (LEIS) permits to analyze the composition of the outermost surface when the sample of interest is bombarded with noble gas ions in the energy range around 0.5 – 5 keV. Because of the high neutralization probability inside a solid, the surface peak is mostly due to binary collisions with atoms in the sample surface. Therefore, it is possible to deduce the masses of the scattering partners from the energy positions of these peaks [1].

An ESA – LEIS setup was used to investigate the influence of oxygen on the charge exchange between He^+ ions and a Ta surface. To this aim, the sputter cleaned Ta sample was exposed to oxygen until further exposure did not lead to significant changes in the ion yields.

The presented experiments were performed in an energy range where the resonant charge exchange processes (reionization and neutralization in the collision) occur in addition to Auger Neutralization (AN). Therefore, the ion fraction P^+ includes both the surviving ions which not undergone AN, and the projectiles which were neutralized on their way in and reionized again on their way out of the sample:

$$P^+ = \underbrace{P^+_{in} \cdot (1 - P_{RN}) \cdot P^+_{out}}_{survivals} + \underbrace{(1 - P^+_{in}) \cdot P_{RI} \cdot P^+_{out}}_{reionized} . \quad (1)$$

The reionized projectiles lead to a pronounced reionization background (tail) in the energy spectra of Ta, which starts at a threshold energy E_{th} of about 300 eV [2].

2. RESULTS

The yields A^+_{Ta} and A^+_O of He^+ ions backscattered from Ta or O atoms, respectively, were detected. A linear behavior between these two signals was observed, as shown in Fig. 1. As a result, one can extrapolate the Ta signal to the case of clean Ta, i.e. when the O signal vanishes. With this information and the experimental parameters one can determine the ion fraction for He^+ scattered from Ta, P^+_{Ta}. From the slopes of the $A^+_O(A^+_{Ta})$ lines the ion fraction for scattering from oxygen, P^+_O, is obtained directly, since the cross sections are known for He-Ta and He-O scattering. The resulting ion fraction values are presented and discussed.

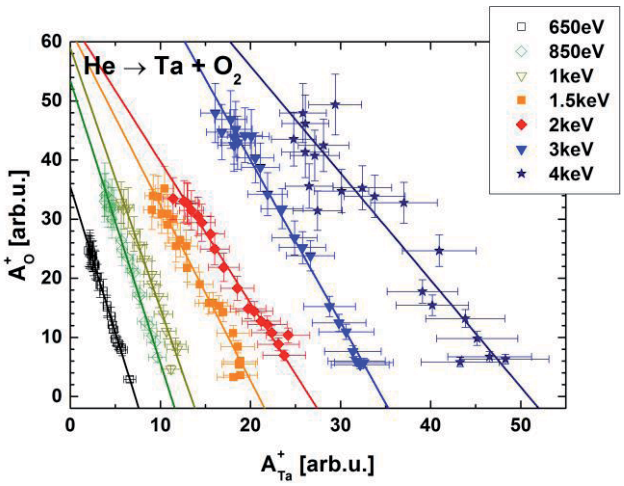

Figure 1: Ion yield A^+_O for He^+ scattered from O atoms as a function of ion signal A^+_{Ta} for He^+ backscattered from Ta atoms under oxygen exposure for different primary energies.

REFERENCES

[1] H.H. Brongersma, M. Draxler, M. de Ridder and P. Bauer, *Surf. Sci. Rep.* (**2007**) 62, 63.

[2] N.P. Wang et al., *Phys. Rev. A* (**2001**) 64

[*] Corresponding author e-mail address: barbara.bruckner@jku.at

TOWARDS THE UNDERSTANDING OF MECANISMS RESPONSIBLE OF THE THERMAL HYSTERESIS SUPPRESSION BY HIGLY CHARGED IONS COLLISIONS IN THIN FILMS

S. Cervera[1], M. Trassinelli[1], M. Marangolo[1], L. Bernard Carlsson[1], M. Eddrief[1], V.H. Etgens[1], V. Garcia[2], S. Hidki[1], E. Lamour[1], A. Levy[1], S. Mace, C. Prigent[1], J.-P. Rozet[1], S. Steydli[1], Y. Zheng[1] and D. Vernhet[1]

[1] CNRS, UMR 7588, Institut des NanoSciences de Paris (INSP), 4 Place Jussieu, 75005 Paris, France
Sorbonne Universités, UPMC Univ. Paris 06, INSP, UMR 7588, F-75005 Paris, France
[2]Unité Mixte de Physique CNRS/Thales, 1 Avenue A. Fresnel, 91767 Palaiseau, France and Université Paris-Sud, 91405 Orsay, France

1. INTRODUCTION

Modifications of magnetic properties induced by ion impact have been extensively studied in the last decades. Previous studies on the effect of ion impact were focused mostly on materials exhibiting a second-order magnetic transition and with singly charged ions. In the last years, our group started to investigate the effect of highly charged ion collisions on thin films presenting a first-order magnetic transition, like MnAs. These types of materials are characterized by a giant magnetocaloric effect (GMCE) associated to the magneto-structural transition close to room temperature making them promising materials for magnetic refrigeration applications. However, they suffer from a large thermal hysteresis, typical of first-order transitions, which cripples thermodynamic cycles in real refrigerator systems. In previous work [1], we demonstrated that the thermal hysteresis of the MnAs thin film can be entirely suppressed, by impact of Ne^{9+} at 90 keV, whereas other structural and magnetic properties are barely affected. To understand the mechanisms responsible of the thermal hysteresis suppression, different irradiation conditions and magnetocaloric materials are explored.

2. RUNNING EXPERIMENTS

With our present knowledge, both ions implantation and ion-induced defects or constraints could be responsible for the suppression of thermal hysteresis in the MnAs. To discriminate between these two possible mechanisms, we are running new experiments with different irradiation conditions allowing to tune the ratio between implanted ions and induced defect densities. As illustrated Figure 1, for a MnAs layer of 150 nm thick on a GaAs substrate, capped with 10 nm of Al, this ratio can be drastically changed by varying the incident ion energy and impact angle.

For investigating further on the thermal hysteresis suppression, other thin films exhibiting first-order transitions are also considered, like FeRh. In MnAs, the structural transition triggers the magnetic transition. Differently, the magnetic phase transition in FeRh, also affected by a thermal hysteresis, is accompanied by a lattice expansion [2] [3]. Studies of FeRh thin film will then allow us to gain new insights on the role of the ion impact. The experiments are running at present and new results will be presented at the workshop.

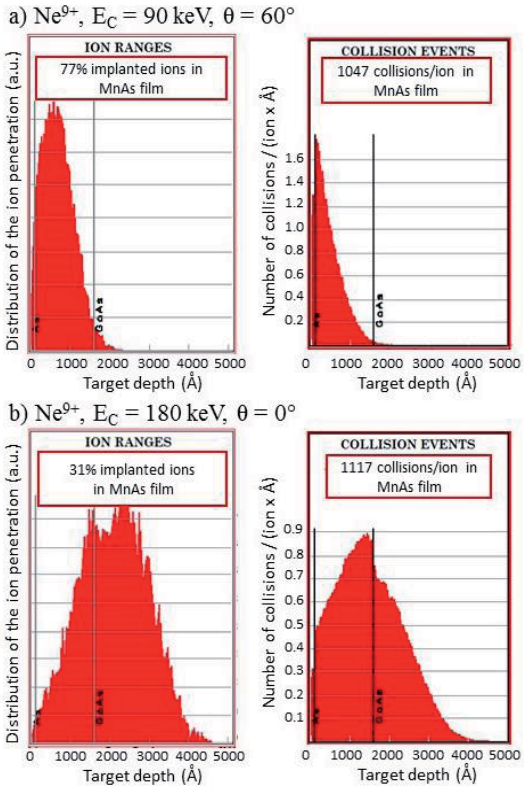

Figure 1: TRIM simulations for different irradiation conditions of Ne^{9+} on MnAs thin film: a) at 90 keV of kinetic energy with an incident angle of 60° with respect to the normal of the surface b) at 180 keV and 0° of incident angle for the second couple of diagrams.

Acknowledgments

This work was partially supported by French state funds managed by the ANR within the Investissements d'Avenir programme under reference ANR-11-IDEX-0004-02, and more specifically within the framework of the Cluster of Excellence MATISSE led by Sorbonne Universités.

3. REFERENCES

[1] M. Trassinelli, et. al. , Appl. Phys. Lett. **104**, 081906 (2014).

[2] F. de Bergevin and L. Muldawer, C.R. Hebd. Seances. Acad. Sci. **252**, 1347 (1961)

[3] T. Zhou, et.al., Phys. Lett. A **377**, 3052 (2013).

* sophie.cervera@insp.upmc.fr
* martino.trassinelli@insp.upmc.fr

Modifications of gallium phosphide single crystals using swift heavy ions and slow highly charged ions

A.S. El-Said[1,*], R.A. Wilhelm[2], R. Heller[2], S. Fascko[2] and C. Trautmann[3,4]

[1]Physics Department, King Fahd University of Petroleum and Minerals, Dhahran 31261, Saudi Arabia
[2]Institute of Ion Beam Physics and Materials Research, Helmholtz-Zentrum Dresden-Rossendorf, 01328 Dresden, Germany
[3]GSI Helmholtz Centre for Heavy Ion Research, 64291 Darmstadt, Germany
[4]Technische Universität Darmstadt, 64289 Darmstadt, Germany

1. INTRODUCTION

Ion-solid interaction is an exciting multidisciplinary field of research, which is not only leading to valuable outputs from interesting basic phenomena but also to promising technological applications in various fields. As nanotechnological tool, both swift heavy ions (SHI) and slow highly charged ions (HCI) were successfully utilized in nanostructuring of various materials by single ion impacts [1,2]. The formation of the nanostructures are mainly attributed to the strong electronic excitations created by the electronic energy loss of SHI and to the potential energy deposition of HCI [3]. Here, we are studying the modifications induced by SHI and HCI, in one of the most promising semiconductors, namely gallium phosphide (GaP).

2. EXPERIMENT

GaP single crystals were irradiated with ^{197}Au ions of equilibrium charge state and of kinetic energies between 374 MeV and 2.2 GeV at the Universal Linear Accelerator (UNILAC) facility of GSI Darmstadt, Germany. For slow highly charged ions (HCIs), the samples were irradiated with 114 keV $^{129}Xe^{Q+}$ (Q=33+ to 40+) from the Electron Beam Ion Trap (EBIT) facility of HZDR, Dresden, Germany. After irradiation, the samples were investigated using scanning force microscope (SFM) to investigate the surface modifications induced by ions. Moreover, ellipsometry measurements were performed in order to explore the SHI-induced modifications in the bulk.

3. RESULTS

In case of swift heavy ions, the topographic SFM images showed nanohillocks protruding from the GaP surfaces, see Fig. 1(a). Each hillock is produced by a single Au ion. In contrast to SHI, no observable topographic changes were observed after irradiation with HCI, as shown in Fig. 1(b). This result indicates that higher potential energy threshold (E_{pot} > 38.5 keV) is required for surface nanostructuring of GaP.

We also noticed that SHI-irradiated crystals become darker by using higher kinetic energy of the Au ions (Figure 2). This was confirmed by measuring a higher extension coefficient in the visible light region for the sample area that was exposed to 2.19 GeV than the one exposed to 374 MeV (see Fig. 2).

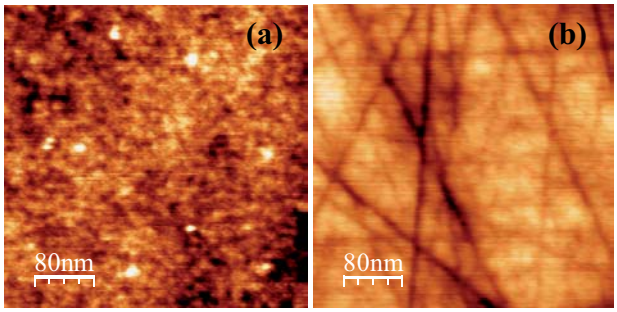

Figure 1: Topographic SFM image of GaP surface irradiated with 1.5 GeV ^{197}Au (a) and 114 keV Xe^{36+} (b) ions.

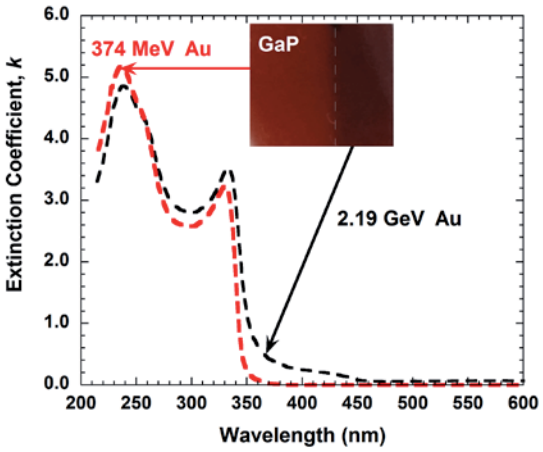

Figure 2: Extinction coefficient as a function of wavelength for GaP surface irradiated with 374 MeV and 2.19 GeV ^{197}Au ions. The inset shows a photo of the sample illustrating the coloring effect of the beam.

4. ACKNOWLEDGEMENTS

The support by KFUPM (Projects: RG1326 and FT131018) is greatly acknowledged.

5. REFERENCES

[1] A.S. El-Said, R.A. Wilhelm, R. Heller, S. Facsko, C. Lemell, G. Wachter, J. Burgdüorfer, R. Ritter, F. Aumayr, Phys. Rev. Lett. 109 (2012).
[2] O. Ochedowski, O. Osmani, M. Schade, B. Kleine Bussmann, B. Ban-d`Etat, H. Lebius, M. Schleberger, Nature Communications 5, 3913 (2014).
[3] F. Aumayr, S. Facsko, A. S. El-Said, C. Trautmann, and M. Schleberger, J. Phys. Condens. Matter 23, 393001 (2011).

* Corresponding author e-mail address: elsaid@kfupm.edu.sa

ELECTRON EMISSION INDUCED BY HIGHLY CHARGED ION IMPACT ON SINGLE LAYER GRAPHENE

A. Fuchs-Fuchs[*], *J. Schwestka*[*], *E. Gruber, Y. Y. Wang, and F. Aumayr*

Institute of Applied Physics, TU Wien, Wiedner Hauptstr. 8-10/E134, 1040 Vienna, Austria

1. INTRODUCTION

Single layer graphene (SLG) is an ultimately thin membrane made of sp2-hybridized carbon atoms with unique electronic properties. Since its discovery [1] SLG has been considered as an excellent candidate for future nanoelectronics. Disorder, as induced e.g. by collisions with energetic electrons or ions, effects the electronic structure and opens the possibility to modify and tailor the properties of this true 2D material. Collision studies between ions and free-standing SLG are also of fundamental interest, because they bridge the gap between atomic collisions in gaseous and those in solid targets.

For the transmission of slow highly charged ions through slightly thicker 1 nm carbon nanomembranes (CNMs) we have recently observed two distinct exit charge state distributions accompanied by a strong charge state dependent energy loss [2] as well as the creation of nano-sized pores for Xe^{q+} projectiles in charge states $q \geq 25$ mainly by deposition of their potential energy [3].

2. EXPERIMENTAL SETUP

To learn more about the microscopic interaction mechanism we have built a new experimental setup (figure 1), which allows us to determine the numbers statistics of electrons emitted during the transmission of slow multiply charged Ar^{q+} ions through SLG (and CNMs in comparison).

Slow Ar^{q+} ions ($q \leq 11$) are extracted from an ECR-ion source [4], mass analyzed and collimated before traversing a free standing SLG or CNM target (mounted on a TEM grid which is fixed onto a rotatable manipulator) and being registered by a position sensitive multichannel plate detector (MCP). Electrons emitted from the interaction region are extracted by a weak electric field through a highly transparent grid and accelerated onto a surface barrier type detector biased at +30 kV, where their statistical distribution is measured in the usual way (see, e.g. [5, 6]).

By changing the orientation of the target film from 45° to 135° with respect to the incident beam direction, electrons emitted from the front (= ion entrance side) and back side (= ion exit side) can be distinguished.

To separate emission events originating from ion transmission through SLG from ion impact on the (solid) TEM grid support, only electrons registered in coincidence with an ion signal on the MCP are counted.

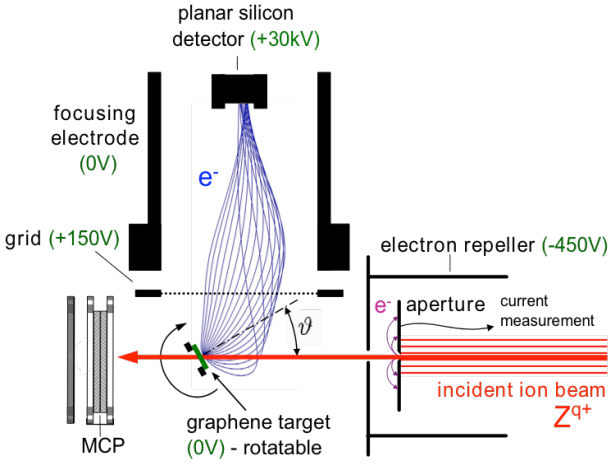

Figure 1: Experimental setup (c.f. text).

Since electron emission and projectile charge exchange are closely related, in a next step it is planned to register the electrons in coincidence with a particular projectile exit charge state.

3. REFERENCES

[1] A. K. Geim and K. S. Novoselov, Nature Mater. **6**, 183 (2007).
[2] R. A. Wilhelm, et al., Phys. Rev. Lett. **112** 153201 (2014).
[3] R. Ritter, et al., Appl. Phys. Lett. **102** 06311 (2013).
[4] E. Galutschek et al., J. Phys. Conf. Ser. **58** 395 (2007).
[5] F. Aumayr et al., Appl. Surf. Sci. **47** 139 (1991).
[6] K. Töglhofer et al., Surf. Sci. **281** 143 (1993).

[*] Corresponding author e-mail address: fuchsfuchs@iap.tuwien.ac.at, schwestka@iap.tuwien.ac.at

INTERACTION OF MULTIPLY CHARGED IONS WITH SINGLE LAYER GRAPHENE: CHARGE EXCHANGE AND ENERGY LOSS STUDIES

V. Smejkal[1], E. Gruber[1,], M. Kralik[1], R. A. Wilhelm[2], R. Heller[2], S. Facsko[2], and F. Aumayr[1]*

[1] Institute of Applied Physics, TU Wien, Wiedner Hauptstr. 8-10/E134, 1040 Vienna, Austria
[2] Helmholtz-Zentrum Dresden-Rossendorf, Inst. of Ion Beam Physics & Materials Research, 01328 Dresden, Germany

1. INTRODUCTION

Due to its unique electronic properties, single layer graphene (SLG) has attracted enormous attention since its discovery [1] as an excellent candidate for future nanoelectronics. SLG can be considered as the ultimately thin membrane made of sp2-hybridized carbon atoms. Disorder as induced e.g. by collisions with energetic electrons or ions effects the electronic structure and opens the possibility to modify and tailor the properties of this true 2D material. Collision studies between ions and free-standing SLG are also of fundamental interest, because they bridge the gap between atomic collisions in gaseous and those in solid targets.

2. EXPERIMENTAL SETUP

For the transmission of slow highly charged ions through slightly thicker 1 nm carbon nanomembranes (CNMs) we have recently observed two distinct exit charge state distributions accompanied by a strong charge state dependent energy loss [2] as well as the creation of nano-sized pores for Xe^{q+} projectiles in charge states $q \geq 25$ mainly by deposition of their potential energy [3].
To learn more about the microscopic interaction mechanism we have extended our studies to the case of slow multiply charged Ar^{q+} ions transmitted through SLG (and CNMs in comparison). In a new experimental setup in Vienna, slow Ar^{q+} ions ($q \leq 9$) are extracted from an ECR-ion source [4], mass analyzed and collimated before traversing a free standing SLG or CNM target mounted on a TEM grid. The ions exiting the target foil are analyzed in a spherical electrostatic energy analyzer (COMSTOCK AC-903B) equipped with a channelplate detector. A typical spectrum (intensity vs. analyzer voltage) recorded for 144 eV/amu Ar^{4+} ions through a CNM is shown in figure 1.

3. RESULTS

Such spectra give information on both the exit charge state distribution (i.e. charge exchange between multiply charged ions and SLG) as well as the mean value of the energy loss and the energy loss distribution (see the insert of fig. 1) as a function of the charge state and kinetic energy of the primary projectile. E.g., figure 1 clearly shows that charge equilibrium of the projectile has by far not been reached within the 1 nm thick foil and therefore non-equilibrium effects can be studied. Further information on the interaction is derived from the comparison between results for SLG and CNMs.

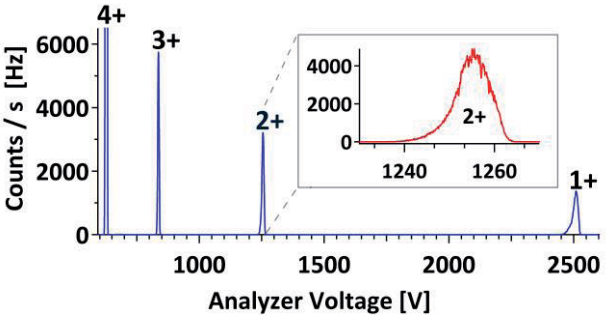

Figure 1: Charge state and energy spectrum (e.g. see insert for ions exiting as Ar^{2+}) of 5.76 keV Ar^{4+} projectile ions after transmission through a 1 nm thick carbon nanomembrane.

Work supported by Austrian FWF (Proj.No. I 1114-N20).

4. REFERENCES

[1] A. K. Geim and K. S. Novoselov, Nature Mater. **6**, 183 (2007)
[2] R. A. Wilhelm, et al., Phys. Rev. Lett. **112**, 153201 (2014)
[3] R. Ritter, et al., Appl. Phys. Lett. **102**, 06311 (2013)
[4] E. Galutschek et al., J. Phys. Conf. Ser. **58**, 395 (2007)

* Corresponding author e-mail address: egruber@iap.tuwien.ac.at

Time of Flight Backscattering and Secondary Ion Mass Spectrometry in a Helium Ion Microscope

N. Klingner[1], *R. Heller*[1], *G. Hlawacek*[1], *P. Gnauck*[2], *S. Facsko*[1], *and J. von Borany*[1]

[1]Helmholtz-Zentrum Dresden-Rossendorf, Bautzner Landstr. 400, 01328 Dresden, Germany
[2]Carl-Zeiss-Microscopy GmbH, D-73447 Oberkochen, Germany

Abstract

Helium ion microscopes (HIM) have developed into a frequently used imaging device in several laboratories around the world. Beside a sub nano-meter resolution and a high depth of focus the latest generation of HIM devices (Zeiss Orion NanoFab) offers the ability to make use of Neon ions enabling additional possibilities for surface modifications on the nm scale [1].

While the image generation in a HIM is based on evaluating the amount of secondary electrons (SE) the information carried by the energy of the backscattered He/Ne projectiles (BS) is not taken into consideration at the moment. Thus the HIM offers excellent topographic imaging capabilities but chemical information (in terms of elemental composition) of the surface is barely accessible. Nevertheless back-scattered particles carry that information and may be used to provide additional contrast mechanism(s). First attempts to measure BS energy spectra were carried out by Sijbrandij *et al.* [2] and gave evidence for the general feasibility but also revealed that a quantitative chemical analysis of thin layers would require the development of more sophisticated detection concepts than those used in their experiments (silicon surface barrier detector).

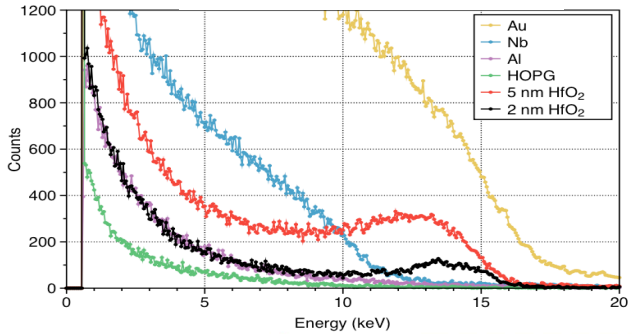

Figure 1: ToF-BS spectra of different elemental bulk samples and thin layers of HfO_2 on Si measured in the HIM by using 25keV Ne ions.

Since the primary He/Ne energy is rather low (10-35 keV) back-scattering spectrometry is suffering various difficulties like high contribution of multiple scattering, non-Rutherford backscattering cross sections and an energy dependent charge fraction. Further the angular spread in the collision cascade as well as the high sputtering yields in this energy regime define physical limits on the maximum achievable lateral resolution and the detection sensitivity. In this contribution we will address these challenges and present our experimental approach and the corresponding results of performing BS spectrometry in a HIM.

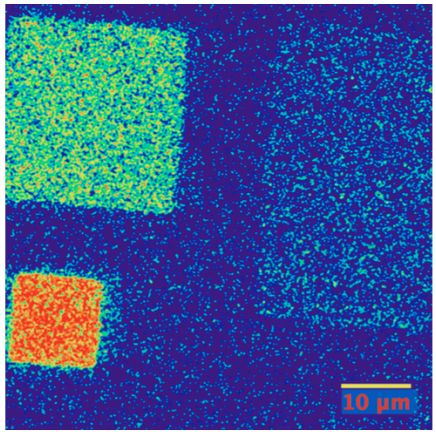

Figure 2: ToF-BS image of a carbon sample covered with rectangular patterns of Si, Ni and Au. The color scale corresponds to the time of flight of the BS particles. In contrast to SE imaging this technique reveals well-defined elemental contrast.

We show that pulsing the primary ion beam and measuring the Time of Flight (ToF) of the BS He/Ne ions presents a promising technique of performing BS spectrometry in a HIM in terms of sensitivity, energy resolution and lateral resolution.

Our approach enables us also to perform Secondary Ion Mass Spectrometry (SIMS) by just biasing the sample to a positive potential (of several 100V). Advantages and limitations of this technique will be discussed and compared to those of BS spectrometry.

REFERENCES

[1] [1] G. Hlawacek, V. Veligura, R. van Gastel, and B. Poelsema, J. Vac. Sci. Technol. B **32**(2), 2014, 020801.

[2] [2] S. Sijbrandij, B. Thompson, J. Notte, B. W. Ward and N. P. Economou, J. Vac. Sci. Technol. B, **26**(6), 2008, 2103-2106

* Corresponding author e-mail address: r.heller@hzdr.de

MONTE CARLO SIMULATION OF CHARGE EXCHANGE PROCESSES IN He^+/Cu SCATTERING

K.Khalal-Kouache[1,*], *B.Bruckner*[2], *D.Roth*[2], *D.Goebl*[2] *and P.Bauer*[2]

[1] Université des Sciences et de la Technologie Houari Boumediene (USTHB), Faculté de Physique, Laboratoire SNIRM, Bab-Ezzouar, 16111 Algiers, Algeria
[2] Institut für Experimentalphysik, Abteilung für Atom- und Oberflächenphysik, Johannes Kepler Universität Linz, 4040 Linz, Austria

Keywords: Low energy ion scattering, Charge exchange processes, Neutralization, Reionization, Ion fraction, Monte Carlo simulation.

Low energy ion scattering (LEIS) is a surface analysis technique widely used for quantitative composition and structure analysis [1]. A solid surface is bombarded with low energy noble gas ions and the scattered ions are detected. Many investigations have been carried to study charge exchange processes between the projectile and the target [1]. In the case of the scattering of He^+ ions from a copper surface, it is well known that Auger Neutralization (AN) plays an important role [2, 3]. The probability to escape AN is given by [4]:

$$P^+ = \exp\left(-\int \Gamma \, dt\right) \quad (1)$$

where Γ is the Auger neutralization rate. P^+ can also be written as:

$$P^+ = \exp\left(-V_c / V_{per}\right) \quad (2)$$

V_c is a characteristic velocity witch is a measure of the neutralization efficiency. V_{per} is the projectile perpendicular velocity.

When the projectile energy E is larger than a threshold energy E_{th}, charge exchange processes during 'close collisions' become possible. In these collisions, the minimum distance reached between the projectile and the target atom is lower than a critical value r_{min}. Thus, P_{CIN} and P_{CIR} are defined respectively as the neutralization and reionization probabilities in 'close collisions'. They have to be taken into account in the calculation of the ion fraction in the reionization regime (E > Eth).

In this contribution, results of the scattering of He^+ ions from a polycrystalline copper surface are presented. P^+ values are calculated using a Monte Carlo simulation [5] where models of charge exchange processes are included. To describe the interaction between the projectile and the target atom, the Thomas-Fermi-Molière potential is used with a correction factor to the screening length C_a=0.75 [6].

Calculated P^+ values at normal incidence and for a scattering angle θ=136° show a good agreement with experimental ion fractions.

REFERENCES

[1] H. Brongersma, M. Draxler, M. Deridder, and P. Bauer, Surf. Sci. Rep. **62** (2007) 63.
[2] M.Draxler, R. Gruber, H.H. Brongersma and P. Bauer, Phys. Rev. Lett. **89** (2002) 263201.
[3] D. Primetzhofer, M. Spitz, E. Taglauer and P. Bauer, Surf. Sci. **605** (2011) 1913.
[4] H.D. Hagstrum, Phys. Rev. **96** (1954) 336.
[5] K. Khalal-Kouache, A.C. Chami, M. Boudjema, Y. Boudouma, P. Benoit-Cattin and C. Benazeth, Alg. J. Adv. Mater. **3** (1999) 1.
[6] D. Primetzhofer, S.N. Markin, M. Draxler, R. Beikler, E. Taglauer, P. Bauer, Surf. Sci. **602** (2008) 2926.

* Corresponding author e-mail address: kkouache@yahoo.fr

MULTIPLE SCATTERING OF LOW ENERGY H^+ IONS IN MATTER: MEAN ENERGY APPROXIMATION WITH THE SIGMUND AND WINTERBON MODEL

A.Mekhtiche[1,2] *and K.Khalal-Kouache*[1,*]

[1]Université des Sciences et de la Technologie Houari Boumediene (USTHB), Faculté de Physique, Laboratoire SNIRM, Bab-Ezzouar, 16111 Algiers, Algeria
[2] Faculté des Sciences et de la Technologie, Université Yahia Farès de Médéa, Algeria

In this contribution, angular distributions of slow H^+ ions transmitted through different targets (Al, Ag and Au) are calculated using the model of Sigmund and Winterbon (SW) [1] in the multiple scattering theory. Valdés and Arista (VA) developed a method extending the SW model by including the effect of energy loss in the calculation of angular distributions of transmitted ions [2]. Another method has been proposed for such calculations: one can consider the SW model by using an average value for the energy of the ions inside the target.
In this contribution, a new expression is proposed for the mean energy which gives a better agreement with the VA model than the precedent one at low energy. Different potentials have been considered to describe the interaction projectile-target atom in this study and the new expression is found to be independent of the interaction potential.

Keywords: Multiple scattering; Energy loss; Angular distributions; Stopping power; Mean energy function.

REFERENCES

[1] P. Sigmund, K.B. Winterbon, Nucl. Instr. and Meth. **119** (1974) 541.
[2] J. E. Valdès and N. R. Arista, Phys. Rev. A **49**, 2690 (1994).

* Corresponding author e-mail address: kkouache@yahoo.fr

Magnetic Property of Ferromagnetic Material multi-layer with High Brightness and Highly Spin-polarized LEEM

T. Koshikawa[1], *M. Suzuki*[1)], *K. Kudo*[2)], *K. Kojima*[3)], *T. Yasue*[1)], *N. Akutsu*[1)], *A. Dino*[3)], *H. Kasai*[3)], *E. Bauer*[4)], *T. Nakanishi*[5)], *X.G.Jin*[6)] *and Y. Takeda*[7]

[1] Osaka Electro-Communication University, Japan
[2] Ochanomizu University, Tokyo, Japan
[3] Osaka University, Osaka, Japan
[4] Arizona State University, Tempe, USA
[5] School of Science, Nagoya University, Nagoya, Japan
[6] KEK, Tsukuba, Japan
[7] Aichi Synchrotron Light center, Aichi, Japan

We have already developed a novel very high brightness and high spin-polarized low energy electron microscope (SPLEEM) [1-4].

[CoNix] multi-layer is known to exhibit perpendicular magnetic anisotropy and is expected as a material for the devices with low operation current. We investigated magnetic property during growth of the [CoNix]y multi-layer with our SPLEEM [1-4] and. Numerical simulations based on the Landau-Lifshitz-Gilbert (LLG) equation was also carried out for [$CoNi_2$] on W(110) [5,6].

Detailed experimental results will be shown on the magnetic property for different pairs of Co/Ni systems, i.e., Co/Ni2, Co/Ni3 and Ni2/Co on W(110). Fig.1 shows that the changing angle between the in-plain and the out-of-plain for the same kinds of materials. Three systems show the similar property and the contribution of Ni layer is not large. The main contribution to the perpendicular magnetization would cause with the un-isotropy of the interface of Co and Ni layer.

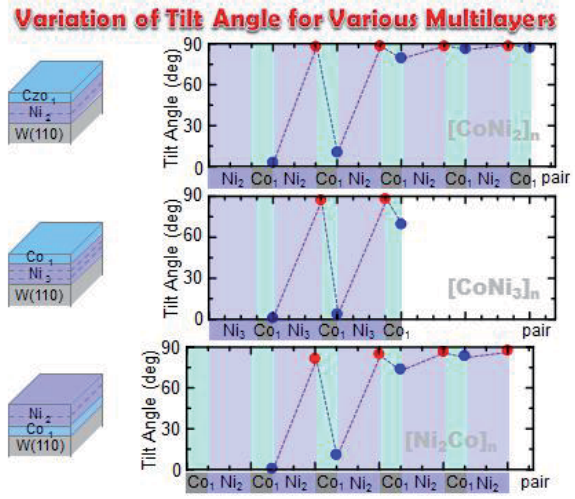

Figure 1: Magnetic direction of Co/Ni2, CoNi3 and Ni2/Co multi-layers on W(110)

.

REFERENCES

[1] N.Yamamoto *et al*., J. Appl. Phys. **103**, 064905 (2008).
[2] X.G. Jin *et al*., Appl. Phys. Express **1**, 045602 (2008).
[3] M.Suzuki *et al*., Appl. Phys. Express **3**, 026601 (2010).
[4] T.Yasue et.al., Rev. Sci. Instrum., 85, 043701 (2014).
[5] M.Suzuki et.al., J.Phys.Condens.Matter. **25**, 406001 (2013).
[6] K.Kudo et.al., J.Phys. Condens.Matter. **25**, 395005 (2013).

Nanostripes and nanoripples: surface modifications by swift heavy ions

M. Karlušić[1,*], *M. Buljan*[1], *H. Lebius*[2], *B. Ban-d'Etat*[2], *Z. Siketić*[1], *I. Bogdanović-Radović*[1], *B. Šantić*[1], *N. Radić*[1], *M. Jakšić*[1], *S. Bernstorff*[3], *M. Schleberger*[4]

[1] Ruđer Bošković Institute, Bijenička cesta 54, 10000 Zagreb, Croatia
[2] CIMAP, CEA-CNRS-ENSICAEN-UCN, BP 5133, 14070 Caen Cedex 5, France
[3] Elettra-Sincrotrone Trieste, SS 14 km 163.5, 34149 Basovizza, Italy
[4] Fakultät für Physik and CENIDE, Universität Duisburg-Essen, D-47048 Duisburg, Germany

Swift heavy ion (SHI) irradiation is a powerful tool for materials modification on the nanoscale. When irradiated at grazing incidence angle, surface modifications in the form of long surface ion tracks can be observed [1,2,3]. Recently, it was demonstrated that grazing incidence SHI irradiation can also be applied for modification of graphene [4] and other 2D materials. In the present contribution, we present two new developments along this line of research, demonstrating the usability of SHI for nanoscale modifications of surfaces and custom made 2D materials.

Grazing incidence SHI irradiation of GaN [5] yields the formation of two different kinds of surface ion tracks. While chains of nanohillocks were observed for higher values of electronic stopping power, chains of nanoholes were found by AFM for lower stopping power values. In addition, surface tracks were investigated using grazing incidence small angle X-ray scattering (GISAXS). This novel method yields good statistics and avoids typical difficulties in measurements due to the (unknown) AFM tip size. Preferential loss of nitrogen found by *in situ* TOF-ERDA measurements indicates a thermal decomposition of GaN as origin of the chains of nanoholes observed on its surface.

Second experiment shown is grazing incidence SHI irradiation of thin ITO films. Here we also found two different surface ion track morphologies: for lower stopping powers, usual ion tracks were observed, but for high stopping power values nanostripes in the form of double tracks were found (Fig. 1a). After higher fluence SHI irradiation, yet another new feature was found: in a narrow range of stopping powers, straight uniform nanoscale ripples were observed for the first time (Fig. 1b.).

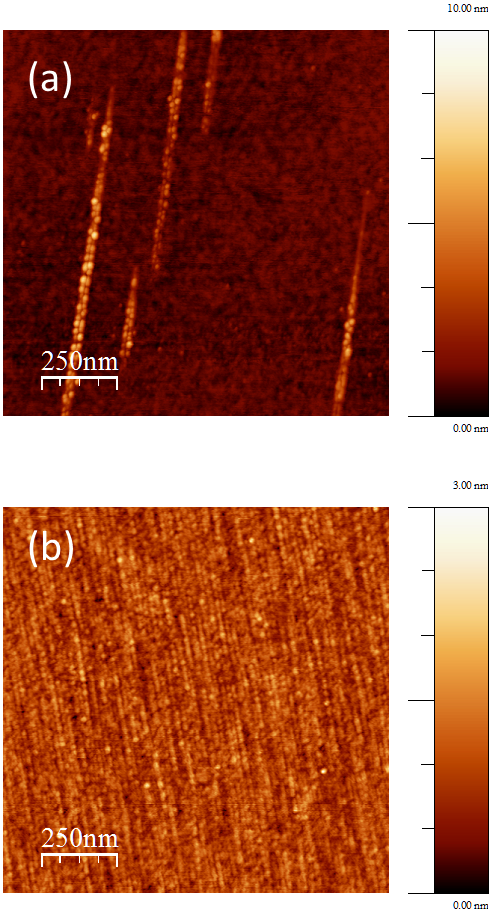

Figure 1. (a) Nanostripes (double tracks) in thin ITO film after grazing incidence irradiation using 92 MeV Xe ions (b) Nanoripples in thin ITO film after grazing incidence irradiation using 15 MeV Si ions.

[1] E. Akcöltekin, T. Peters, R. Meyer, A. Duvenbeck, M. Klusmann, I. Monnet, H. Lebius, M. Schleberger, Nature Nanotech. **2**, 290 (2007)
[2] M. Karlušić, S. Akcöltekin, O. Osmani, I. Monnet, H. Lebius, M. Jakšić, M. Schleberger, New J. Phys. **12**, 043009 (2010)
[3] O. Ochedowski, O. Osmani, M. Schade, B.K. Bussmann, B. Ban d'Etat, H. Lebius, M. Schleberger, Nature Comm. **5**, 3193 (2014)
[4] S. Akcöltekin, H. Bukowska, T. Peters, O. Osmani, I. Monnet, I. Alzaher, B. Ban d'Etat, H. Lebius, and M. Schleberger, Appl. Phys. Lett. **98**, 103103 (2011)
[5] M. Karlušić, R. Kozubek, H. Lebius, B. Ban d'Etat, R.A. Wilhelm, M. Buljan, Z. Siketić, F. Scholz, T. Meisch, M. Jakšić, S. Bernstorff, M. Schleberger, and B. Šantić, J. Phys. D: Appl. Phys. (accepted)

* Corresponding author e-mail address: marko.karlusic@irb.hr

Transmission secondary ion mass spectroscopy of a peptide using 5 MeV C_{60}^+ ions

T. Marumo[1], *K. Yamamoto*[1], *K. Nakajima*[1,*], *K. Narumi*[2], *Y. Saitoh*[2], *K. Hirata*[3] *and K. Kimura*[1]

[1] Department of Micro Engineering, Kyoto University, 615-8540 Kyoto, Japan
[2] Takasaki Advanced Radiation Research Institute, JAEA, Takasaki, Gumma 370-1292, Japan
[3] Nation Metrology Institute of Japan, AIST, Tsukuba, Ibaraki 305-8565, Japan

1. INTRODUCTION

In the last two decades, secondary ion mass spectrometry (SIMS) has been much improved in sensitivity to large molecules by use of large clusters as primary ions, such as C_{60} ions [1], argon gas cluster ions [2] and water cluster ions [3]. However higher sensitivity to macromolecules is still desired for application of SIMS to imaging of biological samples. Recently, we have demonstrated that a strong enhancement of intact molecular ion yield of an amino acid (phenylalanine) can be achieved when secondary ions emitted in the forward direction from thin-film samples were detected under transmission with 5 MeV C_{60}^+ primary ions [4]. The enhancement can be explained in terms of density of energy deposition on the sample surface to be analyzed. It is of great interest whether a similar enhancement occurs for larger molecules.

In this work, secondary ions emitted in the forward direction from a peptide, Leucine-enkephalin were analyzed under transmission of 5 MeV C_{60}^+ and 6 MeV Cu^{4+} primary ions. It was found that a significant enhancement of intact molecular ion yield from the peptide can be achieved using C_{60}^+ primary ions.

2. EXPERIMENT

Leucine-enkephalin was used as a target peptide. This peptide consists of 5 amino acids (Tyr-Gly-Gly-Phe-Leu) and the molecular weight is 555.6 Da. It was dissolved in distilled water and the solution of 3–10 µl was dropped on cleaned self-supporting amorphous SiN membranes (50 nm thick). Then the samples were ex-situ dried in a vacuum prior to the SIMS measurements. In the SIMS measurements, the samples were irradiated from the SiN side with 5 MeV C_{60}^+, and also with 6 MeV Cu^{4+} for comparison. Positive secondary ions emitted in the forward direction under transmission of primary ions through the sample were mass-analyzed using time-of-flight techniques.

3. RESULTS AND DISCUSSION

Figure 1 shows mass spectra of positive secondary ions from a sample for 5 MeV C_{60}^+ and 6 MeV Cu^{4+} primary ions, respectively. There are many peaks corresponding to fragment ions as well as intact molecular ions. For example, the peaks at m/z 136 and 279 can be assigned as Tyrosine and Tyrosine-Glycine-Glycine, respectively. Several peaks at m/z 550–600 are assigned as intact molecular ions, such as $[M+H]^+$, $[M+H_3O]^+$, $[M+Na]^+$, $[M+K]^+$ and so on. Yields of both fragment ions and intact molecular ions are higher for C_{60}^+ primary ions than for Cu^{4+} primary ions. In detail, the enhancement factor of the yield of intact molecular ions with 5 MeV C_{60}^+ compared to with 6 MeV Cu^{4+} is as high as ~5, while that of fragment ions is only ~2. This indicates that the combination of 5 MeV C_{60}^+ primary ions with the forward detection in the transmission geometry leads to preferential enhancement of the yield of intact molecular ions from Leucine-enkephalin as well as from phenylalanine. These results could be qualitatively explained again in terms of density of energy deposition on the peptide surface. The comparison with the case of phenylalanine will be also discussed in the presentation.

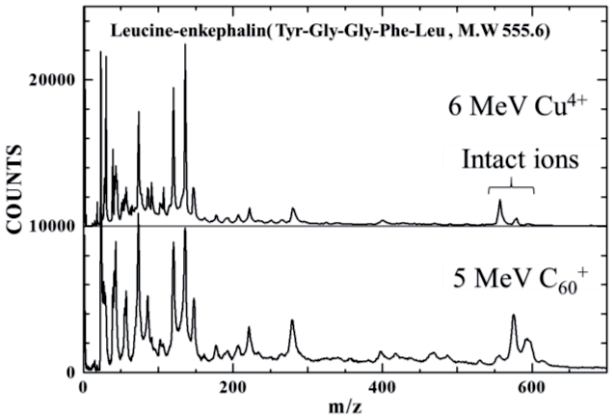

Figure 1: Mass spectra of positive secondary ions emitted in the forward direction from a Leucine-enkephalin film on an amorphous SiN membrane under transmission of 5 MeV C_{60}^+ and 6 MeV Cu^{4+}, respectively.

4. REFERENCES

[1] E. A. Schweikert, M. J. van Stipdonk, R. D. Harris, *Rapid Commun. Mass Spectrom*. **10**, 1987 (1996).
[2] N. Toyoda, J. Matsuo, T. Aoki, I. Yamada, D. B. Fenner, *Appl. Surf. Sci*. **203-204**, 214 (2003).
[3] K. Mori, D. Asakawa, J. Sunner, K. Hiraoka, *Rapid Commun. Mass. Spectrom*. **20**, 2596 (2006).
[4] K. Nakajima, K. Nagano, M. Suzuki, K. Narumi, Y. Saitoh, K. Hirata, and K. Kimura, *Appl. Phys. Lett*. **104**, 114103 (2014).

* Corresponding author e-mail address: nakajima.kaoru.4a@kyoto-u.ac.jp

SECONDARY MOLECULAR ION EMISSION FROM LIQUIDS UNDER AMBIENT PRESSURE

J. Matsuo[1,2*], *M. Kusakari*[1], *M. Fujii*[1,2] *T. Seki*[1,2] *and T. Aoki*[1,2]

[1] Quantum Science and Engineering Center, Kyoto University, Uji, 611-0011 Kyoto, Japan
[2] SENTAN, Japan Science and Technology Agency (JST), Chiyoda, 102-0075 Tokyo, Japan

1. INTRODUCTION

Secondary particle emission under ion irradiation provides unique opportunities for further insight on ion collision with matter and material analysis. In particular, secondary molecular ion emission from organic or biological molecules is of interest, not only for fundamental studies on excitation of molecules, but also for practical applications, such as secondary ion mass spectrometry (SIMS). It has been reported that secondary molecular ion yields of biological molecules with swift heavy (MeV) ions are much higher yields than that with monomer ions with energy of a few tens keV [1-3]. In this energy range (MeV), most of the deposited energy by incoming ions is used for electronic excitation, although nuclei excitation is dominant for low energy (keV) ions. In case of MeV ions, delta electrons are generated in the infratrack and these electrons stimulate ejection of intact molecules from the outer region ("ultratrack"). We have been demonstrated molecular imaging technique with secondary molecular ions emitted by swift heavy ion beams for biological material analysis under low vacuum pressure [4].
We recently succeed to detect secondary molecular ions emitted from liquids, such as fatty acid, alcohol and water under ambient pressure.

2. RESULTS AND DISCUSSIONS

6 MeV Cu^{4+}, which has 35 mm projection range in ambient pressure, was extracted and collided to liquid samples. MeV ion beam from a tandem ion accelerator was focused with a quadrupole lens. In order to avoid degradation of vacuum pressure in both quadrupole lens and mass spectrometer, fine nozzles were placed in between the sample chamber. The distance between the nozzle and a sample has to be shortened in order to reduce ionization of gas phase molecules. The incident angle of the primary beam was 45 º with respect to the normal to the sample surfaces.
An orthogonal acceleration (oa) time-of-flight (TOF) mass spectrometer with quadrupole ion guide was used to measure secondary ions. Vacuum pressure of TOF chamber was kept below 10^{-5} Pa, when the sample chamber was at atmospheric pressure.

Secondary ion mass spectrum from liquid water was depicted in figure 1. The droplet of water (20μL) disappeared within 20 minutes even under atmospheric pressure, because of the high vapor pressure Not only monomer water ion $[H_2O+H]^+$ but also many water cluster ions $[nH_2O+H]^+$ were found in the spectrum. The water cluster ions $[nH_2O+H]^+$ were only generated at the liquid surface, but monomer water ion $[H_2O+H]^+$ could be generated at both at the liquid surface and the gas phase. Those water cluster ions $[nH_2O+H]^+$ suddenly disappeared, when water droplet was gone. This result indicates that secondary molecular ions from liquid are clearly observed as secondary cluster ions.
Detail of this new technique and possibility to investigate liquid-solid interface will be presented.

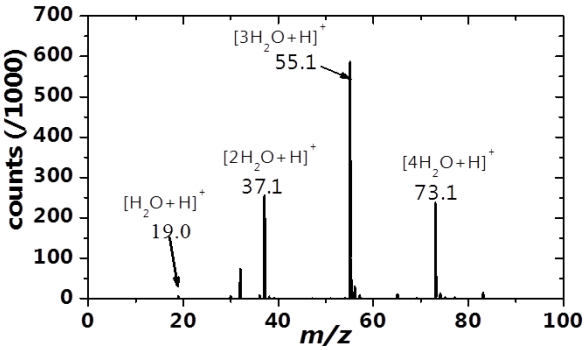

Figure 1: Secondary ion mass spectrum from liquid water measured under ambient pressure. 6 MeV Cu^{4+} was irradiated to water droplet, which disappeared within 20 minutes.

3. REFERENCES

[1] A. Hedin, P. Hakansson, M. Salchpour and B. U. R. Sundqvist, Phys. Rev. B, 35, 7371, (1987)
[2] Y. Nakata, Y. Honda, S. Ninomiya, T. Seki, T. Aoki and J. Matsuo, J. Mass Spectro., 44, 128 (2009)
[3] Y. Wakamatsu, H. Yamada, S. Ninomiya et al., Nucl. Instr. and Meth. B, 269, 2251 (2011)
[4] J. Matsuo, S. Ninomiya, H. Yamada, K. Ichiki, Y. Wakamatsu, M. Hada, T. Seki, T. Aoki, Surf. Interface Anal., 42, 1612 (2010)

* Corresponding author e-mail address: adam. lack@ hite.

QUALITATIVE AND QUANTITATIVE DESCRIPTION OF SiC GROWN GRAPHENE CORRUGATION BY GRAZING INCIDENCE FAST ATOM DIFFRACTION.

M. Debiossac, Z. Mu, P. Lunca-Popa, P.Roncin and A. Zugarramurdi

ISMO, Université Paris Saclay, CNRS-Université Paris-Sud, Orsay F-91405, France

Recently grazing incidence fast atom diffraction (GIFAD or FAD) was applied [1] to investigate the moiré-like pattern of SiC-grown graphene with high precision. This diffractive technique based on the scattering of fast He atoms, is only sensitive to the topmost layers of the surface, and thus is well suited for the extraction of corrugation parameters from graphene. This is true when compared to other techniques such as STM, where corrugation depends on the voltage used to sample the surface, or x-ray diffraction, where pure surface contributions are difficult to isolate.

In GIFAD, the scattering of the atomic beam can be modeled in a 2D space [2], obtained from the averaging of the 3D surface along the beam-incidence low-index direction. The relevant quantity determining the diffraction of the beam of total energy E_0, is the corresponding perpendicular energy $E_\perp=E_0 \sin\theta^2$, where θ is the small polar angle of incidence. Despite the reduced dimensionality of the problem, description of Moiré surfaces requires large computational resources owing to their large superlattice. From the point of view of developing GIFAD as a real-time surface analysis tool, the availability of quick analysis tools of the diffraction data is important.

Here a fast and simple approach based on the hard corrugated wall (HCW) model to perform the analysis of the GIFAD data from corrugated graphene is tested. The HCW model is motivated by the exponential repulsive barrier felt by the He atom when getting close to the surface. Thus most of the momentum transfer to the He projectile takes place around the classical turning points, which define a corrugated surface. The HCW model considers semi-classical diffraction by this infinitely repulsive surface Z(y) and assuming free propagation above it . This model has been successfully applied to simple surfaces, however, as shown by Winter and Schüller [3], corrugation can be overestimated by almost 20% percent for a LiF surface along <110>. Based on HCW, we derive an empirical description of the graphene surface in terms of Gaussian bumps, representing the surface corrugation, on top of a sinusoidal oscillation, representing the carbon backbone. Comparing to exact diffraction results [1], a good quantitative agreement is achieved for the graphene backbone interaction potential. Along the [100] direction also called zigzag, only the carbon backbone is visible [1] due to geometric properties of the hexagonal structure. Corresponding diffraction curves plotted in Figure 1 show that the diffracted intensity ratios are well reproduced (dotted lines) by a simple Bessel function solution $I_m=J_m(x)^2$ where $x=k_\perp \cdot h_{tp}$. with $k_\perp$ the wave vector associated with $E_\perp$ and h_{tp} the full amplitude associated with a sinusoidal corrugation function. The agreement in the low energy region is even better (full lines) if a 10 meV attraction energy is added to the perpendicular energy $E_\perp$. Alternately, one could allow the corrugation to be energy dependent to fit the data. The same procedure can be applied to the [110] direction (armchair) where only the moiré-like structure is visible. A Bessel adjustment indicates a sinusoidal amplitude of 0.13 to 0.14 Å perfectly in line with the scaled value proposed in Ref. [1]. The excellent quantitative agreement here is attributed to the fact that the carbon-helium interaction potential is very short range.

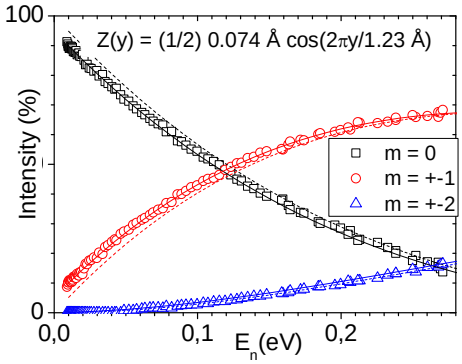

Figure 1 Diffracted intensities from ref[1] along the [100] direction as a function of $E_\perp$. the lines are simple Bessel functions obtained for a sinusoidal HCW of 2.13 Å period and a full corrugation amplitude of 0.074 Å.

In conclusion, with help of exact quantum mechanical calculations [1] we show that, in the case of graphene, the HCW provide a quantitatively correct solution to the analysis of GIFAD data.

Acknowledgment. We are grateful to Andrei Borisov for fruitful advices. This research has been supported by Triangle de la physique (2012-040T-GIFAD) and by the Agence Nationale de la Recherche ANR-11-EMMA-0003.

REFERENCES

[1] A. Zugarramurdi *et al.* Appl. Phys. Lett. **106**, 101902 (2015)

[2] A.Zugarramurdi and A.G. Borisov Phys. Rev. A **87**, 062902 (2013) or Z et al. Phys. Rev. A 88, 012904 (2013)

[3] H. Winter and A. Schüller Progress in Surface Science **86** 169ï 221 (2011)

* Corresponding author e-mail address: philippe.roncin@u-psud.fr

A COMPACT, LARGE AREA, TIME AND POSITION SENSITIVE DETECTOR FOR TIME OF FLIGHT MEASUREMENTS

M. Albaret, A. Husseen, S. Lupone, S. Damois, N. Briand, M. Debiossac, Z. Mu, S. Tall and P.Roncin

Institut des Sciences Moléculaires dôOrsay, Université Paris Saclay, CNRS-Université Paris-Sud, Orsay F-91400, France

Micro channel plate based position sensitive detectors are now widely used in atomic and molecular physics as well as in surface science [1-6]. Such detectors can be place in the focal plane of an electrostatic analyzer [1-3] or, for grazing incidence, it can be placed downstream to record the scattering profile [4-6]. In this later case, if the beam is pulsed, the arrival time provides energy loss spectra for each scattering angle and charge state [4].

Each detector is characterized by its performances in terms of spatial and time resolution but also by it geometric form factor as well as it compatibility to UHV conditions. The design presented here is UHV compatible and very compact offering a 40 mm diameter open area. With a 63CF to 40CF conical reducer it is designed to be mounted on DN40 tube for time of flight.

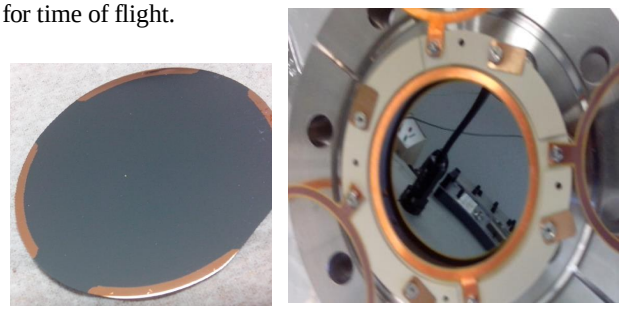

Figure 1: Left; Resistive anode made of high impedance 2ò silicon wafer with four collecting stripe of evaporated Cu. Right; Vacuum side view of the detector on its DN63CF flange. before mounting the MCP.

Recently, grazing incidence fast atom diffraction have shown to be bring simple and accurate informationôs both under static condition [5] and during growth [6]. In this later case the diffracted intensity is reduced because atoms, island and steps decorate the terminal layer each time a new layer is growing. Since the keV beam of atom is still present, some of the violent collisions with these obstacles can be used to provide chemical identification of the surface atoms by TOF analysis of the forward or backscattered particles. The larger the detector, the larger the collection efficiency. At variance a good mass resolution requires that the detector is small to limit kinematic aberration (the fact that peak position varies rapidly with the angle). The easy way to circumvent these antagonist requirements is to design a position sensitive detector. For UHV compatibility, we have decided to use high purity single crystal silicon wafer produced at few euro by the semi-conductor industry (fig. 1). To allow direct mounting of the detector on its flange the electrical feed troughs have been threaded before welding. Such short connections allow very easy decoupling of the high voltage immediately on the flange as well as a very clean timing signal without any ringing.

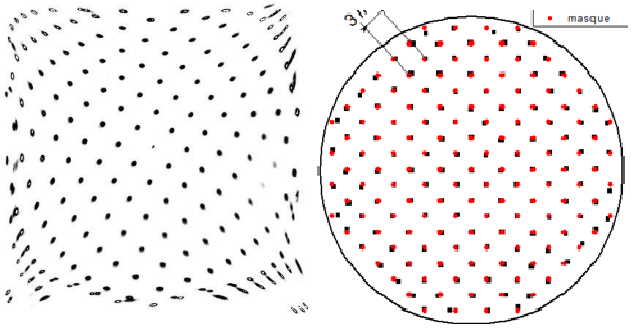

Figure 2: A mask with holes every 3mm is used to calibrate the detector. Aberrations are very important (left) but reduced after hyperbolic and polynomial corrections (right)

As shown on fig. 2, the main drawback of this compact design is that serious distortions are present close to the collection anodes. However a polynomial correction is applied online to correct for distortions (right hand side). We will present the key feature, the correcting algorithm and the final resolution and linearity after corrections.

Acknowledment. We are grateful to O. Jagutzki from Roentdek Gmbh for kindly giving us a circular glass anode with evaporated Ge to test our approach. We are also indebted to X. Fléchard for help in finding the correction algorithm. This work has been supported by Agence Nationale de la Recherche ANR-07-BLAN-0160.

REFERENCES

[1] C. L. Knibbeler *et al* Rev. Sci. Instrum. **58**, 125 (1987)
[2] M. Lampton and C. W. Carlson Rev. Sci. Instrum. **50**, p1093 (1979)
[3] P. Roncin *et al*. J. Phys. E Sci. Instrum **19**, 1 p37 (1986)
[4] P. Roncin *et al*. Phys. Rev. Lett. 89, 043201(2002)
[5] M. Debiossac *et al*. Phys. Rev. B 90, 155308 (2014)
[6] P. Atkinson, *et al* Appl. Phys. Lett. 105, 021602 (2014)

* Corresponding author e-mail address: philippe.roncin@u-psud.fr

Active correction of the tilt angle of the surface plane with respect to the rotation axis during azimuthal scan

M. Séréno, S. Lupone , A. Momeni A. Husseen, M. Debiossac, and P.Roncin

ISMO Université Paris Saclay, CNRS-Universitée Paris-Sud, Orsay F-91400, France

For grazing incidence observation, azimuthal rotation of the surface requires a very high mounting accuracy. For diffraction experiments, this is usually achieved with a goniometer. We present here a simple strategy to allow azimuthal scan of sample for which the positioning accuracy would otherwise prohibit such analysis.

Grazing incidence fast atom diffraction (GIFAD or FAD) has recently merged as a new surface science technique with very high surface sensitivity as well as high structural resolution. In this technique a beam of keV atoms impinges the surface at angles of incidence θ on the order of one deg. When the beam is aligned with a low index crystal direction, diffraction can take place, provided that the surface quality is good enough in terms of flatness and coherence length. First discovered with single crystal of ionic insulator [1,2] such as LiF, NaCl etc GIFAD has shown successful with metal [3], semi-conductors[4] and even molecular layers of alanine[5].

In this later case, diffraction is not as sharp as with bulk crystal or inorganic layer [6] probably because the molecular layers have more structural defects. Fortunately, triangulation technique [7] easily reveals the direction were the absorbed molecules align to each other and even faint diffraction signal is enough to derive the lattice parameter of the molecular organization [5]. It has also been suggested [8] that azimuthal scans could reveal the range of the interaction potential above the surface. These techniques however require azimuthal rotation of the surface, ideally without changing the angle of incidence. This turns out to be more tricky than expected since it is not straightforward to put a goniometer under UHV and most sample transfer systems as well as rotation devices do not allow for ultraprecise positioning of the sample. Most often the surface normal has a residual tilt angle Γ of the order of a degree with respect to the rotation axis. This is enough to prevent easy application of azimuthal scan.

If both the azimuthal and polar movement are motorized, an online correction is possible and is described in this contribution. The general problem is not complex and ray tracing or graphical software offer direct solution but extracting a simple analytic formula is not straightforward. To make things simpler we consider that the beam impacts the surface exactly on its intersection with the rotation axis. Since the detector is usually far away from the surface, this kind of far field approximation is fully justified. To simulate the correction outside vacuum, we have used a laser beam reflecting onto a polished silicon wafer acting as a perfect mirror and placed on top of a stepper motor. A second stepper motor is used to control the polar angle (to vary the angle of incidence θ). The reflected laser beam is imaged onto a screen at a distance L a few meters downstream and captured by a camera. Defining x, y as the coordinate on the screen, the ideal situation would be x=0 and y=L tan(2θ)~2.L.θ, both values independent of the azimuthal angle ϕ.

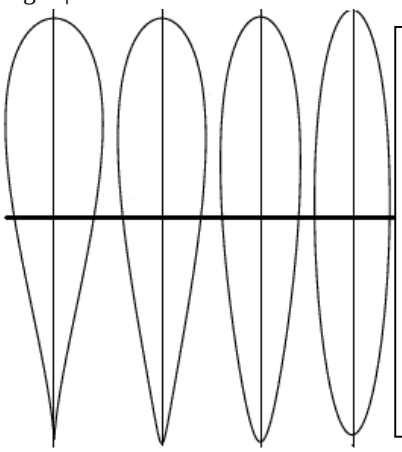

From left to right, the ratio of tilt angle Γ to incidence angle θ decreases from Γ/θ=1 to 0.1 approaching a perfect ellipse. Horizontal and vertical scales are different.

Figure 1: normalized trajectories of reflected beam..

When the tilt angle is in the scattering plane, it produces a drastic effect ; the effective angle of incidence goes from θ+Γ to θ–Γ. At variance when the tilt angle is perpendicular to the plane defined by the primary beam and the rotation axis, the effect is reduced and the impact position x is simply shifted by L. tanθ.tanΓ, typically 57.3 time smaller.

Two parameters are needed to apply a correction, the value of the tilt angle, and a reference azimuth angle. Both the equations, the strategy to measure these values and to apply the correction will be described.

REFERENCES

[1] P. Rousseau *et al*. Phys. Rev. Lett. **98**, 016104 (2007)
[2] A. Schüller *et al*.Phys. Rev. Lett. **98**, 016103 (2007)
[3] N. Bundaleski *et al* Phys. Rev. Lett. **101**, 177601 (2008)
[4] H. Khemliche *et al* Appl. Phys. Lett. **95**, 151901 (2009)
[5] J. Seifert *et al*. Phys. Rev. Lett. **111**, 137601 (2013)
[6] M. Busch *et al*. Phys. Rev. B **86**, 241402(R) (2012)
[7] R. Pfandzelter, T. Bernhard, and H. Winter, Phys. Rev. Lett. **90**, 036102 (2003)
[8] M. Debiossac & P. Roncin Phys. Rev. A **90**, 054701 (2014)

* Corresponding author e-mail address: philippe.roncin@u-psud.fr

IONOLUMINESCENCE AND MICROSTRUCTURAL CHANGES OF FUSED SILICA UNDER SWIFT ION IRRADIATION

R.Saavedra[1,*], *D. Jiménez-Rey*[1,2], *P. Martin*[1] *and R. Vila*[1]

[1] Fusion Materials Research Unit, National Fusion Laboratory, CIEMAT, Av Complutense, 40, 28040, Madrid, Spain
[2] Centre for Micro Analysis of Materials, Universidad Autónoma de Madrid, Cantoblanco, 28049, Madrid, Spain

1. INTRODUCTION

Optical and electrical properties of silica are strongly influenced by defects, which are introduced during the manufacturing process or produced by energetic photons (UV light, X-ray or γ ray) and/or particles (ions, electrons or neutrons) [1]. Optically polished samples of vitreous silica with different hydroxyl and impurity content were irradiated with high energy Si^{4+}, O^{4+} and He^{+} ions. The electronic excitation was the predominant process of energy transfer in these ion irradiations.

The ionoluminescence (IL) spectra were recorded during the irradiations, in order to study the evolution of different defects. Important changes in the spectra of the distinct silica grades were observed, particularly at low fluence.

2. EXPERIMENTAL

The samples used in this work were high purity fused silica with different OH content: KU1 (OH ~ 820ppm) and KS-4V (OH < 1ppm), known as highly radiation resistant and considered as reference materials in fusion reactors, and also a silica with higher metallic impurity content, Infrasil 301from Heraeus (Al ~ 20 ppm and OH < 8 ppm)

Samples were irradiated with high energy Si^{4+} (24.4 MeV), O^{4+} (13.5 MeV) and He^{+} (2.5 MeV) ions at various fluences (from 5 x 10^{12} to 1.6 x 10^{15} ions/cm^2). A copper mask defines a homogeneous irradiation area of 5x5 mm^2 and also avoids electrical discharges. Ion bombardment was performed at the Centre for Micro Analysis of Materials (CMAM) of the Autónoma University of Madrid using a 5 MV linear tandem accelerator, in the Standard beam line, at a vacuum of 10^{-4} Pa.

The ionoluminescence emission was collected and guided towards a compact spectrometer QE6500 (Ocean Optics Inc.) configured with a multichannel CCD array detector that could measure simultaneously the spectral range from 200 to 900 nm with an integration time of 3 s.

3. RESULTS

The main IL bands observed in the three silica grades are: 650nm (1.9 eV) red band related to NBOHC centers, 460 nm (2.7 eV) blue band, its origin can be attributed to oxygen vacancy defects ODC(II) and self-trapped excitons (STE) and another band at 540nm (2.3 eV) related to STE. The UV band at 280 nm (4.4 eV) was detected only under He ion irradiation. I301 samples exhibit at low fluences a 400 nm (3.1 eV) luminescence band, related to Ge ODC, this band disappears when fluence increase. An example of the measured IL spectra is shown in the figure 1.

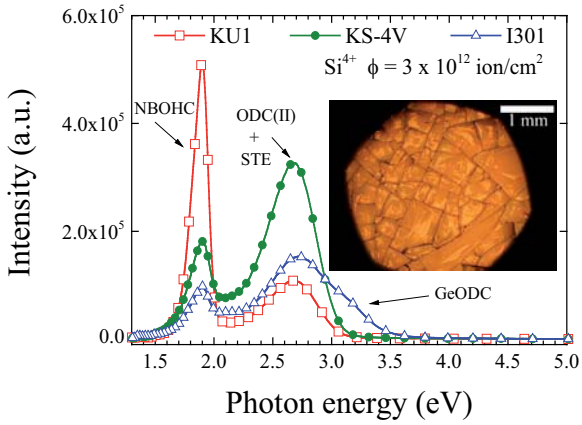

Figure 1. KU1, KS-4V and I301 ionoluminescence spectra for Si irradiation (fluence 3 x 10^{12} ion/cm^2). The inset shows a picture of cracked surface.

Macroscopic surface cracking was observed for O and Si irradiated samples at low fluence. However, no macroscopic cracks were detected when samples were exposed to higher fluence. Cracks were not detected after He^{+} irradiations. Cracks could be due to density fluctuations on nanometer length scale if the material is not completely covered by ion tracks.

A saturation of the optical absorption spectra of the Si and O irradiated samples with increasing ion fluence was measured [2], which can be due to point defects density saturation. The change in the surface structure of the irradiated face of silica samples was measured by means of IR reflectance spectroscopy.

4. REFERENCES

[1] G. Pachioni, L. Skuja and D. L. Griscom (eds.) *Defects in SiO_2 and Related Dielectrics: Science and Technology* Kluver Academic Publishers (2000).

[2] P. Martin, D. Jiménez-Rey, R. Vila, F. Sánchez and R. Saavedra, Fus. Eng. Design 89 1679-1683 (2014).

* Corresponding author e-mail address: rafael.saavedra@ciemat.es

RECENT RESULTS FROM THE ION BEAM LABORATORIES AT CLEMSON UNIVERSITY

C.E. Sosolik[1,*], *D.D. Kulkarni*[1], *D.A. Field*[1], *E.S. Srinadhu*[1], *D.B. Cutshall*[2], *W.R. Harrell*[2] *and J.E. Harriss*[1]

[1] Department of Physics and Astronomy, Clemson University, Clemson, South Carolina, USA
[2] Holcombe Dept. of Electrical and Computer Engineering, Clemson University, Clemson, SC, USA

1. INTRODUCTION

We present recent results obtained at Clemson University in the area of singly- and multiply-charged ion interactions with surfaces. For singly charged ions, measurements were made using a custom-built low-to-hyperthermal energy ion source, beamline, and target chamber centered around a Colutron ion source [1]. In the area of multiply-charged ions, we have a newly established facility that features a DREEBIT designed electron beam ion trap source which can produce decelerated beams for surface studies [2].

2. SINGLY CHARGED IONS

Utilizing both noble gas and alkali species, we have investigated radiation effects and ion-derived transport characteristics of insulating targets. These include the utilization of encapsulated insulators within metal-oxide-semiconductor (MOS) targets, which show that the energy loss of singly charged ions implanted near-surface give rise to below-surface oxide defects analogous to other energetic sources, e.g. UV radiation. In fact, for MOS structures, a superlinear dependence on ion impact energy is seen for interface states that are buried hundreds of Angstroms below the impacted surface (see Fig. 1) [3]. In the area of ion-derived transport, we have explored the geometric parameter space for keV energy ion transport through both metallic and insulating capillary structures. This spans the range of dimensions from macro-to-micro capillaries and also includes a novel approach based on an embedded electrode design. Finally, we have measured both ion scattering and charge exchange for alkali species from oxide surfaces that support well-defined metal nanostructures.

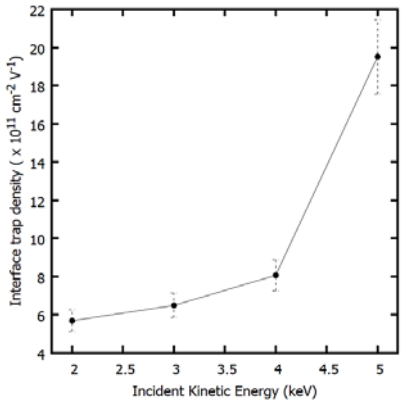

Figure 1: Interface trap density for an MOS structure irradiated by Na^+ ions.

3. MULTIPLY CHARGED IONS

With decelerated beams of multiply charged Argon ions, we have explored the effects of the ion potential energy on a range of material surfaces (insulators, metals, and polymers). An extension of our MOS results from singly charged ions is included here, where we find evidence for charge-state dependent energy loss in the capacitance-voltage signatures of each irradiated device (see Fig. 2). These results are compared directly with power law predictions for the stopping power of these ions. Also, we have explored the role of point defect formation in metallic and two-dimensional systems by measuring the low temperature resistance properties and surface topography of irradiated noble metal wires and graphene substrates. Finally, multiply charged ions have been used to modify polycarbonate substrates, where post-irradiation data obtained by contact angle and x-ray photoelectron spectroscopy reveal selective bond breaking that is charge-state dependent.

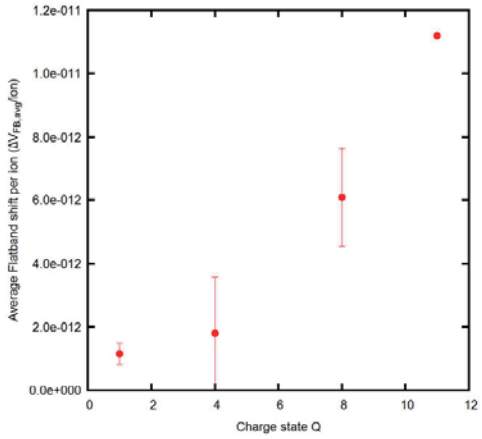

Figure 2: Normalized flat band shifts for Ar^{Q+} irradiated oxides obtained from MOS capacitance measurements.

4. REFERENCES

[1] M.P. Ray, R.E. Lake, S.A. Moody, V. Magadala, and C.E. Sosolik, Rev. Sci. Instrum. **79**, 076106(2008).

[2] R. Shyam, D.D. Kulkarni, D.A. Field, E.S. Srinadhu, D.B. Cutshall, W.R. Harrell, J.E. Harriss, and C.E. Sosolik, AIP Conf. Proc. **1640**, 129(2015).

[3] R. Shyam, D.D. Kulkarni, D.A. Field, E.S. Srinadhu, J.E. Harriss, W.R. Harrell, and C.E. Sosolik, IEEE Trans. Nucl. Sci., submitted and under review.

* Corresponding author e-mail address: sosolik@clemson.edu

TRANSMISSION OF ELECTRONS THROUGH INSULATING PET FOILS: CHARGE DEPOSITION, ANGULAR AND ENERGY DEPENDANCE

D. Keerthisinghe[1], *B. S. Dassanayake*[2], *S. Wickramarachchi*[1], *N. Stolterfoht*[3] *and J. A. Tanis*[1,*]

[1] Department of Physics, Western Michigan University, Kalamazoo, Michigan, 49008, USA
[2] Department of Physics, University of Peradeniya, Peradeniya, Sri Lanka
[3] Helmholtz-Zentrum Berlin für Materialien und Energie, D-14109, Berlin, Germany

1. INTRODUCTION

The transmission of electrons through insulating nanocapillaries was studied [1] following the landmark paper on the guiding of highly charged ions (HCIs) through insulating polyethylene terephthalate (PET) nanocapillaries [2]. In the present work the transmission of electrons through PET was studied as a function of the charge deposition, angular and incident energy dependences. It is found that self-organized charge patch formation guides electrons through PET similar to the way that HCIs are guided by PET [2].

2. EXPERIMENT

The present work was conducted for two different samples with 100 nm and 200 nm diameters and 5 x 10^8 and 5 x 10^7 pores/cm^2 densities, respectively. The first sample was studied for incident current densities ~1.5-4.2 nA/mm^2, while for the second sample densities of ~14-43 nA/mm^2 were used. The samples were mounted on a goniometer which was isolated from ground so that the current on the sample could be read directly. The detector (spectrometer) and the goniometer angles were measured with respect to the incident beam direction. The energy of the transmitted electrons was analyzed using an electron spectrometer that was stepped in voltage over the desired energy range.

3. RESULTS

Electron transmission depended on the charge deposited as shown by the results for 500 eV incident electrons in Figure 1a, where the transmission started after a time delay and increased rapidly afterwards. The small characteristic charge constant value, Q_c (rate of change of charge), at the smallest tilt angle (0.0^o) shows the rapid charge up at this angle. The larger values of Q_c for tilt angles away from zero (+0.3^o and -1.7^o) show that charge deposition increases more slowly at these angles. Measurements were also performed for the angular and incident energy dependence (not shown) [3]. Three different regions of the transmission, referred as *direct*, *transition and guiding* depending on the tilt angle, were observed as shown in Fig. 1b. These three regions result from the overlap, partial overlap and non-overlap of the exit and entrance openings of the capillaries in the foil sample as seen by the beam passing through. Transmission from these regions can be attributed to elastic and inelastic transmission giving rise to two peaks in the energy spectra for the transition region as seen in Fig. 1b. It has been found that inelastic transmission of electrons through insulating PET nanocapillaries is largely due to self-organized charge patch formation.

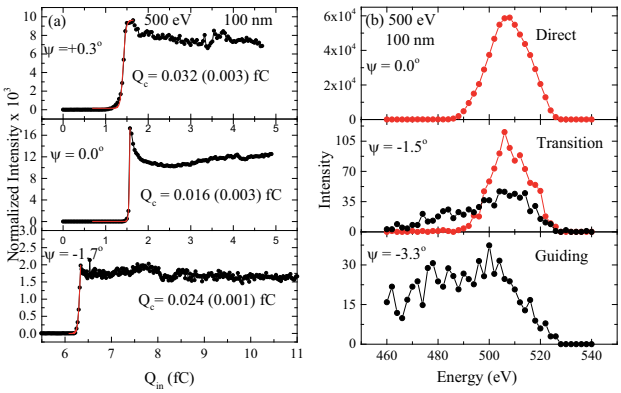

Figure 1: (a) Normalized intensity vs. charge entering per capillary (Q_{in}) at ψ = +0.3^o, ψ = 0.0^o and ψ = -1.7^o at 500 eV for the sample with 100 nm diameter capillaries. The red line represents the exponential growth function fitted to the fast rise of transmission and Q_c is the characteristic charge constant. (b) Energy spectra for selected sample tilt angles ψ = 0.0^o, -1.5^o and -3.3^o at 500 eV for the same sample. Red points represent the intensity for elastically transmitted spectra while black points represent the intensity of inelastically transmitted spectra.

4. REFERENCES

[1] S. Das, B. S. Dassanayake, M. Winkworth, J. L. Baran, N. Stolterfoht, and J. A. Tanis, Phys. Rev. A 76, 042716 (2007).

[2] N. Stolterfoht, J.-H. Bremer, V. Hoffmann, R. Hellhammer, D. Fink, A. Petrov, and B. Sulik, Phys. Rev. Lett. 88, 133201 (2002).

[3] D. Keerthisinghe, B. S. Dassanayake, S. J. Wickramarachchi , N. Stolterfoht, and J. A. Tanis, Phys. Rev. A (2015), to be published.

* Corresponding author e-mail address: darshika.keerthisinghe@gmail.com

INCIDENT ENERGY AND CHARGE DEPOSITION DEPENDENCES OF ELECTRON TRANSMISSION THROUGH A MICROSIZED TAPERED GLASS CAPILLARY

S. J. Wickramarachchi[1], T. Ikeda[2], B. S. Dassanayake[3], D. Keerthisinghe[1], and J. A. Tanis[1]

[1]Department of Physics, Western Michigan University, Kalamazoo, MI 49008, USA
[2] RIKEN Nishina Center for Accelerator Based Science, Wako, Saitama, 351-0198, Japan
[3]Department of Physics, Faculty of Science, University of Peradeniya, Sri Lanka

1. INTRODUCTION

Beam transmission through insulating capillaries has attracted intensive interest offering potential applications in surface modifications and biology [1]. This followed the discovery of slow (keV) ions guided through an array of nanocapillaries in a polyethylene terephthalate (PET) foil [2]. In this work we investigate the incident energy and charge deposition dependences of electron transmission through a single microsized tapered glass capillary.

2. RESULTS

Experimental measurements of 500 eV and 1000 eV (nominal energies) incident electron transmission through a glass capillary with inlet/outlet diameters of 800/100 µm were performed. The experimental setup has been previously described [3]. Electrons were transmitted for tilt angles up to ~6.5° and ~9.5° (measured laboratory angles) for 500 and 1000 eV, respectively.

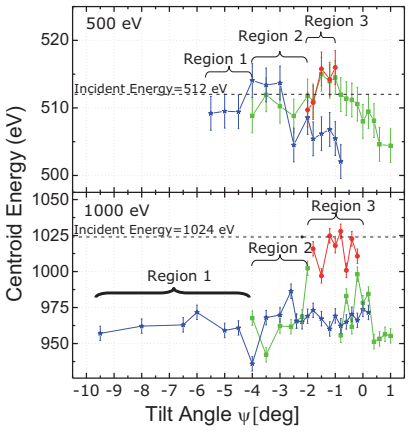

Figure 1: Centroid energy (obtained from associated energy spectra) vs. tilt angle for 500 and 1000 eV.

Figure 1 shows the results for the centroid energies of the transmitted electron spectra vs. the tilt angle. The centroid energies for 500 (actually 512) eV lie around the incident energy showing elastic transmission for all the tilt angles due to deflection by negative charge patches on the capillary wall. For 1000 (actually 1024) eV the transmitted electrons always had inelastic components (green and blue data points) for all the tilt angles. Moreover, for 1000 eV the red points show the events without energy loss corresponding to the transmitted electrons that do not touch the capillary wall. For both 500 and 1000 eV three transmission regions were identified in the angular beam profiles plotting the measured intensities vs. the observation angle (not shown). Region 3 consisted of three peaks in the profile that resulted from directly transmitted electrons as well as electrons scattered from the opposite walls of the capillary. Two peaks in the angular profile, referred to as Region 2, are produced by electrons scattered from the two sides of the capillary without directly transmitted electrons, while one peak occurs in Region 1 for the beam scattered only from one side of the capillary.

Figure 2 shows primarily elastic transmission for 500 eV and primarily inelastic transmission for 1000 eV as a function of the charge deposited into the capillary. The transmission intensity for 500 eV, after an initial quiet time, increased with a charge-up constant of ~67 nC following which transmission continued with infrequent intensity breakdowns up to ~450 nC when near complete blockage occurs. For 1000 eV the initial charge-up constant is ~3 nC followed by frequent breakdowns occurring for the entire studied range of incident charge into the capillary.

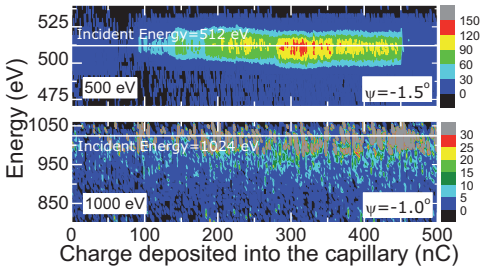

Figure 2: Energy vs. charge deposited into the capillary for 500 and 1000 eV, with color representing the intensity.

3. REFERENCES

[1] V. Mäckel, W. Meissl, T. Ikeda, M. Clever, E. Meissl, T. Kobayashi, T. M. Kojima, N. Imamoto, K. Ogiwara and Y. Yamazaki, Rev. Sci. Instrum. **85**, 014302 (2014).

[2] N. Stolterfoht, J. H. Bremer, V. Hoffmann, R. Hellhammer, D. Fink, A. Petrov, and B. Sulik, Phys. Rev. Lett. **88**, 133201 (2002).

[3] S. J. Wickramarachchi, T. Ikeda, D. Keerthisinghe, B. S. Dassanayake, and J. A. Tanis, Nucl. Instrum. Meth. Phys. Res. B **317**, 101 (2013).

* Corresponding author e-mail address: samanthi.j.wickramarachchi@wmich.edu

Nanostructure formation on CaF_2, Al_2O_3, c-SiO_2 and MgO single crystal surfaces by highly charged ions and swift heavy ions impact

Y. Y. Wang[1, 2,*], *C. Grygiel*[3], *I. Monnet*[3], *E. Gruber*[2], *H. Lebius*[3], *B. Ban d'Etat*[3], *J. R. Sun*[1], *Y. T. Zhao*[1], *Z. G. Wang*[1], *G. Q. Xiao*[1], *and F. Aumayr*[2]

[1] Institute of Modern Physics, Chinese Academy of Sciences, Lanzhou 730000, China
[2] Institute of Applied Physics, TU Wien, 1040 Vienna, Austria
[3] CIMAP-GANIL, CEA-CNRS-ENSICAEN-University of CAEN, F-14070 Caen, France

1. INTRODUCTION

Individual highly charged ions (HCI) in the keV energy regime are able to induce surface modifications on a nanometric scale [1]. Swift heavy ions (SHI) with kinetic energies in the MeV to GeV range can also induce severe structural modifications at the surface and in the bulk [2]. These modifications result from the deposition of potential energy carried by HCI in the topmost surface layers or from electronic energy loss of SHI along its trajectory. In both cases several keV/nm^3 are deposited within a few femtoseconds into the target's electronic system and subsequently transferred to the lattice atoms via electron-phonon coupling. This similarity between HCI and SHI was pointed out [1, 3] in order to establish a qualitative link between surface modifications by potential energy and electronic energy loss.

2. EXPERIMENTS AND RESULTS

2.1. Highly charged ion impact

In the energy range of a few MeV hillock formation on single crystal surfaces induced by highly charged heavy ions has recently been studied on the 320 kV highly charged ions physics platform in IMP-CAS. This study has shown an additive effect between depositions of kinetic energy and potential energy for surface nanostructure formation on CaF_2 [4].

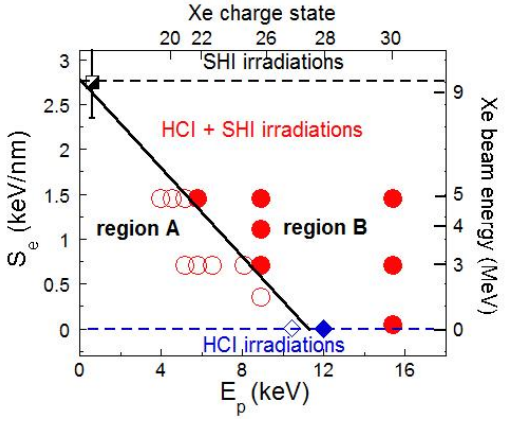

Figure 1: "Phase diagram" with potential energy (E_p) and electronic energy loss (S_e) (from ref. [4]).

2.2. Swift heavy ions impact

We have now extended these investigations to other insulating materials including Al_2O_3, c-SiO_2 and MgO single crystals. As a first step we have irradiated these materials by 100 MeV Pb ions delivered by the IRRSUD beamline at GANIL. The aim of these investigations is to find the S_e threshold for the SHI case. Unfortunately on several crystals the surface roughness or present surface contaminations prevented an unambiguous identification of ion-induced nanostructures. In these cases irradiation were also conducted under grazing angles of incidence. Surface tracks usually take the form of a chain of hillocks [5] and are therefore more easily to identify than single ion-induced hillocks under normal incidence. Our results for SHI irradiation of Al_2O_3, c-SiO_2 and MgO will be presented at the conference.

This work has been supported by the French-Austrian collaboration SIISU, co-financed by ANR (France, ANR-12-IS04-0005-01) and FWF (Austria, Project No. I 1114-N20), as well as by the French-Chinese cooperation project IiN by PICS-CNRS (France) and NSFC (China, No. 11411130112).

3. REFERENCES

[1] F. Aumayr, et al, J. Phys. Cond. Matt. **23**, 393001 (2011)
[2] M. Toulemonde, et al, Phil. Mag. A **58**, 799 (1988)
[3] A. El-Said, et al, Phys. Rev. Lett. **100**, 237601 (2008)
[4] Y.Y. Wang, et al, Sci. Reps. **4**, 5742 (2014)
[5] E. Akcöltekin, et al, Nature Nanotechnology **2**, 290 (2007)

* Corresponding author e-mail address: wangyuyu@impcas.ac.cn

EFFECTS OF SWIFT HEAVY ION IRRADIATION IN A FeSiNbZrB AMORPHOUS ALLOY

Jianrong Sun [1,*], *Zhiguang Wang*[2], *Yuyu Wang*[1], *Peng Song*[1], *Tianyu Deng*[1], *and Fashen Li*[2]

[1] Institute of Modern Physics, Chinese Academy of Sciences, Lanzhou, China
[2] Key Laboratory for Magnetism and Magnetic Materials of the Ministry of Education, Lanzhou University, Lanzhou 730000, China

Amorphous alloy (also known as metallic glass) is a kind of new alloy material synthesized by using modern rapid solidification metallurgical technology, owning excellent mechanical, physical and chemical properties that general metal and glass have. The unique glassy structure makes metallic glass have some high performances such as high strength, corrosion resistance, great ductility, and having a wide supercooled liquid region, etc. which usually belong to the high-quality magnetic functional materials, and hence showing enormous potential for development and application in the fusion reactor [1-3]. In this work, SHI irradiation as a kind of special non-equilibrium and exogenous energy deposition process will be applied to the study on modification of the structural and magnetic properties of the amorphous alloys.

Amorphous FeSiNbZrB alloy ribbons were prepared by melt spinning, and then the amorphous ribbons were irradiated at RT with 2.01 GeV Kr^{26+} ions for fluence range from 1×10^{11} to 1×10^{14} ions/cm^2 on the materials research terminal of the HIRFL-SSC (IMP, Lanzhou). X-ray diffraction (XRD), transmission electron microscopy (TEM), vibrating sample magnetometer (VSM), superconducting quantum interference device (SQUID) and mössbauer spectra (MS) were used to measure the structural and magnetic properties of the pristine and irradiated samples.

It's obviously that before and after SHI irradiation, such amorphous FeSiNbZrB alloy systems do not have a long-range order in atomic arrangement and exhibit only a short-range order. Under SHI irradiation at RT, local crystallization phenomenon of amorphous FeSiNbZrB alloy ribbons has been confirmed and formation of finer α-Fe(Si) phases precipitations with diameter of 1-2 nm has been observed. In addition, after irradiation, magnetic anisotropy considerably changes from its original in-plane direction. Possible mechanism of structural and magnetic properties modification after SHI irradiation is discussed briefly.

References

[1] A.L. Greer, Science 267 (1995) 1947.
[2] H.S. Barnard, Z.S. Hartwig, et.al., Fusion Engineering and Design 87 (2012) 248.
[3] J.R. Sun, Z.G. Wang, Y.Y. Wang, et.al., Nucl. Instr. Meth. B 307 (2013) 486.

* Corresponding author e-mail address: sunjr@impcas.ac.cn

A ballistic transport model for electron excitation energy induced by particle impact

S. Hanke, C. Heuser, B.Weidtmann and A.Wucher

University of Duisburg-Essen, 47048 Duisburg

1. INTRODUCTION

The electronic excitation following atomic particle bombardment can be experimentally observed in kinetic electron emission into the vacuum or, for instance, in internal electron emission in ion bombarded metal-insulator-metal junctions.

Whereas the physical mechanisms underlying the kinetically induced electronic excitation have been discussed in great detail in terms of electronic friction and hard binary collisions, by far less attention has been devoted to the transport of excitation energy away from the spot of its generation. In a series of works a we have in the past employed a nonlinear diffusion model using ad hoc diffusivity parameters describe secondary ion emission and external kinetic electron emission. Due to the fact, that the corresponding typical electron mean free path is larger than the standard simulation system volume, however, the validity of the diffusion model on the fs time scale of primary particle impact appears questionable [1].

Therefore, the present contribution aims at a more fundamental physical investigation of the transport characteristics of electronic excitations generated by the projectile at the very early stage of the cascade. In this context, the description of transport by means of the classical Boltzmann transport equation (BTE) constitutes a promising approach to tackle the problem of the relatively large electron mean free paths and the restriction of the diffusion model statistical equilibrium conditions.

Once the electron-electron scattering potential is determined, the BTE allows the calculation of temporal and spatial dynamics of the distribution function $f(k,r,t)$ for a given initial distribution of electron k-vectors. Different kinds of electronic excitations can be prepared by occupying selected k-states above the Fermi-level and be followed numerically solving the corresponding BTE. The aforementioned procedure is carried out for two different types of electronic excitation, namely

1. an initial set of k-vectors corresponding to a Fermi distribution at elevated electron temperature.
2. a ground state distribution complemented by “peak” excitation realized in form of a few occupied k-states with energies above Fermi-level (isotropic and anisotropic)

The calculation shows that the temporal evolution of the local distribution function can be approximated by a quasi-diffusive approach , even though the dynamics are caused by a combination of ballistic and collisional transport. The results are used to extract effective diffusivity parameters for comparison with the tacit assumptions formerly made in the diffusion model.

2. REFERENCES

[1] S. Hanke, A. Duvenbeck, C.Heuser, B. Weidtmann, D. Diesing, M. Marpe and A. Wucher, Nucl. Instrum.Meth. B. **303**, 55 (2013)

* Corresponding author e-mail address: adam.black@white.zz

HELIUM ATOM SCATTERING FROM GRAPHENE: TESTING THE PAIRWISE POTENTIAL ANSATZ

Asier Zugarramurdi[1,*], *Torbjörn Björkman*[2], *and Martti J. Puska*[3]

[1] COMP Centre of Excellence, Department of Applied Physics, Aalto University School of Science, P.O. Box 11100, FI-00076 Aalto, Finland

Graphitic surfaces are one of the most common systems for studying the interaction between He gas atoms and surfaces [1]. The corrugation of the equipotential surfaces of this interaction can, under proper conditions, produce the diffraction of He atoms. Nowdays two different scattering regimes are available where diffraction of atom projectiles can be observed: thermal energy helium atom scattering (HAS or TEAS) and grazing incidence fast atom diffraction (FAD or GIFAD) [2, 3]. Analysis of diffraction intensities in these techniques allows extraction of accurate information on the surface structure and dispersion forces.

Motivated by a recent joint experimental-theoretical study of the corrugation of graphene by GIFAD [4], we have further theoretically investigated the interaction potential between He and graphitic surfaces [see Figure 1(a)]. This potential is often represented as a pairwise sum:

$$V_{surf}(\mathbf{r}) = \sum_j V_{He-C}(\mathbf{r} - \mathbf{R}_j), \qquad (1)$$

where V_{He-C} is an effective He-C interaction potential contributing for each atom at $\mathbf{R}_j$. This ansatz has been very useful to obtain efficient descriptions of He-surface interactions. However, the interaction between the projectile and surface atoms is not pairwise additive, and thus *ab initio* approaches for the calculation of this interaction require full description of the surface. Even in that case, approximations to exchange-correlation (xc) energy functionals within density-functional theory (DFT) prevent accurate predictions of the dispersion forces. Indeed, as illustrated in Figure 1(b) for the He-C interaction potential, theoretical predictions strongly depend on the particular xc functional.

In our work we present *ab initio* DFT calculations of the interaction potential between He atom projectiles and corrugated graphene surfaces. Diffraction intensities are calculated with these potentials and compared to available experimental data in order to assess their quality. We focus on the transferability of the resulting pairwise potentials from the parameterization of Eq. (1) for different degrees of surface corrugation. Calculations are performed for several xc functionals, with special emphasis on those including corrections to the van der Waals interaction.

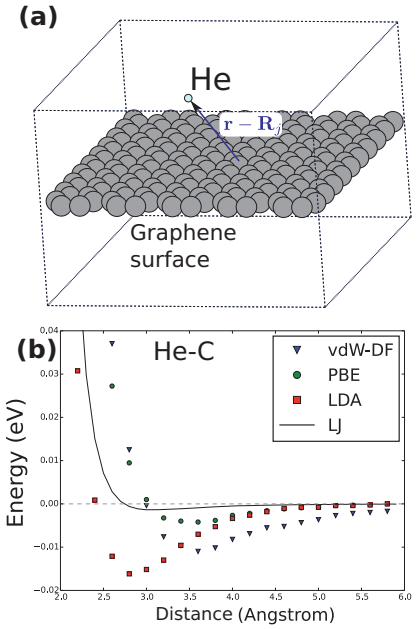

Figure 1: (a) The system under study: A helium atom on top of a graphene layer. (b) Calculated interaction potential between He and a C atom as function of the interatomic distance, for different exchange-correlation functional approximations (symbols). The solid line corresponds to the Lennard-Jones (LJ) pairwise potential [4] derived from He-graphite diffraction experiments.

1. REFERENCES

[1] H. Hoinkes, Rev. Mod. Phys. **52**, 933 (1980).

[2] A. Schüller, S. Wethekam, and H. Winter, Phys. Rev. Lett. **98**, 016103 (2007).

[3] P. Rousseau, H. Khemliche, A. G. Borisov, and P. Roncin, Phys. Rev. Lett. **98**, 016104 (2007).

[4] A. Zugarramurdi, M. Debiossac, P. Lunca-Popa, A.J. Mayne, A. Momeni, A.G. Borisov, Z. Mu, P. Roncin, H. Khemliche, Appl. Phys. Lett. **106**, 101902 (2015).

*Corresponding author e-mail address: asier.zugarramurdi@aalto.fi

DENSITY FUNCTIONAL THEORY STUDY OF NITROGEN ATOMS INTERACTIONS WITH A FE(111) SURFACES

M. A. Nosir[1,*], *Ludovic Martin Gondre*[2], *G. A. Bocan*[3], *and R. Díez Muiño* [1,4]

[1] Centro de Física de Materiales CFM/MPC (CSIC-UPV/EHU), Donostia-San Sebastián, Spain
[2] Institut UTINAM - University of Franche-Comté, Besançon, France
[3] CONICET and Centro Atómico Bariloche (CNEA), Argentina
[4] Donostia International Physics Center (DIPC), Donostia-San Sebastián, Spain

1. ABSTRACT

We present Density Functional Theory (DFT) calculations for the investigation of the structural relaxation of Fe(111), as well as for the study of the interaction of nitrogen atoms and molecules with this surface. We perform spin polarised DFT calculations using VASP (Vienna Ab-initio Simulation Package) code. We use the supercell approach and up to 19 slab layers for the relaxation of the Fe(111) surface. We find a contraction of the first two interlayer distances with a relative value of Δ_{12} = -21.7 % and Δ_{23} = -7.8 % with respect to the bulk reference. The third interlayer distance is however expanded with a relative change of Δ_{34} = 9.7 %. Early experimental studies of the surface relaxation using Low Energy Electron Diffraction (LEED) [1] and Medium Energy Ion Scattering (MEIS)[2] showed contradictory results, even on the relaxation general trend. Our current theoretical results support the LEED conclusions and are consistent qualitatively with other recent theoretical calculations [3, 4, 5]. In addition, we study the interaction energy of nitrogen atoms and molecules on the Fe(111) surface. Our results show that the bridge site with adsorption energy (5.6 eV) is the most favourable site for atomic adsorption. For the molecular case, we find two minima with similar adsorption energies corresponding to the nitrogen molecule perpendicularly adsorbed on top and hcp sites.

2. REFERENCES

[1] J. Sokolov, F. Jona and PM. Marcus, Phys. Rev. B **33**, 2 (1986).

[2] C. Xu and D.J. O'connor, Nuclear Instruments and Methods in Physics Research Section B: Beam Interactions with Materials and Atoms, **51**, 3 (1990).

[3] P. Błoński and A. Kiejna, Vacuum, **74**, 2 (2004)?

[4] P. Błoński and A. Kiejna, Surface science, **601**, 1, (2007) .

[5] Michelle JS Spencer, Andrew Hung, Ian K Snook, and Irene Yarovsky. Surface Science, **(513)2, 2002.**

*Corresponding author e-mail address: mohamed_ahmed@ehu.es

INVESTIGATION OF ELEMENTARY PROCESSES OF ION-SURFACE-INTERACTION AND HYDROGEN RETENTION IN FUSION-RELEVANT MATERIALS

H. R. Koslowski, M. Hellwig, Ch. Linsmeier*

Forschungszentrum Jülich GmbH, Institut für Energie- und Klimaforschung - Plasmaphysik, 52425 Jülich, Germany

1. INTRODUCTION

Present and future fusion experiments apply carbon, beryllium, tungsten, and reduced activation ferritic martensitic steel (e.g. Eurofer) as first wall materials [1, 2]. There is growing need to assess specific properties of these materials with respect to erosion and hydrogen retention. Ion beam experiments allow to investigate erosion and surface modification under well controlled conditions and complement studies on tokamaks and linear plasma devices.

2. EXPERIMENT

The UHV apparatus ALI (= **A**uger, **L**EED, **I**on scattering), formerly build and operated in IPP Garching, has been transferred to FZ Jülich and is presently under commissioning. Figure 1 shows a schematic view of the apparatus and the installed components.

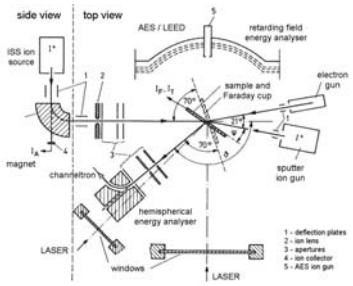

Figure 1: Schematic view of ion beam experiment ALI.

An experiment to study the effect of surface roughness on ion reflection has been performed using the mass selected ISS ion source and a specially constructed target holder with a titanium catcher foil [3].

3. INFLUENCE OF SURFACE ROUGHNESS ON ^{13}C ION REFLECTION FROM A W SURFACE

The investigation of castellated tungsten structure in the TEXTOR and DIII-D tokamaks has shown that deposited carbon is found only close to the plasma facing top surface. Very little deposition has been detected deep in the gaps. The roughness of the tungsten surface and its influence on sticking probability and angular distribution of scattered particles has been put forward as a possible explanation of the experimental findings. A dedicated experiment using a $^{13}C^{+}$ ion beam impinging under angles of $30°$ and $80°$ on tungsten samples with roughness R_a of $5.9\,\mathrm{nm}$ and $20.5\,\mathrm{nm}$ has been performed. The reflected ^{13}C atoms were collected on a titanium catcher foil and the relative amount of deposited ^{13}C has been analysed by SIMS. In addition, NRA measurements to quantify the remaining C content on the W targets have been done.

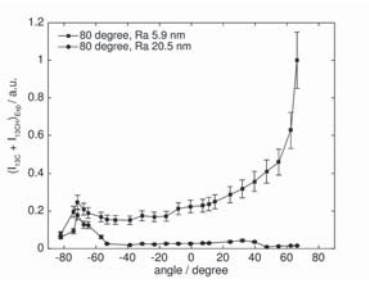

Figure 2: Angular distribution of scattered ^{13}C atoms from smooth and rough W surfaces [3].

The result for $80°$ incident angle (which corresponds to $-80°$ in the reference frame) is shown in figure 2. The angular distribution of particles scattered from the smooth surface shows a strong specular shape, but scattering from the more rough surface yields in a strong backscattering contribution. Since curves are normalised to NRA measurements and incoming fluence, the rough surface shows less reflection and higher sticking. Detailed modelling using the SDTrimSP code [4] is underway.

4. SUMMARY AND CONCLUSION

Ion beam experiment are well suited to perform well defined experiments on erosion and study detailed aspects in the field of plasma wall interaction. The reflection of ^{13}C atoms from rough surfaces has been measured. The angular distributions show large differences and it is doubtful if present codes will adequately reproduce the experimental results.

Acknowledgements. We thank Dr. R. A. De Souza and Ch. Schwab (Institut für Physikalische Chemie, RWTH Aachen) for the SIMS measurements.

5. REFERENCES

[1] G. Federici et al., Nucl. Fusion **41**, 1967-2137 (2001)
[2] J. Roth et al., J. Nucl. Mater. **454**, 1-6 (2014)
[3] M. Hellwig, PhD thesis, Ruhr-Universitt Bochum (in preparation)
[4] W. Eckstein et al., IPP-Report 12/3 (2007)

*Corresponding author e-mail address: h.r.koslowski@fz-juelich.de

ABSTRACTS

Wednesday 21st October 2015

TUNNELING AT SURFACES: ATOMIC PROJECTILES AND LOCALIZED PLASMONS.

A.G. Borisov

ISMO, UMR 8214 CNRS-Université Paris-Sud,
Bât 351, Université Paris-Sud, 91405 ORSAY Cedex, FRANCE

Electron tunneling between atomic and molecular species and metal surfaces is one of the central research subjects of the Surface Science. Indeed, not only electron capture and electron loss determines the charge fractions in the scattered/sputtered beams, but the efficiency of the electron transfer process is of paramount importance for the chemical reactions at surfaces. Too short lifetime of the excited state will harm the energy transfer between electrons and nuclei and therefore the reaction yields will be reduced. It is thus of paramount importance to be able to predict the tunneling rates, which implies development of parameter free approaches and comparison between experimental and theoretical data on the absolute scale.

In this respect experiments performed in grazing scattering geometry offer particularly well adapted playground because the projectiles are softly scattered from the topmost surface layer without violent collisions with surface atoms which might lead to eventual ionization/excitation. Another peculiarity of the grazing scattering geometry is the orders of magnitude difference between the speeds of the slow motion of the projectile perpendicular to the surface and fast motion parallel to the surface. The latter leads to the necessity of account for the dynamic effects (translational factors) between the electronic states of the metal and these of the projectile. All over, the projectile motion brings *dynamics* at the core of the problem, where the knowledge of the static properties of the system does not necessarily implies ability to predict the final results.

Over the years, the extremely high quality experimental data and original ideas provided by the group of Prof. H. Winter allowed elaboration of many theoretical concepts and approaches. (1) Parallel velocity assisted resonant and Auger electron transfer at metal surfaces; (2) Polarization of the light resulting from the electron capture at the excited projectile states; (3) The effect of the projected band structure; (4) Many-body aspects of the charge transfer for the open-shell projectiles; (5) Neutralization of the multi-charge ions and dynamic surface response; (6) Charge transfer processes at insulating surfaces of ionic crystals - this would be by far not complete list of the major advances in the field.

I my contribution I will show how these theoretical approaches and concepts developed in the context of the projectile/surface charge transfer can be used to address various aspects of the dynamics of excited states at pristine, nanostructured, and adsorbate coated surfaces. In this way we could provide parameter-free explanation for the results obtained in time-resolved two photon photoemission and scanning tunneling microscopy, i.e. in experimental conditions quite distant at first glance from the original grazing incidence of the projectile beams. The most recent examples of the importance of the electron tunneling at surfaces concern many-body electronic excitations (plasmons) in metal nanoparticle pairs. In this case, establishment of the tunneling currents between “superatoms” separated by the narrow junction leads to the marked change in the optical response of the system, as first predicted in Time Dependent Density Functional Theory Calculations and then confirmed experimentally.

Corresponding author e-mail address: andrei.borissov@u-psud.fr

IISC, IONS, AND SURFACES – THE FIRST FOUR DECADES

H. Winter[*]

Humboldt Universität Berlin, Institut für Physik, Newtonstr. 15, D-12489 Berlin, Germany

1. INTRODUCTION

In July 1976 a workshop on *Inelastic Ion-Surface Collisions (IISC)* was organized by N. Tolk and J.C. Tully at Bell Laboratories (Murray Hills, USA). This workshop with some ten participants became the starting point of a series of meetings which will face its 21st edition in Donostia/San Sebastian (Spain) from 18 to 23 October 2015. In the preface of the proceedings published in 1977 [1] one finds the statement: "There are a number of contributions on newly observed and in some instances controversial phenomena. These new topics include oscillations in the energy dependence of backscattered ions, wake riding states, or optical polarization effects from beam transmission through tilted foils and from particle bombardment of surfaces under grazing incidence. Clearly this area is in its infancy and holds great promise for equally dynamic and exciting growth in the future".

In looking back, one can state that these early judgments on the developments of the field were fully justified where the close interactions between experiment and theory played a paramount role.

2. GRAZING ION SURFACE SCATTERING

In this presentation we will discuss some specific topics on the interactions of atoms and ions with surfaces which came up over the years and which were also discussed on the IISC-meetings. In following first work on this issue presented already on the workshop at Bell labs in 1976 [1], we will focus on the scattering of ions from surfaces under a glancing angle of incidence, developed over the years to a powerful method for studies on the interaction mechanisms as well as an interesting surface analytical tool [2].

In this respect, we will discuss studies on the effect of the image charge in front of metal surfaces which modifies the trajectories of ions during the scattering process. A fairly spectacular effect is "skipping motion" predicted by Ohtsuki [3] and which was observed later on in experiments.

Image charge effects on trajectories played a crucial role in investigations on the interaction mechanisms of highly charged ions with surfaces [4] – a topic which was also treated at IISC meetings over the years – and in the quantitative understanding of the neutralization of He^+ ions in front of metal surfaces [5]. This topic dates back to the pioneering work of Hagstrum which was presented on the early IISC meetings [1].

The defined trajectories for grazing scattering can be exploited to study energy loss phenomena by a type of tomographic method [6] which was applied in detailed tests on theoretical predictions concerning the dependence of "Z_1-oscillations" as function of the density of an electron gas [7].

Further topics comprise the emission of electrons [8] and production of negative ions [9] during scattering of atomic projectiles from insulator surfaces, the observation of "Resonant Coherent Excitation"[10], studies on growth of ultrathin films [11], as well as high resolution atomic spectroscopy [12].

Finally we will outline some basic features and achievements on the recently observed quantum scattering of fast atoms from surfaces ("Fast Atom Diffraction") [13].

3. REFERENCES

[1] N. Tolk et al. (eds), *Inelastic Ion Surface Collisions* (Academic, New York, 1977).
[2] H. Winter, Phys. Reports **367**, 387 (2002).
[3] Y.H. Ohtsuki, K. Koyama, Y. Yamamura, Phys. Rev. B **20**, 5044 (1979).
[4] A. Arnau et al., Surf. Sci. Reports **27**, 113 (1997).
[5] R. Monreal, Prog. Surf. Sci. **89**, 80 (2014).
[6] K. Kimura, M. Hasegawa, M. Mannami, Phys. Rev. B **36**, 7 (1987).
[7] P.M. Echenique, R.M. Nieminen, R.H. Ritchie, Solid State Commun. **37**, 779 (1981).
[8] H. Eder et al., Phys. Rev. A **62**, 52901 (2000).
[9] C. Auth, A.G. Borisov, H. Winter, Phys. Rev. Lett. **75**, 2292 (1995).
[10] C. Auth et. al., Phys. Rev. Lett. **79**, 4297 (1997).
[11] Y. Fuji et al., Appl. Phys. Lett. **63**, 2070 (1993).
[12] A. Schirmacher, H. Winter, Phys. Rev. Lett. **69**, 257 (1992).
[13] A. Schüller et al., Phys. Rev. Lett. **98**, 016103 (2007); P. Rousseau et al., Phys. Rev. Lett. **98**, 016104 (2007).

[*] Corresponding author e-mail address: winter@physik.hu-berlin.de

Ions in Extreme UltraViolet lithography tools

M. van Kampen[1], *D. Smeets*[1], *A. Lassise*[1], *C. Berendsen*[1], *R. Hoekstra*[2], *J. Pijnenburg*[1]

[1] ASML, De Run 6501, 5504 DR, Veldhoven, The Netherlands
[2] ARCNL, Science Park 102, 1098 XG Amsterdam, The Netherlands

1. INTRODUCTION

To enable the continuing shrink of semiconductor devices ASML has developed lithography systems operating in the Extreme UltraViolet (EUV), at a wavelength of 13.5 nm. This huge step from the current standard of 193 nm pushes down the diffraction-limited feature sizes that can be printed on wafers. The step to the EUV regime comes with challenges, amongst others the generation and the transport of this ionizing radiation.

1.1. EUV SOURCE

Current high power EUV sources are based on a Laser-Produced Plasma (LPP) of tin [1]. Highly ionized tin ions (7^+ - 12^+) show line emission around 13.5 nm, allowing for a reasonably efficient conversion of laser energy into a band around 13.5 nm [2]. A typical source layout is shown in Figure 1. Tin fuel is injected in the form of small droplets that are subsequently irradiated by a ~20 kW pulsed laser. The EUV radiation emitted by the illuminated droplet is collected by a parabolic mirror and reflected towards the scanner part of the lithography tool.
An LPP emits not only radiation, but also energetic, keV ions, c.f. Figure 2. Without mitigation, these ions sputter and implant in the collector mirror, rapidly degrading its performance: a tin layer of only 1 nm reduces the reflectivity already by ~20%. As mitigation measure, hydrogen gas is injected at low pressure. Tin ions collide with the buffer gas, loose energy and charge, and eventually thermalize. The thermalized ions are flushed away by the hydrogen flow. Energetic ions will, however, exert a force on the gas and cause strong heating. This changes the flow profile and gas density, affecting the mitigation scheme.

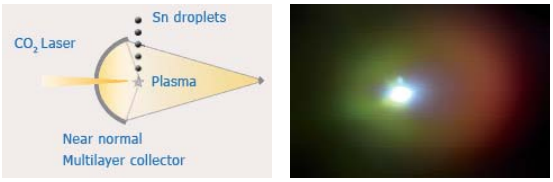

.

Figure 1: Left: schematic representation of a LPP EUV source. Right: Visible emission from a LPP tin plasma in a hydrogen atmosphere (laser from right). Red emission from H_α, green emission from Sn.

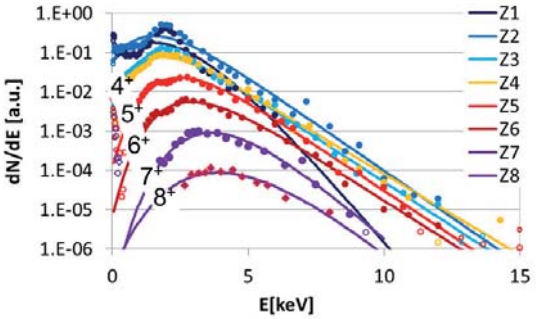

Figure 2: Charge-resolved tin ion energy spectrum from a laser-produced plasma using a 1 μm drive laser.

Measuring and modeling these dynamic ion-gas interactions is a challenging task.

1.2. EUV-INDUCED PLASMA

EUV radiation is strongly absorbed by matter, including low pressure gasses. With an energy of 92 eV the photons have ample energy to ionize the gas and create energetic photo-electrons. The resulting EUV-induced plasma is dense enough [3] to affect materials. For example, carbon can be etched from EUV mirrors by EUV-generated hydrogen ions [4].

2. This talk

In this talk I will discuss the challenges imposed on EUV lithography tools by ions. Specifically, I will address ion-gas and ion-mirror interactions in the tin-based laser-produced plasma EUV source, and the interaction of the secondary EUV-induced hydrogen plasma with its environment.

3. REFERENCES

[1] A. A. Schafgans *et al.*, Proc. of SPIE Vol. 9422 94220B-1
[2] J. White *et al.*, J. of App. Phys. 98, 113301 (2005)
[3] R. M. van der Horst, J. Beckers, S. Nijdam, and G. M. W. Kroesen, J. Phys. D: Appl. Phys. 47 (2014) 302001
[4] A. Dolgov *et al.*, Phys. D: Appl. Phys. 47 065205

* Corresponding author e-mail address: maarten.van.kampen@asml.com

IMAGING MASS SPECTROMETRY IN FORENSIC SCIENCE – NEW TOOLS, NEW APPLICATIONS

Melanie Bailey[1], Catia Costa[1], Tara Salter[2], Marcel de Puit[3,4], and Roger Webb[1]

[1] University of Surrey, Guildford, Surrey, GU2 7XH, UK
[2] National Physical Laboratory, Teddington, TW11 0LW, UK
[3] Netherlands Forensic Institute, The Hague, The Netherlands
[4] Delft University of Technology, Delft, The Netherlands

Imaging mass spectrometry techniques have been used sparingly in forensic investigations, despite their potential to provide unique information about certain types of sample. In this presentation, we will demonstrate how secondary ion mass spectrometry (SIMS) and desorption electrospray ionisation (DESI) (which also uses a beam of charged particles to generate ions from the sample) can be used for the chemical imaging of fingerprints, and how this may be used to give new evidence in casework such as visualising undeveloped fingermarks, determining the deposition order of fingerprints and inks on documents and determining drug use from a fingerprint. We will also present new results, showing the potential for MeV-SIMS (a technique being developed at Surrey, which provides micron scale imaging under ambient conditions) in forensic investigations.

* Corresponding author e-mail address: adam.black@white.zz

DYNAMICAL STUDIES OF OPTOELECTRONIC MODIFICATION ARISING FROM HEAVY ION INDUCED POINT DEFECTS USING COHERENT ACOUSTIC PHONONS

N. H. Tolk[1,*], H. Krzyzanowska[1]. A. Baydin[1] and L. C. Feldman[2]

[1] Department of Physics and Astronomy, Vanderbilt University, Nashville, TN, USA
[2] Inst. for Advanced Materials, Devices and Nanotechnology, Rutgers University, Piscataway, NJ, USA

We have applied coherent acoustic phonon spectroscopy to the characterization of ion-irradiated GaAs, [1] diamond, [2] and silicon [3] specimens to determine the implantation-induced modulation of the opto-electronic properties of these materials as a function of depth.

In semiconductors, point defects play a critical role in the performance of electrical devices. Such effects become increasingly important as size scales approach the order of tens of nanometers or less, where single defects can affect a significant fraction of the material and the "local" influence of a single defect may significantly alter the entire device performance. Under these circumstances it is extremely important to identify both the location and concentration of defects as well as their effect on the local electronic structure. Traditionally, either optical or ion beam analysis methods have been used to characterize point defect distributions. On one hand, while optical methods can deliver information regarding the average electronic structure, depth-dependent information is typically lost in measurement. Ion beam analysis, while providing some depth resolution, creates damage in a sample similar to that which is being studied. Scanning or transmission electron microscopy can be useful in characterizing local electronic structures, though they are destructive techniques and unsuitable for *in situ* experiments.

To overcome these disadvantages, we have demonstrated the use of a novel application of an ultrafast pump-probe technique perfectly suited for *simultaneous* measurement of depth-dependent defect concentrations and their effect on local electronic structure. This technique, known as coherent acoustic phonon (CAP) spectroscopy or picosecond ultrasonics [1–3] is employed to generate and monitor a picosecond strain wave which transiently modifies the material as it passes through a substrate of interest. The resulting time-resolved optical response is highly sensitive to local changes in a material's photoelastic constant. By deploying a probe pulse to monitor the strain wave as it travels (at the longitudinal speed of sound), the sample is effectively probed layer by layer as a function of depth.

Here we present data wherein CAP studies are carried out on GaAs wafers exposed to varying levels of He^+ irradiation [1]. Similar studies have been carried out on diamond and silicon samples. [2,3]. The irradiation creates a strongly depth-dependent damage profile whose dominant species types are vacancy and self-interstitial point defects. Generally, defects may modify the ideal GaAs electronic structure by opening deep-level defect states and causing strain-induced band-tailing effects. Thus, in regions where defect populations exist, local electro-optical properties are modified, and the photoelastic constants become strongly non-linear [7,8] and extremely sensitive to the presence of defects. This effect allows quantitative measurement of the depth-dependent total defect concentration caused by the radiation in the GaAs sample. Our measurements extend over four orders of magnitude in defect concentration, and provide a tabletop method for non-invasive and non-destructive defect characterization, which is two orders of magnitude more sensitive than any other method. Comparison with TRIM code simulations show excellent agreement in the full-width, peak depth, and estimated concentration as shown in Figure 1 below.

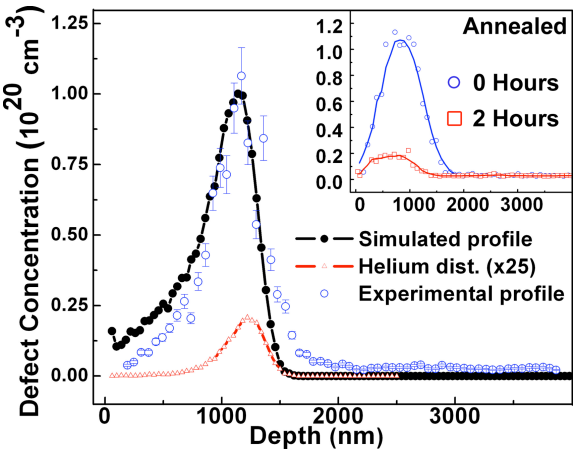

Figure 1: Defect concentrations arising from He+ implanted GaAs, obtained experimentally using CAP compared to TRIM code simulations.

The fact that materials may be transiently strained by the CAP wave suggests that, in addition to characterization, using ultrafast laser pulses, we can selectively deliver energy in a spatially and temporally localized manner as a function of depth. We will discuss the implications of this for (a) non-thermal localized permanent material modification and (b) studies of the dynamics of high electronic energy density relaxation paths and rates far from equilibrium.

We acknowledge financial support through the Department of Energy and from the Army Research Office.

REFERENCES

[1] A. Steigerwald, A. B. Hmelo, K. Varga, L. C. Feldman, and N. Tolk, J. Appl. Phys. **112**, 013514 (2012).

[2] J. Gregory, A. Steigerwald, H. Takahasi, A. Hmelo, and N. Tolk, Applied Physics Letters 101, 181904 (2012)

[3] H. M. Lawler, A. Steigerwald, J. Gregory, H. Krzyzanowska and N. H. Tolk Materials Research Express 1 (2014) 025701

* Corresponding author e-mail address: norman.tolk@vanderbilt.edu

HIGHLY CHARGED IONS IMPACT, A PROMISING ROUTE TO EXPLOIT THE REFRIGERATION POWER OF GIANT MAGNETOCALORIC THIN FILMS

M. Trassinelli[1,*], *M. Marangolo*[1], *L. Bernard-Carlsson*[1], *S. Cervera*[1], *M. Eddrief*[1], *V.H. Etgens*[1], *V.Gafton*[1,2], *S. Hidki*[1], *E. Lamour*[1], *A. Lévy*[1], *S. Macé*[1], *C. Prigent*[1], *J.-P. Rozet*[1], *S. Steydli*[1], *Y. Zheng*[1] *and D. Vernhet*[1]

[1] CNRS, UMR 7588, Institut des NanoSciences de Paris (INSP), 4 Place Jussieu, 75005 Paris, France
Sorbonne Universités, UPMC Univ. Paris 06, INSP, UMR 7588, F-75005 Paris, France
[2] *Alexandru Ioan Cuza University, Faculty of Physics, 11 Carol I Blv, Iasi 700506, Romania*

1. INTRODUCTION

Conventional magnetic materials heat up when they are placed in a magnetic field and cool down when they are removed. This phenomenon is known as the magnetocaloric effect (MCE). The discovery of compound with a giant magnetocaloric effect (GMCE) close to room temperature pushed the development of magnetic refrigeration as an environmentally friendly and energy-efficient technology alternative to gas compression refrigeration commonly employed for everyday applications. Up to now, the practical application of GMCE materials is blocked by the fact that these compounds are also characterized by a magnetic transition of first-order. This type of transition suffers intrinsically from large thermal hysteresis making their use in thermal machine inefficient. In the last decades many but mostly vane efforts have been explored (doping, external constrains, etc.) [1–3] for eliminating the thermal hysteresis keeping the GMCE properties. Here we present a new approach based on slow highly charged ions interacting with a GMCE thin film resulting in the successfully suppression of the thermal hysteresis without affecting the other material properties.

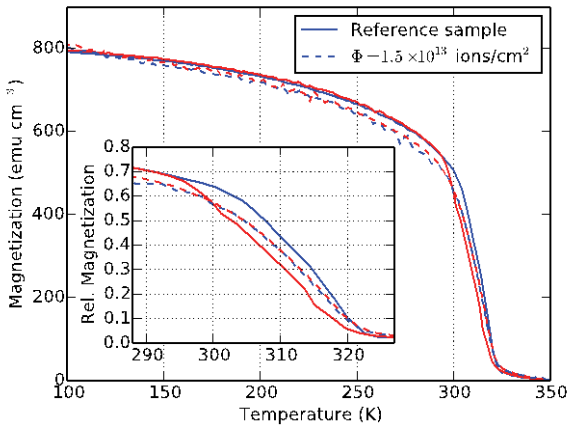

Figure 1: (color online) Magnetization as a function of temperature for the reference (solid lines) and for the irradiated samples (dashed lines). Data obtained by a temperature increase (from colder temperatures) and decrease (from hotter temperatures) are presented in blue and red, respectively.

2. EXPERIMENT, RESULTS AND DISCUSSION

The thin film considered here is composed by MnAs produced by molecular beam epitaxy on a Ge(100) substrate. MnAs is characterized by a GMCE associated to its phase transition close to room temperature (fig. 1) and is one of the most promising candidates for magnetic refrigeration. The ion irradiation is performed at the slow highly charged ion beam facility SIMPA [4] where samples are irradiated with Ne^{9+} at E_{kin} = 90 keV (v = 0.4 a.u.). After irradiation, thin films magnetic and structural properties are characterized by X-ray diffraction, Magnetic Force Microscope and SQUID magnetometer to reveal which properties are modified or not. As main effect, the ion irradiation suppress completely the thermal hysteresis on the MnAs thin film. As small grains of dust in a glass of champagne, the defects induced by the ion impact act as seeds for the nucleation of one phase with the other during the transition. Consequently, facilitating the transformation from one phase to the other, the thermal hysteresis is entirely suppressed (fig. 1, dashed lines) whereas other structural and magnetic properties are only slightly affected. In particular, the large refrigeration power of MnAs thin films related to GMCE is preserved [5]. At present, we extend our investigations to different collision conditions (ions type and kinetic energy) and to other type of samples exhibiting GMCE for providing new insights on the full understanding on the thermal hysteresis suppression mechanism (see also [6]).

Acknowledgments

This work was partially supported by French state founding ANR-11-IDEX-0004-02 and by the Romanian strategic grant POSDRU/159/1.5/S/137750.

3. REFERENCES

[1] B.G. Shen, J.R. Sun, F.X. Hu, H.W. Zhang, and Z.H. Cheng, Adv. Mater. **21**, 4545-4564 (2009)
[2] J. Liu, T. Gottschall, K.P. Skokov, J.D. Moore, and O. Gutfleisch, Nature Mater. **11**, 620-626 (2012)
[3] X. Moya, L.E. Hueso, F. Maccherozzi *et al.*, Nature Mater. **12**, 52-58 (2013)
[4] A. Gumberidze, M. Trassinelli, N. Adrouche *et al.*, Rev. Sci. Instum. **81,** 033303-10 (2010)
[5] M. Trassinelli, M. Marangolo, M. Eddrief *et al.*, Appl. Phys. Lett. **104**, 081906 (2014)
[6] S. Cervera, M. Trassinelli *et al.*, contribution to IISC-21 (2015)

* martino.trassinelli@insp.upmc.fr

ABSTRACTS

Thursday 22nd October 2015

Tungsten as Plasma Facing Material: Hydrogen Transport Studies and Defect Creation

T. Schwarz-Selinger[1,*], *J. Bauer*[1], *S. Markelj*[2], *A. Manhard*[1], *and K. Schmid*[1]

[1] Max-Planck-Institut für Plasmaphysik, Boltzmannstrasse 2, D-85748 Garching, Germany
[2] Jožef Stefan Institute, Jamova cesta 39, 1000 Ljubljana, Slovenia

1. INTRODUCTION

Tungsten is successfully applied in present day tokamaks such as ASDEX Upgrade and JET as armor material for the plasma-wetted areas [1, 2]. Besides its resilience against erosion by energetic particles and high melting point, the low uptake of hydrogen isotopes makes tungsten the material of choice also for the high-heat-flux areas of the international fusion experiment ITER as well as a promising candidate for a future fusion demonstration power plant DEMO. While for present-day devices as well as for ITER hydrogen retention and transport will be of minor concern [3] extrapolation to DEMO is not easily possible. Despite decades of work by many research groups theoretical understanding of hydrogen transport in tungsten is still incomplete. Because the heat of solution of hydrogen in the tungsten lattice is positive, the solubility in defect free material is extremely low. In practice transport and retention of hydrogen in tungsten is governed by defects such as vacancies, dislocations or grain boundaries as well as impurities where hydrogen can be trapped. The concentration of traps depends on the material grade as well as on the thermal treatment. In addition, defects will be created close to the surface by eV-keV particle bombardment during plasma exposure. As a consequence the scatter in the experimental data is still large. Besides intrinsic and plasma-induced defects, in a future thermonuclear fusion device displacement damage will be created throughout the tungsten bulk by MeV neutrons [4]. Because hydrogen isotopes will be trapped by these additional defects diffusive transport will slow down but retention will increase.

In this talk the present status of hydrogen retention in different tungsten materials will be reviewed with a special emphasis on the influence of defects created at the very surface and in the bulk. Dedicated small scale laboratory experiments will be shown that allow to reveal the influence of defect density and plasma loading parameters on hydrogen retention [5].

Until very recently only mono isotopic experiments (mostly deuterium) were reported in literature, which only yield the final state but not the underlying dynamics. In this presentation in-situ isotope exchange experiments will be presented that allow to benchmark existing codes by also revealing the trapping/de-trapping dynamics. In a recent work it was shown that isotope exchange is an important tool for the understanding of hydrogen diffusion, retention and release in general [6]. It demonstrates that hydrogen transport is a sequence of trapping, de-trapping and diffusion events. It will be shown that common diffusion trapping models which are successful in predicting transport for typical mono isotopic ion implantation and thermal degassing experiments fail at describing experiments on isotope exchange at low temperatures. A novel approach is briefly introduced which is based on fill-level-dependent de-trapping, where each trap site can contain an integer number of hydrogen atoms and the de-trapping energy depends on the current fill level [7].

In order to study hydrogen transport and retention in defect rich material, defects are deliberately prepared by implantation of MeV ions. Implantation of heavy ions causes dense cascades which resemble those created by neutron irradiation. Tungsten self-implantation is used as a proxy for neutron-damaged materials as it adds no additional impurity. Exposure of this so-called self-damaged tungsten to low flux, low energy D plasma or D atom beams allows to characterize these defects as well as to test existing D transport parameters for both mono-isotopic as well as hydrogen-deuterium isotope exchange experiments.

REFERENCES

[1] R. Neu et al.: “Overview on plasma operation with a full tungsten wall in ASDEX Upgrade”, J. Nucl. Mater. 438, S34 (2013).
[2] L. Horton and JET EFDA contributors: “The JET ITER-Like Wall Experiment: First Results and Lessons for ITER”, Proceedings of the 28th Symposium on Fusion Technology SOFT, San Sebastian, (2014) to be published.
[3] J. Roth et al., “Recent analysis of key plasma wall interactions issues for ITER”, J. Nucl. Mater., Vol. **390-391**, No. 1, (2009).
[4] M. Shimada et al.: “Irradiation effect on deuterium behaviour in low-dose HFIR neutron-irradiated tungsten”, Nucl. Fusion **55,** 013008 (2015).
[5] A. Manhard, PhD thesis, University of Augsburg, Germany 2012.
[6] J. Roth et al.: „Hydrogen Isotope Exchange in Tungsten: Discussion as Removal Method for Tritium“. J. Nucl. Mater. **432**, 341 (2013).
[7] K. Schmid et al: “Transport of hydrogen in metals with occupancy dependent trap energies”; J. Appl. Phys **116** 134901 (2014).

This work has been carried out within the framework of the EUROfusion Consortium and has received funding from the Euratom research and training programme 2014-2018 under grant agreement No 633053. The views and opinions expressed herein do not necessarily reflect those of the European Commission.”

* Corresponding author e-mail address: thomas.schwarz-selinger@ipp.mpg.de

SURFACE MORPHOLOGIES OF HE-IMPLANTED TUNGSTEN

M. E. Bannister[1,*], *H. Hijazi*[1], *F. W. Meyer*[1], *K. A. Unocic*[2], *L. M. Garrison*[2], *and C.M. Parish*[2]

[1] Physics Division, Oak Ridge National Laboratory, Oak Ridge, TN 37831-6371, USA
[2] Materials Science and Technology Division, Oak Ridge National Laboratory, Oak Ridge, TN, USA

1. INTRODUCTION

Tungsten, with its high melting point, low sputtering yield, and low tritium retention rate, is the leading candidate for plasma facing material in next-generation fusion reactors. However, high-flux irradiation of tungsten surfaces by He ions at temperatures typical of burning reactors can induce significant morphological changes, including the formation of nano-fuzz [1]. Using experimental capabilities unique to our laboratory, tungsten targets were exposed to high fluxes of He ions ranging in energy from 200 eV to 200 keV and their surface morphologies were investigated using electron microscopy. To gain insight into the mechanisms for these changes, we also measured thermal desorption spectra for He after implantation in the tungsten targets.

2. EXPERIMENTAL

Helium ion beams were produced by two ECR ion sources, one installed on a 250-kV platform yielding ion energies up to 500 keV He^{2+}. The second ECR ion source is equipped with a custom deceleration section [2] to achieve He-ion energies down to 200 eV while maintaining fluxes exceeding $2x10^{16}$ cm^{-2} s^{-1}, needed for nano-fuzz formation [3]. Flux-mapping of the ion beams permits correlation of surface morphology changes to varying ion fluxes in a single exposure [4]. High-purity polycrystalline tungsten samples were positioned in the ion beams using triple-axes manipulators, and heated up to 1500 C using electron-beam heaters.

Thermal desorption spectra for helium were measured using a residual gas analyzer tuned to mass 4. The parameters of the heater controller were adjusted to ensure a linear ramp of the sample temperature from 200 C to 1150 C. The spectra were made absolute by comparing the desorption measurements to the RGA signals for a calibrated He leak.

3. RESULTS

Figure 1 shows SEM and FIB/SEM images of polycrystalline W after exposure to 218-eV (top images) and 100-keV (bottom images) He^+ ions with fluxes exceeding 10^{16} cm^{-2} s^{-1}. The 218-eV ions are below the displacement damage threshold for W, whereas the 100-keV ions create significant damage to the W lattice, producing additional trapping sites for the He atoms. For this reason, the minimum flux required for the production of nano-fuzz is lower for the 100-keV ions.

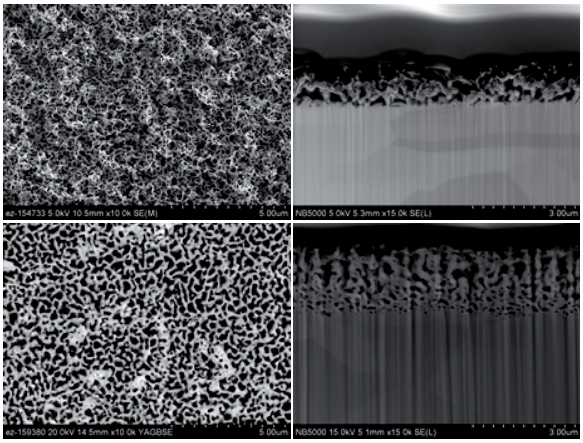

Figure 1: SEM and FIB/SEM images of W surfaces after exposure to 218-eV (top) and 100-keV (bottom) He^+ ions.

Thermal desorption spectroscopy is being employed to investigate the mechanisms driving the changes in the W surface morphologies, seeking to understand and differentiate the helium nucleation processes in both the low- and high-energy implantation regimes, including the role of damage induced by the implantation of He ions for energies above the displacement damage threshold.

4. REFERENCES

[1] M. J. Baldwin and R. P. Doerner, Nucl. Fusion **48**, 035001 (2008).
[2] H. Hijazi and F. W. Meyer, Rev. Sci. Instrum. **84**, 033305 (2013).
[3] F. W. Meyer *et al.*, Proceedings of PFMC-15 (to be published).
[4] M. E. Bannister *et al*, Nucl. Instrum. Methods Phys. Res. **B339**, 75 ((2014).

Research sponsored by the LDRD Program of Oak Ridge National Laboratory, managed by UT-Battelle, LLC, for the US Department of Energy, and the DOE Office of Fusion Energy Sciences. SEM and FIB/SEM instruments supported by Oak Ridge National Laboratory's Shared Research Equipment (ShaRE) User Program, which is sponsored by the Office of Basic Energy Sciences, U.S. Department of Energy.

* Corresponding author e-mail address: bannisterme@ornl.gov

THE ROLE OF THE ADATOMS DIFFUSION IN THE TUNGSTEN FUZZ GROWTH

D. Trufanov[1], *E. Marenkov*[1,*], *and S. Krasheninnikov*[1,2]

[1] National research nuclear university MEPhI, Russia
[1,2] University of San Diego, USA

Tungsten (W) is considered as a primary candidate material for high heat load plasma-facing components in the next generation magnetic fusion devices, in particular ITER. Being a high-Z material W demonstrates very low sputtering under plasma bombardment and has one of the highest melting temperatures among metals. At the same time, plasma irradiation causes its modification, creating lattice defects, changing surface morphology etc. It was experimentally observed that filamentary nano-structures, called fuzz, can grow on W surfaces irradiated with plasma containing helium. Necessary conditions for the formation of fuzz are the bombardment by He^+ ions with energies above 20 – 30 eV and the target surface temperature within 1000 – 2000 K. A morphological modification of plasma-facing materials due to the fuzz growth can provoke intensive erosion due to arcs formation, surface overheating and other processes. Therefore, understanding of the fuzz growth process is of significant practical interest.

However, the physical mechanism of the fuzz growth is not completely clear. Recent experiments at PISCES linear simulator have shown, that there is a stage in fuzz formation, when the length of the fibers increases, while their mass remains constant. This "thinning" of the fuzz fiber can be associated with surface diffusion of W atoms. It was proposed in [1] that helium irradiation, although incapable of real surface sputtering due to very low energy of incident ions, weakens surface atoms bonds, leading to formation of adatoms. Movement of the adatoms along the surface can be responsible for fiber prolongation. Nevertheless, such diffusion is possible in both directions: towards the top or bottom of the fiber. Only if there is an external force making movement towards the top preferential, the fiber can grow.

We assume that this force is due to change of the surface binding energy of the adatom while it moves to a fiber top. To verify this assumption a Molecular Dynamics (MD) simulations were performed. The fiber was modelled by a cone. By adding W atoms at different places on the surface, surface binding energies of adatoms at different positions were obtained. It was found that the surface binding energy increases towards the tip which supports our assumption. Simulations show that the dependence of the binding energy, E_b on the surface curvature, ρ, can be written as:

$$E_b = E_0 \left(1 + \frac{a}{\rho + \rho_0}\right) \qquad (1)$$

where E_0 is the binding energy on the plane surface, a is the lattice constant, and ρ_0 is a parameter, defined from the calculations.

A differential equation coupling the adatoms flow and fiber length change was obtained from geometrical considerations. Solving this equation, we obtain the following expression for the fiber length:

$$l(t) = \left[\frac{\sqrt{qD}}{(R+\rho_0)^2}\frac{atE_0}{n}\right]^{1/2} \qquad (2)$$

Here D is the adatoms diffusivity, q is the rate of adatoms formation, n is the density (atoms/cm^3), T is the surface temperature.

This expression gives a correct dependence of the fiber length on time: $l \propto \sqrt{D_{eff}t}$. Values of D_{eff} obtained from experimental observations, were found in literature [2] for different surface temperatures. Our estimations based on eq. (1) and (2), are in good agreement with experimental results. For example, for the surface temperature $T = 1120$ K we have $D_{eff} = 9.6 \cdot 10^{-12}$ cm^{-2}s^{-1} while the experimental value $D_{exp} = 6.6 \cdot 10^{-12}$ cm^{-2}s^{-1}.

1. REFERENCES

[1] Yu. V. Martynenko and M. Yu. Nagel, Fizika Plazmy **38**, 12 (2012)

[2] M. Baldwin and R. Doerner, Nucl. Fusion **48**, 035001 (2008).

*Corresponding author e-mail address: edmarenkov@mephi.ru

EROSION OF FUSION-RELEVANT WALL MATERIALS UNDER ION BOMBARDMENT STUDIED WITH A QUARTZ CRYSTAL MICROBALANCE TECHNIQUE

B. M. Berger[1,*], *R. Stadlmayr*[1], *G. Meisl*[2], *M. Cekada*[3], *K. Sugiyama*[2], *M. Oberkofler*[2], *T. Schwarz-Selinger*[2] *and F. Aumayr*[1]

[1]Institute of Applied Physics, Fusion@ÖAW, TU Wien, Wiedner Hauptstr. 8-10/E134, 1040 Vienna, Austria
[2] Max-Planck-Institut für Plasmaphysik, Boltzmannstr. 2, 85748 Garching, Germany
[3] Jožef Stefan Institute, Jamova 39, 1000 Ljubljana, Slovenia

1. INTRODUCTION

Nitrogen seeding is presently used in nuclear fusion devices with a tungsten divertor to reduce the local power load on highly exposed surfaces by enhanced radiative cooling [1]. The formation of tungsten-nitride (WN) layers upon N ion implantation and their erosion during D and N bombardment is therefore a topic of current research [2]. Low activation steels (e.g. EUROFER) are considered for recessed areas. Preferential sputtering of W-containing steels could lead to a surface enrichment with tungsten, thereby reducing the erosion yield and increasing the lifetime of these components. A profound understanding of the interaction of deuterium ions with tungsten-nitride and tungsten-containing steels is hence highly desirable.

2. EXPERIMENTS

We have studied the interaction of mono-energetic deuterium projectiles with 300 nm thick tungsten-nitride WN and iron-tungsten (FeW) model films at 465 K using a highly sensitive quartz crystal microbalance (QMB) technique. The overall mass change rate of the two model systems under D_2^+ ion impact at ion energies between 250 and 1000 eV/D is investigated in situ and in real-time. Measurements were performed at a typical flux of 10^{18} $m^{-2}s^{-1}$. For WN films a strong dependency of the observed mass change rate on the deuterium fluence is found. The mass loss is initially higher than for pure W and drops with fluence finally reaching the same steady state value as for pure W sputtering. At 1 keV/D impact energy a D-fluence of 10^{23} D/m^2 is necessary to obtain steady state conditions. The QMB results for WN are supported by SDTRIM.SP calculations, which indicate that preferential sputtering of N in the WN matrix proceeds until a N-depleted W surface develops. Similar measurements have been performed for Fe films containing 1.5 at% of W as a model system for EUROFER steel. At low ion fluences measured erosion yields are comparable to those for pure Fe. However with increasing fluences (up to 10^{23} D m^{-2}) a noticeable decrease of the sputtering yield for FeW is observed, indicating a W enrichment of the near surface layer.

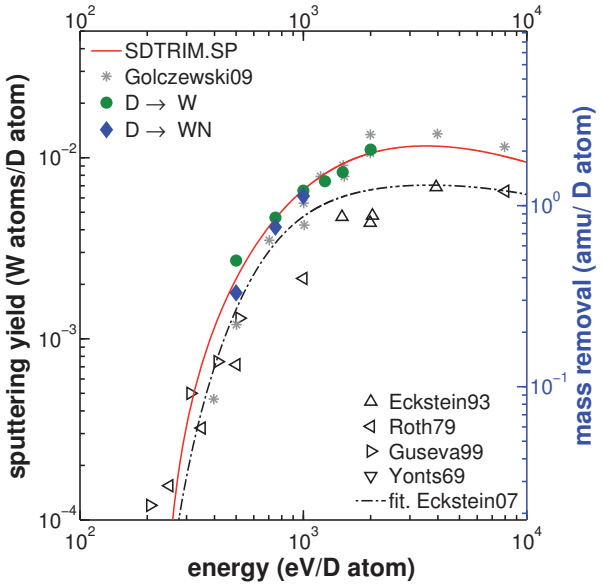

Figure 1: Measured sputtering yield of W and WN for the impact of D_2^+ ions. For the WN measurements steady state conditions are obtained, where the removal of W atoms is expected to dominate the mass change rate. For comparability the projectile energy as well as the sputtering yield are normalized to the number of D atoms in the incoming beam. We compare our data to the results of previous measurements and semi-empirical fits [3-8].

3. REFERENCES

[1] A.Kallenbach, et al, Plasma Phys. Control. Fusion **52**, 055002 (2010).

[2] G. Meisl, et al, New J. Phys. **16**, 093018 (2014).

[3] A. Golczewski, et al, J. Nucl. Mat. **390**, 1102 (2009).

[4] W. Eckstein, et al, Report IPP 9/82 (Garching, 1993).

[5] J. Roth, et al, Report IPP 9/26 (Garching, 1979).

[6] M. I. Guseva, et al, J. Techn. Phis. **69**, 69 (1999).

[7] O. C. Yonts, BNS Nucl. Fusion Reactor Conf. p. 424 (1969).

[8] W. Eckstein, Sputtering by Particle Bombardment, Springer Berlin Heidelberg, 33-187 (2007).

*Corresponding author e-mail address: berger@iap.tuwien.ac.at

CARBON FOILS FOR SPACE PLASMA INSTRUMENTATION

F. Allegrini[1,2,*] *and R. Ebert*[1]

[1] Southwest Research Institute, San Antonio, Texas, USA
[2] University of Texas at San Antonio, San Antonio, Texas, USA

1. INTRODUCTION

Thin carbon foils are critical components of many space flight instruments used for time-of-flight (TOF) mass spectrometers (e.g., [1]) and energetic neutral atom detection (e.g., [2]). One or both of two fundamental properties of the interaction of the primary particle with the foils are generally employed in these sensors: secondary electron emission and/or charge state conversion. This interaction also creates several adverse effects for the projectile exiting the foil, such as angular scattering and energy straggling, that usually act to reduce the sensitivity and overall performance of an instrument. Because these undesirable factors scale with the thickness of the foils, a significant effort has been made to develop means for handling and supporting extremely thin (<10 nm) foils. Although these foils are extremely fragile, they have proven to be remarkably robust in surviving the rigors of the launch and space environments [3].

In this presentation, we will summarize several studies that have quantified the properties of ions exiting the thin carbon foil and discuss recent work on graphene foils [4,5,6], a promising technology that may be capable of mitigating the undesirable effects associated with these interactions.

2. REFERENCES

[1] M. Wüest, *Measurement Techniques in Space Plasmas: Particles* (Eds. R.F. Pfaff, J.E. Borovsky, and D.T. Young), American Geophysical Union Monograph 102, Washington, DC, pp. 141–155 (1998).

[2] H. O. Funsten, D. J. McComas, and B. L. Barraclough, Optical Engineering 32, 3090–3095 (1993).

[3] D. J. McComas, F. Allegrini, C. J. Pollock, H. O. Funsten, S. Ritzau, and G. Gloeckler, Rev. Sci. Instrum. **75**(11), 4863–4870 (2004).

[4] F. Allegrini, R. W. Ebert, S. A. Fuselier, G. Nicolaou, P. Bedworth, S. Sinton, and K. J. Trattner, Optical Engineering 53 (2), 024101 (2014).

[5] R. W. Ebert, F. Allegrini, S. A. Fuselier, G. Nicolaou, P. Bedworth, S. Sinton, and K. J. Trattner, Rev. Sci. Instrum. **85**(3), 033302 (2014).

[6] F. Allegrini, P. Bedworth, R. W. Ebert, S. A. Fuselier, G. Nicolaou, S. Sinton, Nucl. Instrum. and Meth. B, In press (2015).

* Corresponding author e-mail address: fallegrini@swri.edu

THE IMPACT OF HELIUM IRRADIATION ON REFLECTIVITY OF SELF-DAMAGED MOLYBDENUM MIRRORS AT HIGH DPA VALUES

A. Garcia-Carrasco[1*], *P. Petersson*[1], *E. Fortuna*[2], *J. Grzonka*[2], *A. Hallén*[3] *and M. Rubel*[1]

[1] Department of Fusion Plasma Physics, Royal Institute of Technology (KTH), Association VR, 100 44 Stockholm, Sweden
[2]Faculty of Materials Science and Engineering, Warsaw University of Technology, 02-507 Warsaw, Poland
[3]Department of Physics and Astronomy, Ion Physics, Uppsala University, P.O. Box 516, SE-75120 Uppsala, Sweden

1. INTRODUCTION

Many diagnostics in next-step fusion devices (e.g., ITER, DEMO) will rely on optical systems to determine plasma parameters while maintaining neutron shielding. This is done by using metallic mirrors to guide plasma light through a labyrinthine path across the shielding block. Therefore, optical stability of mirrors is essential to ensure reliability of diagnostics [1]. Plasma-facing mirrors (so-called first mirrors) will undergo modification by plasma-wall interaction processes. Erosion by impinging particles will change roughness and chemical composition of material, while co-deposition of plasma impurities may lead to the formation of thick layers on the mirrors surface. In both cases the degradation of specular reflectivity will occur. Such effects arising from material migration are studied in current devices [2], but neutron-induced radiation damage including helium formation effects are still to be examined. Previous works have shown a detrimental effect of helium irradiation on reflectivity of diagnostic mirrors [3]. However, nothing is known on synergetic effects under neutron and helium fluxes. The aim of the study is to determine whether neutron damage (simulated by high-Z ion impact) enhances the negative effect of helium irradiation on reflectivity of molybdenum mirrors.

2. EXPERIMENTS AND ANALYSES

Two levels of damage were induced in the Mo mirrors to reproduce conditions in ITER and DEMO: 1 and 10 dpa, respectively. Neutron damage was simulated using 30 keV molybdenum ions. Helium irradiation was performed with 10^{18} ions/cm^2 at 2 keV. Irradiation energies were selected to affect the first 30 nm of the material, which is the sensitive layer to light in the visible and near-infrared range. Figure 1 shows the damage profile induced by Mo irradiation and the implantation profile of He as assessed using the SRIM code. The study was performed at room temperature and 300 ºC. Diffuse and total reflectivity of mirrors was determined in the 300-2500 nm wavelength range using a double-beam spectro-photometer. The concentration of helium retained in the samples was measured using elastic recoil detection analysis (ERDA) with a 12 MeV $^{14}Si^+$ beam. Roughness of the samples was measured with atomic force microscopy. Further studies include electron microscopy.

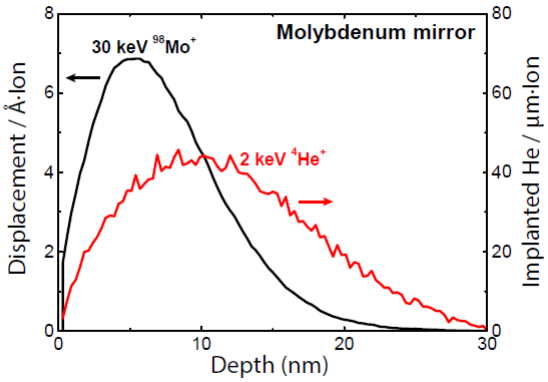

Figure 1: SRIM simulation of Mo irradiation damage profile and He implantation profile on a molybdenum mirror.

3. RESULTS

Total reflectivity of the Mo mirror with 1 dpa decreased only slightly by about 2% in the infrared range while in the visible range it was maintained. However, the reflectivity after 7 dpa decreased 5% in the near infrared range while a slight increase of reflectivity was noted in the visible range, probably due to erosion or reduction of oxides. The same mirror was later irradiated with helium up to the dose of 9 x 10^{17} cm^{-2}. This led to a decrease in reflectivity by 5-15% over the investigated wavelength range. The amount of helium retained in the sample after irradiation was 5 x 10^{16} cm^{-2} as measured by elastic recoil detection analysis. This means that only about 5% of the irradiated helium remained in the sample. One can conclude that damaging of molybdenum by ion irradiation does not affect significantly the reflectivity of the mirror whereas helium irradiation causes significant reductions in reflectivity even though low amounts of He is retained in the subsurface region. Detailed results will be presented and consequences of the mirror damage will be discussed.

4. REFERENCES

[1] A. Costley *et al.*, Fusion Eng. Des. **74**, 1 (2005).
[2] D. Ivanova *et al.*, Phys. Scr. **T159**, 012011 (2014).
[3] K. Ono *et al.*, Phys. Scr. **T138**, 014065 (2009).

* Corresponding author e-mail address: alvarogc@kth.se

DEUTERIUM THERMAL DESORPTION FROM VACANCIES IN TUNGSTEN

S. Ryabtsev*, Yu. Gasparyan, M. Zibrov, and A. Pisarev

National Research Nuclear University MEPhI (Moscow Engineering Physics Institute), Moscow, Russia

1. INTRODUCTION

The investigation of hydrogen (H) isotopes behavior in metals is of great interest for development of fusion reactors. As it is well known, one of the problems in ITER is retention of radioactive tritium in plasma-facing materials, what is a point of safety concern. Tungsten (W) will be used as a plasma-facing material I the divertor region of ITER and its use in future fusion devices is also likely.

The database on H isotopes behavior in W is rather wide, but some of the fundamental aspects of the H-W interaction are not well known yet. First of all, the hydrogen-defect interaction still raises many questions. For example, even the H detrapping energy from a single vacancy in tungsten varies among different researchers [1-3]. It can be shown that the H detrapping energy from a defect can be well determined from the shift of the high temperature desorption maximum in a series of experiments performed with different heating rates under the condition of a high H-H recombination rate at the surface. The detrapping energy E_{dt} in this case is given by

$$\ln\left(\frac{\beta}{T_{\mathrm{m}}^2}\right) = \ln\frac{kA}{E_{dt}} - \frac{E_{dt}}{k}\frac{1}{T_{\mathrm{m}}} \qquad (1)$$

Where β is the heating rate, T_m is the position of the high temperature peak, A – constant, k – Boltzmann constant.

This technique is applied in this work for deuterium (D) detrapping from vacancies in tungsten.

2. EXPERIMENTS

Experiments were performed in the MEDION ion-beam facility (NRNU MEPhI, Moscow). A polycrystalline W foil with a thickness of 25 μm was used as a sample. It was recrystallized at 1800 K for 30 min in order to minimize the amount of natural defects. 10 keV D^+ mass-separated ions with a fluence of 3×10^{19} D/m^2 were used to create defects in the sample. It is expected that mainly vacancies are formed under these conditions [1]. The irradiated sample was heated to 550 K and then held at that temperature for 5 min. Almost all the retained D was released from the sample, but clustering of vacancies is expected to be negligible [1]. The sample prepared in this way was implanted by a 2 keV D_3^+ ion beam to the fluence of 1×10^{19} D/m^2 at room temperature in order to fill vacancies without producing additional displacement damage; and then thermal desorption was performed. This procedure was performed several times in series and the only difference was the TDS heating rate that varied in the range of 0.15-4 K/s.

3. EXPERIMENTAL RESULTS

In the case of irradiation of the annealed W sample by ions with the energy of 0.67 keV/D, which is less than the formation of threshold for the displacement damage, the TDS spectrum has only one peak at 400 K corresponding to a D release from the trapping centers on the surface or from natural defects (dislocations and grain boundaries) in the bulk of the sample [2]. In the case of irradiation of the annealed sample by 10 keV/D ions, the first peak predominates in the TDS spectrum, however, one can see also shoulder at the temperature of 650 K that is corresponding to a D release from point defects created in the sample during the irradiation, and shoulder at 720 K, which, as it is assumed, corresponds to a D release from vacancy clusters. The procedure described above allows obtaining the TDS spectrum with well-resolved second desorption peak, which is associated with a deuterium release from vacancies [2]. Due to that fact, such kind of spectrum and the procedure described above are convenient to use for the experiments with various heating rates.

TDS for the D detrapping from point defects with different heating rates β demonstrated that the second (high-temperature) peak of thermal desorption spectrum moves towards the high temperatures with the increasing of heating rate. The position of the second desorption peak T_m was determined for each β value, and then the Arrhenius-like graph $\ln(\beta/T_m)$ versus $1/T_m$ was plotted. The obtained dependence was then approximated by a straight line, and the D detrapping energy from vacancies in W was calculated from the slope of that line.

4. REFERENCES

[1] H. Eleveld, A. van Veen, J. Nucl. Mater. 191-194, 422 (1992)

[2] O.V. Ogorodnikova, J. Roth, M. Mayer, J. Appl. Phys. 103 (2008)

[3] M. Poon, A.A. Haasz, J.W. Davis, J. Nucl. Mater. 374, 390 (2008)

* Corresponding author e-mail address: ryabtsev91@mail.ru

HIGH RESOLUTION SURFACE TOPOGRAPHY WITH GRAZING INCIDENCE FAST ATOM DIFFRACTION.

P. Atkinson[1] , M. Eddrief[1] , F. Finocchi[1], V. Etgens[2], M. Debiossac[3], A. Zugarramurdi[3], A.G. Borisov[3], M. Mulier[3], B. Lalmi[3], A. Momeni[3,4], H. Khemliche[3], P. Lunca-Popa[3], A. J. Mayne[3] and P. Roncin[3]

1 INSP, Sorbonne Universités, CNRS-Univ. Paris 06, 4 place Jussieu, F-75005 Paris, France
2 VeDeCom-Universitée Versailles Saint-Quentin en Yvelines, Versailles, France
3 ISMO, Université Paris Saclay, CNRS-Universitée Paris-Sud, Orsay F-91400, France
4 Univ. Cergy Pontoise, F-95031 Cergy, France

1. INTRODUCTION

Grazing incidence fast atom diffraction (GIFAD or FAD) has recently developed as an exclusively surface sensitive technique. This is due to the absence of penetration just as in standard helium atom scattering. We will show however that the variable energy ability of GIFAD allows a clear separation of the contributions from Van der Waals forces from those due to the short range repulsion providing the topological resolution. When these later are dominant, GIFAD can be compared to a perfect tip AFM operating in the reciprocal space. Using state of the art DFT calculation and exact diffraction algorithms, both contributions can be compared with GIFAD experiment data.

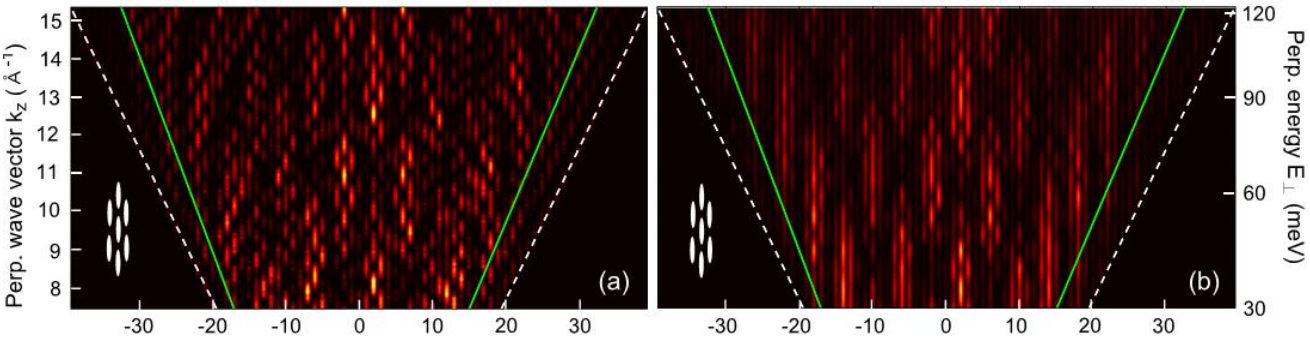

Figure 1. Diffraction charts for 400 eV ^{4}He atoms incident along the [1-10] direction of theβ^2(2×4) reconstruction of GaAs(001). The horizontal axis is the diffraction order and the vertical is plotted both in wavelength and perpendicular energy. a)Theoretical results are from a DFT calculation and a wave packet diffraction code. b) Experimental data.

2. DIFFRACTION CHART

The specific geometry of GIFAD (identical to the one adopted in RHEED) has some definite advantages. High collection efficiency; the full diffraction cone is imaged at once, high detection efficiency of keV atoms and, most of all due to the multiple interaction regime (the atoms interacts more with a row of atoms [1,2] than with individual atoms) the decoherence due to thermal motion of the surface atoms and known as the Debye-Waller factor is reduced. This has two interesting consequences; GIFAD can be operated at elevated surface temperatures such as those needed in Molecular beam epitaxy (MBE) and/or GIFAD can probe the surface with comparatively large perpendicular energy $E_\perp$ therefore probing electronic density closer to the surface atoms where Van der Waals forces are less important. We will present two very different examples were high resolution can be achieved. The first one corresponds to GIFAD images recorded inside a molecular beam epitaxy vessel with the surface temperature of 530°C[3,4]. Changing the angle of incidence θ changes the energy $E_\perp=E\sin^2\theta$ of the motion perpendicular to the surface. This is almost equivalent to illuminating a grating with a variable wavelength. We will show that this analogy allows straight forward qualitative interpretation of the rocking curve also called diffraction chart (fig 1) in terms of the shape of the electronic density profile.

Recent results[5] on the moirée structure of SiC grown Graphene will also be presented.

Acknowledment. The research described here has been supported by Triangle de la physique contract GIFAD and by Agence Nationale de la Recherche ANR-07-BLAN-0160 and ANR-11-EMMA-0003.

REFERENCES

[1] J. R. Manson *et al*. Phys. Rev. B **78**, 155408 (2008)
[2] P. Rousseau *et al* J. Phys. Conf. Ser. **133** 012013 (2008)
[3] M. Debiossac *et al*. Phys. Rev. B **90**, 155308 (2014)
[4] P Atkinson, *et al* Appl. Phys. Lett. **105**, 021602 (2014)
[5] Zugarramurdi *et al.* Appl. Phys Lett **106**, 101902 (2015)

* Corresponding author e-mail address: philippe.roncin@u-psud.fr

Dynamic Grazing Incidence Fast Atom Diffraction: in-situ monitoring of layer-by-layer growth oscillations and surface reconstructions during molecular beam epitaxy

P. Atkinson[1,*], M. Eddrief[1], V. H. Etgens[1,3], M. Debiossac[2], H. Khemliche[2], A. Momeni[2,4], and P. Roncin[2]

[1] *INSP UMR7588 CNRS – Sorbonne Universités, Université Pierre et Marie Curie, Paris 75005, France.*
[2] *ISMO, Université Paris Saclay, CNRS-Univ. Paris Sud Orsay F-91405, France*
[3] *VeDeCom – Université de Versailles Saint-Quentin en Yvelines, Versailles, France.*
[4] *Univ. Cergy Pontoise, F-95031 Cergy, France*

1. INTRODUCTION

Reflection High Energy Electron Diffraction (RHEED) is perhaps the most commonly used in-situ monitoring method for molecular beam epitaxy (MBE), providing quantitative information about surface reconstructions, lattice parameters, growth rates and growth modes, together with semi-quantitative information about surface morphology. We demonstrate here that Grazing Incidence Fast Atom Diffraction (GIFAD), depicted schematically in Figure 1, is fully compatible with conventional MBE growth [1], and is capable of monitoring changes in the surface in real-time during growth as shown in figure 2.

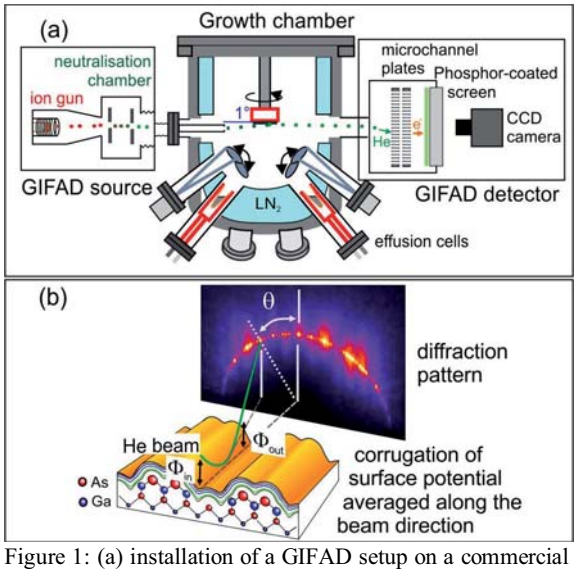

Figure 1: (a) installation of a GIFAD setup on a commercial MBE machine (b) schematic of the GIFAD scattering geometry showing the diffraction pattern obtained from the (2x4)β_2 surface reconstruction of GaAs (100). Due to the shallow angle of incidence, the energy of the atoms perpendicular to the surface is very small giving rise to diffraction of the atom beam from the corrugated surface potential parallel to the beam direction.

2. IN-SITU GROWTH MONITORING

We show here that GIFAD is a robust technique for monitoring layer-by-layer growth allowing variations in surface island coverage to be probed at the same time as observing changes in surface reconstruction induced by growth. The advantages provided by GIFAD over RHEED for understanding growth dynamics and surface reconstructions will be discussed in some detail.

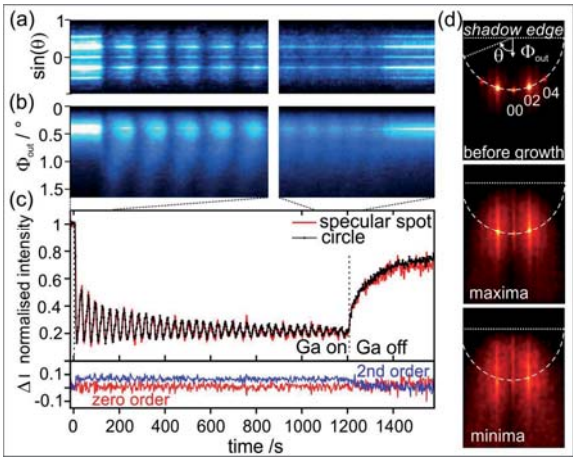

Figure 2: GIFAD intensity oscillations during GaAs growth:
(a) Intensity integration over the Laue circle. All diffraction orders oscillate in phase, unlike in RHEED;
(b) Scattered intensity vs. polar exit angle. The intensity oscillations at super-specular scattering angles precede the specular intensity oscillations for the first few monolayers
(c) Integrated intensity oscillations of the Laue circle (black) and the specular spot (red). The difference in relative intensity of the 00 and 02 diffraction orders is shown in the lower plot. The rearrangement of intensities between different orders may be related to a change in the corrugation of the surface reconstruction during growth.
(d) Diffraction patterns before and during growth.

3. REFERENCES

[1] P. Atkinson, M. Eddrief, H. Khemliche, M. Debiossac, A. Momeni, M. Mulier, B. Lalmi and P. Roncin, *Appl. Phys. Lett.* **105** 021602 (2014)

* Corresponding author e-mail address: atkinson@insp.jussieu.fr

INFLUENCE OF THE LIGHTING ON FAST ATOM DIFFRACTION STUDIED VIA A SEMI-QUANTUM APPROACH

M.. Gravielle[1,*], *and J.E.Miraglia*[1]

[1] Instituto de Astronomía y Física del Espacio (IAFE, CONICET-UBA), Buenos Aires, Argentina

1. INTRODUCTION

The observation of quantum interference effects in projectile distributions originated by grazing scattering of swift atoms off crystal surfaces, now known as Fast Atom Diffraction (FAD), strongly relies on the preservation of quantum coherence [1,2]. In this regard, the collimation conditions of the incident beam, which are associated with the size of the illuminated region of the surface, play an important role [3].

In this work we investigate the influence of the collimation of the incident particles, which determines the shape of the incoming wave packet, by employing a recently developed *semi-quantum* approach for FAD, named Surface-Initial Value Representation (SIVR) approximation [4].

2. THEORY AND RESULTS

The SIVR approach was derived from the Initial Value Representation (IVR) method by Miller [5] by using the corresponding semi-quantum time evolution operator in the frame of a time-dependent distorted-wave formalism. This strategy incorporates an approximate description of classically forbidden transitions on the dark side of rainbow angles, making it possible to avoid the classical rainbow divergence present in previous semi-classical models for FAD, like the Surface-Eikonal (SE) approach [6].

We apply the SIVR approximation to evaluate FAD patterns for He atoms grazingly impinging on a LiF(001) surface, after going through a slit with a transversal width *D*. In order to show the influence of the collimation conditions on FAD spectra, two different values of *D* – *0.2*mm and *1*mm - are considered in Fig. 1. In both cases, simulated spectra are in good agreement with the experimental results.

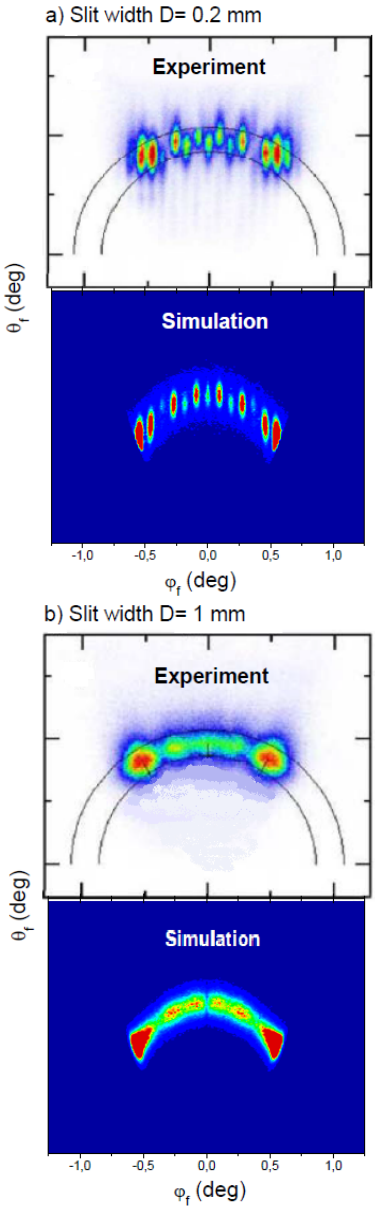

Figure 1: Final angular distribution, as a function of the polar (θ_f) and azimuthal (φ_f) angles, for 1keV ^{4}He atoms impinging on LiF(001) surface along the <110> channel, with a glancing angle θ_i=0.99deg. Expt. from Ref. [3]; simulations with the SIVR approach; both with an incident beam collimation with a slit width: a) D=0.2mm, and b) D=1mm.

3. REFERENCES

[1] J. Lienemann *et al.*, Phys. Rev. Lett. **106**, 067602 (2011).
[2] N. Bundaleski *et al.*, Nucl. Instrum. Meth. Phys. Res. B **269**, 1216 (2011).
[3] J. Seifert *et al.*, Nucl. Instrum. Meth. Phys. Res. B **350**, 99 (2015).
[4] M.S. Gravielle and J.E. Miraglia, Phys. Rev. A **90**, 052718 (2014).
[5] W.H. Miller, J. Phys. Chem. A **105**, 2942(2001).
[6] M.S. Gravielle and J.E. Miraglia, Phys. Rev. A **78**, 022901 (2008).

* Corresponding author e-mail address: msil ia@iafe.u a.ar

The role of the internal degrees of freedom in molecular diffractive scattering under fact grazing incidence

A. S. Muzas[1], *M. del Cueto*[1], *M. F. Somers*[2], *G. J. Kroes*[2], *F. Martín*[1,3] *C. Díaz*[1,*]

[1] Departamento de Química, Módulo 13, Universidad Autónoma de Madrid, Cantoblanco 28049, Madrid, Spain
[2] Gorlaeus Laboratories, Leiden Institute of Chemistry, Leiden University, P. O. Box 9502, 2300 RA Leiden, The Netherlands
[3] Instituto Madrileño de Estudios Avanzado en Nanociencia (IMDEA-Nanociencia), Cantoblanco 28049, Madrid, Spain

1. INTRODUCTION

Diffractive scattering of neutral molecules from surfaces under fast grazing incidence has been widely study, from an experimental point of view, during the last decade (see [1] and refs. therein). However, from a theoretical point of view studying this phenomenon represents a real challenge, which explains that to date only classical and semi-classical approaches have been use to get some insights about this phenomenon (see [2] and refs. therein). During the conference we will show, to our knowledge, the first six-dimensional (6D) quantum dynamics simulations performed to study diffraction of H_2 molecules from a surface, in our case LiF(001).

2. METHOLOGY AND RESULTS

2.1. Theoretical tools

To perform our study, we have worked within the Born-Oppenheimer surface static (BOSS) approximation. In applying the BOSS, we have computed an accurate 6D potential energy surface [3], which have been obtained by applying the corrugation reducing procedure (CRP) [4] to a set of density functional theory (DFT) data. DFT data have been computed within a periodic boundary conditions framework, using the code VASP [5]. To carry out the 6D quantum dynamic simulations, we have used a time-dependent wave packet propagation method, in which the split-operator (SPO) method is used to propagate the wave packet in time [6]. In addition, we have also performed a classical analysis using the method proposed in ref. [7].

2.2. Preliminary results

Three important conclusions can be extracted from our preliminary quantum dynamics results: (I) the initial ro-vibrational state of the molecule may play a fundamental role on the diffraction spectra measured experimentally. This conclusion was already reached from previous classical analysis (see Fig. 1); (II) The molecules exchange a substantial amount of rotational energy with the translational energy during theirs interaction with the surface; (III) The classically simulated diffraction spectra reproduce pretty well the quantum ones (as well as the experimental ones). This result validates the use of the classical trajectory (CT) method to get meaningful conclusions.

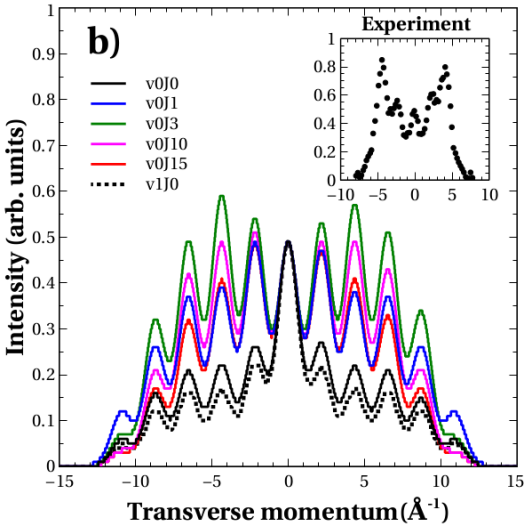

Figure 1: Simulated, using CT, diffraction spectra for H_2/LiF(001), for several vibrational and rotational initial states, along de crystallographic direction <110>. Normal energy 300 meV. The inset show the spectrum measured experimentally. Data taken from Ref. [8]

3. REFERENCES

[1] H. Winter and A. Schüller, Prog. Surf. Sci. **86**, 1169 (2011)
[2] G. J. Kroes and C. Díaz, Chem. Soc. Rev. DOI: 10.1039/c5cs00336a
[3] A. S. Muzas et al. to be published
[4] H. F. Busnengo et al., J. Chem. Phys. **112**, 7641 (2000)
[5] G. Kresse et al., Phys. Rev. B **47**, 558 (1993); Phys. Rev. B **54**, 11169 (1996); Phys. Rev. B **59**, 1758 (1999)
[6] G. J. Kroes, Prog. Surf. Sci. 60, 1 (1999)
[7] C. Díaz el al., J. Chem. Phys. **122**, 154706 (2005)
[8] P. Rousseeau et al., J. Phys.: Conf. Series **133**, 012013 (2008).

* Corresponding author e-mail address: cristina.diaz@uam.es

SOLAR WIND SPUTTERING OF LUNAR SOIL ANALOGS: CHARGE STATE and MASS EFFECTS[#]

H. Hijazi[1 *], *M. E. Bannister*[1], *H. M. Meyer III*[2], *C.M. Rouleau*[3], *and F. W. Meyer*[1]

[1] Physics Division, Oak Ridge National Laboratory, Oak Ridge, TN 37831-6372 USA
[2] Materials Science and Technology Division, Oak Ridge National Laboratory, Oak Ridge, TN 37831-6064 USA
[3] Center for Nanophase Materials Sciences, Oak Ridge National Laboratory, Oak Ridge, TN 37831-6488,

1. INTRODUCTION

In this contribution we report sputtering measurements of anorthite ($CaAl_2Si_2O_8$), an analog mineral representative of the lunar highlands, by singly and multicharged ions representative of the solar wind. The ions investigated include protons, as well as singly and multicharged He, N, O, Ar and Ne ions, and had a fixed solar-wind-relevant impact velocity of ~310 km/s or 500 eV/amu. The goal of the measurements was to determine the sputtering contribution of the heavy, multicharged minority solar wind constituents in comparison to that due to the dominant H^+ fraction.

2. EXPERIMENTAL APPROACH

The measurements were performed at the ORNL Multicharged Ion Research Facility using a quartz crystal microbalance approach for determination of total sputtering yields [1]. QMS measurements were carried out in parallel to compare with earlier measurements using JSC-1A AGGL lunar simulant [2].

The anorthite target was deposited as a thin film onto a gold-coated quartz crystal sensor using Pulsed Laser Deposition (PLD). X-ray Photoelectron Spectrometry (XPS) analysis confirmed the thin film stoichiometry to be close to that expected for bulk anorthite.

2-D spatial profiles of the ion beams incident on the microbalance were measured using a stepper-motor controlled wire scanner under PC control located immediately upstream of the microbalance, and permitted accurate determination of the microbalance response, which depends sensitively on beam size and position. A beam flag insertable in front of the microbalance was used for ion beam current determination during the sputtering measurement.

3. RESULTS AND DISCUSSION

The measurement results are summarized in Figure 1, where the potential sputtering yields are plotted as function of the neutralization potential energy, defined as the sum of binding energies of the electrons removed to reach a particular incident ion charge state, and are in large part consistent with our Ar^{q+} results, which were published in [2]. Of particular importance are the measurements for He^{2+}, since this ion is the most abundant multicharged ion in the solar wind. The experimental physical sputtering yield for He^+ is 9.7 ± 2.1 amu/ion, in rough agreement with the SRIM [3] value of 8.12 amu/ion. The potential sputtering yield for He^{2+} (Fig. 1) is 3.8 ± 0.84 amu/ion. When incorporated into

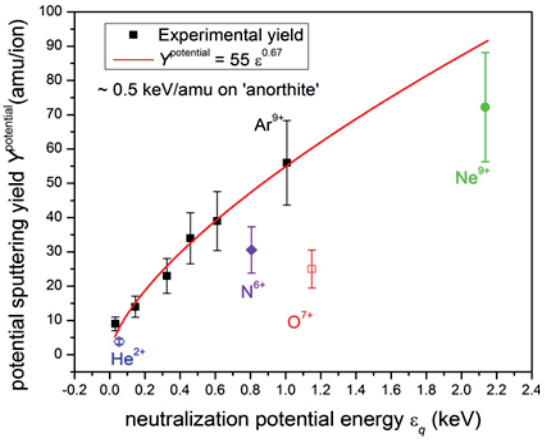

Figure 1: Yield due to the potential sputtering $Y_{potential}$ as a function of the neutralization energy (keV) for various 0.5 keV/amu solar wind ions incident on anorthite.

an abundance-weighted total sputter calculation including all solar wind ions, and physical as well as potential sputtering, the total solar wind sputtering is increased by nearly 50%.

The fact that the N, O, and Ne H-like ion impact results fall below the Ar ion curve, may be due to direct quasi-resonant K-shell filling in collisions with oxygen target atoms, which reduces the available potential energy for sputtering, or, more simply, just a consequence of the large K-Auger electron energies, which constitute significant fractions of the total neutralization potential energies of these ions, but are relatively inefficient in target defect production. These possibilities are currently being investigated by lower charge state measurements for these species.

4. REFERENCES

[1] H. Hijazi et al. J. Geophys. Res: Space Phys. **119**, 8006 (2014).
[2] Meyer F. W. et al. Nucl. Inst. Meth. B, **209**, 1316 (2011).
[3] Ziegler J.F. et al. http://www.srim.org. (1996).
[4] Aumayr F. et al. Phil. Trans. R. Soc. Lond. A, **362**, 77 (2011).

[#]Research supported by NASA grant 10-LASER10-0053, the NASA DREAM2 Solar System Exploration Research Virtual Institute (SSERVI), and by the ORNL LDRD Program.

[*] Corresponding author e-mail address: hussein_hijaze@hotmail.com

ASTROPHYSICAL MATERIAL ANALOGS IRRADIATED BY SWIFT HEAVY IONS

R. Martinez[1,2,*], *E.F. da Silveira*[3], *G. Strazzula*[4], *P. Boduch*[1] *and H. Rothard*[1]

[1] Centre de Recherche sur les Ions, les Matériaux et la Photonique
(CEA/CNRS/ENSICAEN/Université de Caen-Basse Normandie UCBN)
CIMAP-CIRIL-Ganil, Boulevard Henri Becquerel, BP 5133, 14070 Caen Cedex 05, France
[2] Departamento de Física, Universidade Federal do Amapá, Brazil
[3] Departamento de Física, Pontifícia Universidade Católica do Rio de Janeiro, Brazil
[4] INAF-Osservatorio Astrofisico di Catania, Italy

1. INTRODUCTION

Ices (condensed gases) and silicates are the dominant materials of the surfaces of many objects, in specific astrophysical environments. They can e.g. be found on asteroids, on moons of many planets and on dust grains in the interstellar medium. Thus, they are exposed to solar wind, cosmic rays, and energetic ions present in the magnetospheres of the giant planets. The ion populations consist, besides H and He, of multiply charged heavy ions. Ion bombardment (solar wind, cosmic rays, etc.) is able, among other effects, to influence the reflectance spectra of irradiated silicates by inducing physico-chemical changes known as a whole as "space weathering". Sputtered particles also contribute to the composition of the exosphere of planets or moons [1].

2. RESULTS

The sputtering of such astrophysical materials was studied at CIMAP-GANIL and PUC-Rio by time-of-flight mass spectrometry (TOF-SIMS), with projectiles in a wide energy range from ≈ 100 keV to ≈ 600 GeV [1,2]. A general result is the important contribution of cluster emission [2,3,4] to sputtering.

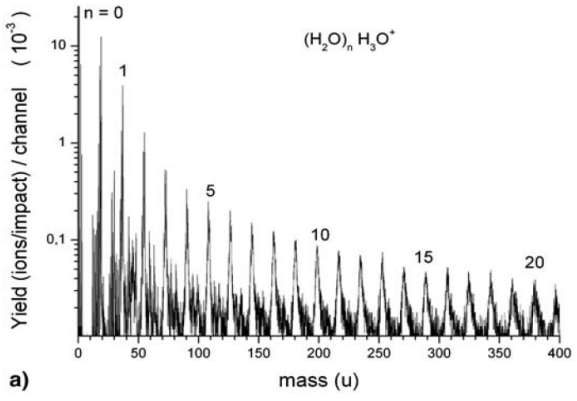

Figure 1: TOF mass spectrum of positive secondary ions of water ice irradiated by ~ 1 MeV/u ions (^{252}Cf FF).

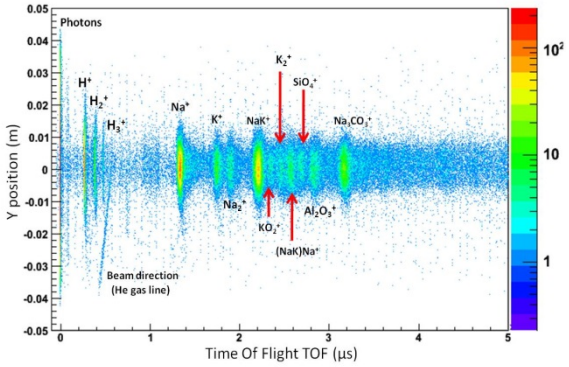

Figure 2: Silicate (nepheline) XY-TOF mass spectrum. Swift heavy and low energy ions produce similar spectra.

Also, imaging XY-TOF-SIMS allows to measure velocity distributions of sputtered secondary ions [1,3,5], which can provide important information about the emission profile of sputtered particles from planetary surfaces.

Acknowledgements:

The CAPES-COFECUB French-Brazilian exchange program, a CNPq postdoctoral grant and the EU Cost Action "The Chemical Cosmos" supported this work. We also acknowledge our co-workers: A. Domaracka, C.R. Ponciano, M.E. Palumbo, H. Hijazi, A. Cassimi.

3. REFERENCES

[1] M.A. Allodi, R.A. Baragiola, G.A. Baratta, M.A. Barucci, G.A. Blake, Ph. Boduch et al., Space Science Reviews (2013) 180, 101-175.
[2] D. P. P. Andrade, A. L. F. de Barros, S. Pilling, A. Domaracka, H. Rothard, P. Boduch, E. F. da Silveira, Monthly Notices of the Royal Astronomical Society (2013) 430, 787-796.
[3] H. Hijazi, H. Rothard, P. Boduch, I. Alzaher, Th. Langlinay A. Cassimi et al, Eur. Phys. J. D (2012) 66:305.
[4] R. Martinez, Th. Langlinay, P. Boduch, A. Cassimi, H. Hijazi, F. Ropars, P. Salou, E.F. da Silveira and H. Rothard, Mater. Res. Express, accepted for publication.
[5] R. Martinez, C.R. Ponciano, and E.F. da Silveira, Eur. Phys. J. D (2012) 66:251

* Corresponding author e-mail address: rafaelmaro@gmail.com

Velocity correlated cluster emission in surface sputtering by a large polyatomic projectile

E. Kolodney[1,*], E. Armon[1], A. Bekkerman[1], Y. Cohen[1], J. Bernstein[1] and B. Tsipinyuk[1]

[1] Schulich Faculty of Chemistry, Technion–Israel Institute of Technology

Haifa 32000, Israel

1. INTRODUCTION

Ion-solid sputtering processes find increasing use in modification and analysis of surfaces at the nanoscale. Recent interest regarding fundamental mechanistic aspects is related with differences between the characteristics of sputtering induced by polyatomic/cluster projectiles as compared with that induced by atomic projectiles. This reflects also an increasing interest in new cluster-surface impact phenomena in general [1]. When compared with the case of surface sputtering with atomic ion projectiles, mechanisms of particle emission following bombardment with large polyatomic ions are generally poorly understood. Here we describe a sputtering phenomenon which is very different for an atomic projectile and a large polyatomic one. It is based on the unique behavior observed for the kinetic energy distributions (KEDs) of surface emitted metallic clusters and carbide nanocrystals following keV surface impact of C_{60}^{-} . A moving precursor model is found to be in good agreement with the experimental results.

2. RESULTS

We have recently reported [2] the emission of large clusters ($Ta_nC_n^+$ (n = 1-10) and Ag_n^+ (n=1-9)) with nearly the same velocity for all cluster sizes (n values) following impact of a large polyatomic projectile (C_{60}^{-} at 14 keV kinetic energy) on Ta /TaC and Ag targets correspondingly. A detailed description of the experimental setup is given elsewhere [3]. As shown in Fig. 1 , the measured kinetic energy distributions (KEDs) of the different clusters ejected by C_{60}^{-} impact were found to behave oppositely to those usually observed using monoatomic projectile ions. The most probable energies are gradually *increasing* with increase in cluster size and the distributions are getting broader (Fig. 1a). We have rationalized our results in terms of a new surface sputtering mechanism where an outgoing, superhot, moving precursor (with a given temperature and some center of mass velocity), is the source of the emitted clusters. In agreement with a successful modelling of the KEDs by a family of shifted Maxwellians. The superhot precursor can tentatively be described either as only partially detached from the surface (just bulging out) at the moment of clusters emission or a fully surface detached large parent cluster (source of the daughter fragments). Additional recent measurements on other target materials and further characterizations will be reported as well.

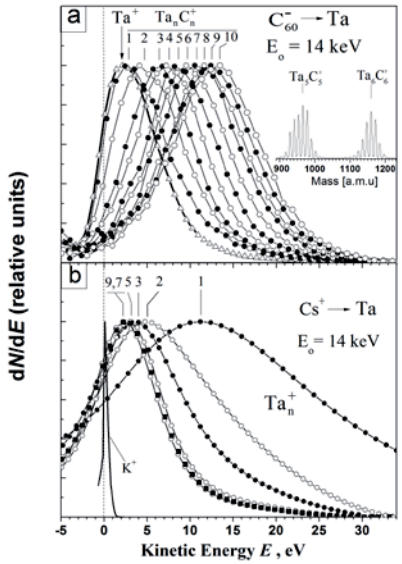

Fig.1. (a) Kinetic energy distributions of $Ta_nC_n^+$ (n=1-10) cluster ions sputtered from pre-grown tantalum carbide layer by C_{60}^{-} impact. Insert shows a representative part of the mass spectrum. (b) Kinetic energy distributions of Ta_n^+ (n=1-9) cluster ions sputtered from a tantalum target by Cs^+ impact.

3. REFERENCES

[1] V. Popok , I. Barke, E.E.B. Campbell and K.- H . Meiwes-Broer, Surf. Sci. Reports **66**, 347 (2011).

[2] E. Armon , A. Bekkerman, Y. Cohen , J. Bernstein , B.Tsipinyuk and E. Kolodney , Phys. Rev. Lett. **113**, 027604 (2014).

[3] Y. Cohen, V. Bernshtein, E. Armon, A. Bekkerman, and E. Kolodney, J. Chem. Phys. **134**, 124701 (2011).

* Corresponding author e-mail address: eliko@tx.technion.ac.il

Secondary particle properties of the ion beam sputter process of Ag, Ge and Ti

C. Bundesmann[*], *R. Feder*[**], *T. Lautenschläger, H. Neumann, and B. Rauschenbach*

Leibniz-Institute of Surface Modification, 04318 Leipzig, Germany

1. INTRODUCTION

Ion beam sputter deposition (IBSD) is a well-known physical vapor deposition (PVD) technique for high-quality thin film production. Its advantage over other PVD techniques is the opportunity to tailor the properties of the film-forming, secondary particles and, hence, the film properties by changing ion beam (ion energy, ion species) and geometrical parameters (Ion incidence angle, emission angle). Here we present systematic investigations of the secondary particle properties in the IBSD process of Ag [1,2], Ge [3] and Ti.

2. EXPERIMENTAL DETAILS

The experimental setup consists of an ion source, a polycrystalline target and an energy-selective mass spectrometer. Ion source and target are mounted on rotary tables on identical rotation axes in order to realize different combinations of ion incidence angel and emission angles.
Ar and Xe were used as primary ions. The ion energy was set to 0.5 keV, 1.0 keV, or 1.5 keV. The minimal detectable emission angle β was 60°, 30°, and 0° for a ion incidence angle α of 0°, 30°, and 60° respectively.

3. RESULTS AND DISCUSSION

Figure 1 shows, exemplary, the measured energy distributions of sputtered Ag ions (a) and backscattered Ar ions (b) for an incidence angle of 30° and an ion energy of the primary Ar ions of 1.0 keV.
In accordance with the predictions by the Thompson formula, the energy distributions of the sputtered particles show a maximum at low energies followed by a E^{-2} decay for small emission angles. When the emission angle increases, a tail or even a broad peak appears. These structures can be assigned to direct sputtering events
The measured energy distributions of the backscattered Ar ions show also a maximum at low energies and up to two additional structures above that: a broad peak with a full width at half maximum of FWHM > 100 eV and a narrower peak with FWHM ~50 eV, which can be assigned to Ar-Ar or Ar-Ag scattering, respectively.
The appearance and energetic position of the additional structures in the energy distributions of the sputtered and backscattered particles depends strongly on the scattering geometry (or scattering angle $\gamma = 180° - \alpha - \beta$) and the ion species, but also on the ion energy.
The experimental data are compared with simulations with the Monte Carlo code TRIM.SP and calculations for simple elastic collision of two particles. These results agree well with the experimental findings, especially for the assignment of the structures related to direct sputtering and scattering events.

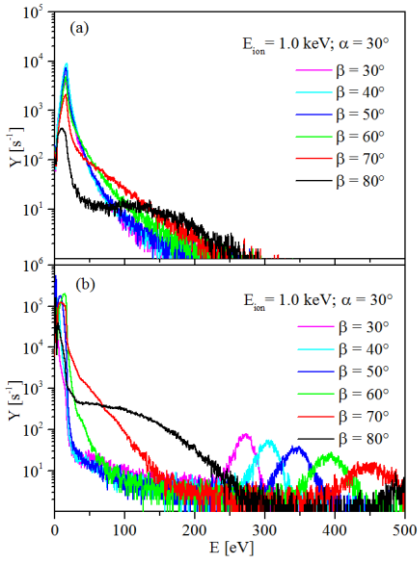

Figure 1: Experimental energy distributions of sputtered Ag ions (a) and backscattered Ar ions (b) for sputtering of an Ag target with Ar ions (ion incidence angle 30°, ion energy 1.0 keV).

For comparison, we also provide experimental results for the ion beam sputter process of Ge and Ti. Due to the different mass of target particles, systematic differences are observed.
The systematic variations of the energy distributions, especially of the backscattered particles, should result in systematic variations in the thin film properties. Indeed, we found systematic dependencies, for instance, of the electrical resistivity of Ag films on the process parameters, especially on the scattering angle and primary ion species [4].

4. REFERENCES

[1] R. Feder, C. Bundesmann, H. Neumann, B. Rauschenbach, Nucl. Instrum. Methods Phys. Res., Sect. B, **316** , 318 (2013).
[2] R. Feder, F. Frost, H. Neumann, C. Bundesmann, B. Rauschenbach, Nucl. Instrum. Methods Phys. Res., Sect. B, **317A**, 137 (2013).
[3] R. Feder, C. Bundesmann, H. Neumann, B. Rauschenbach, Nucl. Instrum. Methods Phys. Res., Sect. B, **334**, 88 (2013).
[4] C. Bundesmann, R. Feder, J.W. Gerlach, H. Neumann, Thin Solid Films **551**, 46 (2014).

[*] Corresponding author e-mail address: carsten.bundesmann@iom-leipzig.de
[**] Now with Clausthal University of Technology, 38640 Goslar, Germany

ABSTRACTS

Friday 23rd October 2015

STUDYING SOLIDS USING THE HELIUM ION MICROSCOPE

T. Kobayashi, H. D. Lee, V. Manichev, S. Shubeita, H. Wang, C. Xu, L. C. Feldman and T. Gustafsson

Department of Physics and Astronomy and Institute for Advanced Materials, Devices and Nanotechnology, Rutgers University, Piscataway, NJ 08854, USA

1. HELIUM ION MICROSCOPY

The Helium Ion Microscope is a relatively new tool for investigating solids. The instrument is similar to an SEM: A charged particle beam is rastered over the sample and the resulting secondary electrons are collected to form an image. The use of a He^+ beam instead of electrons has several advantages: (1) The area emitting secondary electrons (the lateral resolution) is in principle smaller, (2) the use of a positively charged probe means that insulating samples can be studied without applying a conducting overlayer and (3) the depth of focus is large. Another very useful feature is that the massive He ions allow writing and sample modification on the sub-nm scale.

2. RESEARCH EXAMPLES

In this talk, I will after a brief introduction to the technique present some recent results from our group. I will show some examples of sub-nm resolution images of strongly insulating samples, such as shale rock. Imaging of implanted Ag and Au nanoparticles sheds light on the mechanisms for successful analysis of brain tissue. Other examples will involve the creation of a single electron transistor by sample modification and the formation of ultrathin ribbons of graphene by He sculpting. Finally, I will show how by using a novel time-of-flight technique of the back-scattered He ions, one can obtain elemental information in helium ion microscopy.

* Corresponding author e-mail address: adam.black@white.zz

SURFACE MICROSCOPY USING SPIN-POLARIZED METASTABLE HELIUM ATOM BEAMS

Y. Yamauchi[1,2*], *M.Ohtomo*[2], *X, Sun*[1,3], *A. Pratt*[1,4], *M. Kurahashi*[1] *and M. Yoshitake*[1]

[1] National Institute for Materials Science, Tsukuba, Japan
[2]Japan Atomic Energy Agency, Tokai, Japan
[3]University of Science and Technology of China, Hefei, China
[4]University of York, York, U. K.

1. INTRODUCTION

The spin dependence of electron emission induced by He(2^3S) deexcitation provides a unique approach for investigating the properties of magnetic surfaces, i.e., spin-polarized metastable-atom deexcitation spectroscopy (SPMDS). [1] We previously constructed SPMDS apparatus and applied it to the spin analysis of electrons at a variety of magnetic surfaces. Since then, the increasing importance of spintronics has led to demands for a surface spin microscopy. To this end, we have extended SPMDS to surface microscopies, i.e., spin-polarized scanning metastable atom microscopy (SPSMM) followed by spin-polarized metastable-atom emission electron microscopy (SPMEEM).

2. SPMDS

Our previous SPMDS studies clarify that monoatomic layers of organic molecules including graphene exhibit relatively strong interaction with ferromagnetic transition metal surfaces. [2] Since the interaction is expected to be mediated by inserting an insulating monoatomic layer, we have analyzed the surface spin polarization of a h-BN monolayer on a Ni (111) surface and observed the contact-induced spin polarization. [3]

3. HIGH-DENSITY BEAM

A high density of He(2^3S) at the sample position is vital in order to achieve magnification with an acceptable acquisition time for the implementation of a practical microscopy. However, because of charge neutrality, metastable helium atom beams can be bent neither by the Coulomb force nor by the Lorenz force. Instead, He(2^3S) atoms have a total electron spin of 1, which is accompanied by a small magnetic moment of two Bohr-magnetons. This magnetic moment experiences a force in an inhomogeneous magnetic field. By using a sextupole magnet, only He(2^3S) atoms with a spin-up orientation can be collimated or slightly converged. [4] Thus, a single spin state can be selected from the triplet states keeping the beam density high. It is imperative to switch the polarity of the He(2^3S) spin for checking the validity of the spin dependencies. The magnetically selected spin state with respect to the defining field cannot be changed as far as the adiabatic condition holds. Our spin flipper utilizing Majorana transitions under the diabatic condition exhibited superior spin inversion performance with a purity of spin greater than 99%, fulfilling the requirement for accurate spin measurements.

4. SPSMM

Spin polarization images were acquired by scanning a sample with respect to the apertured high-density He(2^3S) beam of 100 μm diameter and measuring the ejected secondary electron signal with a cylindrical mirror analyzer (PHI, 590A) for the transverse magnetic field on and off in the spin flipper. SPSMM images, obtained by subtracting a spin-down count from a spin-up count for each pixel, clearly show magnetic domains of Fe(100) thin films deposited on a MgO(100) substrate.

5. SPMEEM

A single crystal of Fe_3O_4, the outermost surface spins of which have been intensively studied [5], was placed in a PEEM-350 (Staib) and irradiated with a non-apertured high-density He(2^3S) beam. Magnified electron images were then acquired for spin up and down by switching the spin flipper. Spin images, which were obtained by subtracting a spin-down image from a spin-up image, showed clear contrast depending on the three-dimensional spin axes. SPMEEM attains a much higher lateral resolution than SPSMM by sacrificing the fine spectroscopy.

6. REFERENCES

[1] M. Onellion, M.W. Hart, F.B. Dunning and G.K. Walters, Phys. Rev. Lett. 52, 380 (1984)
[2] S. Entani, M. Kurahashi, X. Sun and Y. Yamauchi, Carbon 61 (2013) 134.
[3] M. Ohtomo, Y. Yamauchi, A. A. Kuzubov, N. S. Eleseeva, P. V. Avramov, S. Entani, Y. Matsumoto, H Naramoto and S. Sakai Appl. Phys. Lett. 104 (2014) 051604-1.
[4] W. Schroeder and G. Baum, J. Phys. E 16, 52 (1983)
[5] A. Pratt, M. Kurahashi, X. Sun, D. Gilks, and Y. Yamauchi, Phys. Rev. B 85, 180409(R) (2012)

* Corresponding author e-mail address: yamauchi.yasushi@nims.go.jp

LASER MANIPULATION OF METASTABLE HELIUM ATOMS: APPLICATIONS TO SURFACE ANALYSIS

A. Pratt[1,2*], *J. Zhang*[1] *and Y. Yamauchi*[2]

[1]Department of Physics, University of York, Heslington, York YO10 5DD, U. K.
[2]National Institute for Materials Science, Tsukuba, Ibaraki 305-0047, Japan

1. INTRODUCTION

Laser cooling presents an opportunity to manipulate neutral atoms with the precision and control enjoyed by techniques in charged particle and photon optics for decades. Previously, we have demonstrated how applying methods of laser cooling to collimate and focus a beam of metastable helium (2^3S) atoms can yield an ultra-high intensity probe for performing the extremely surface sensitive analysis technique of metastable de-excitation spectroscopy (MDS) [1,2]. A natural extension of a spectroscopic technique is to develop it into a microscopy to provide spatial information on the surface electronic, magnetic, and chemical properties of a material. Here, we describe the prospects of using laser cooling to generate an ultra-high intensity and nanometer-sized probe of helium atoms for MEEM and MDS applications.

2. METASTABLE-ATOM EMISSION ELECTRON MICROSCOPY

Metastable-atom emission electron microscopy (MEEM) has been demonstrated using conventional He 2^3S sources on a number of occasions, firstly by Harada *et al*. who studied gold and ClAl-phthalocyanine (ClAlPc) monolayer islands grown on a graphite substrate [3]. The 5 μm resolution of the instrument was determined by detecting electrons from only a small area of the sample. The images of the islands were blurred due to aberrations caused by detecting electrons across a wide energy range (0-15 eV), and also because of surface diffusion. Yamamoto *et al.* produced energy-filtered MEEM images of a silicon oxide pattern on a Si(100) surface although the lateral resolution was poor at ~0.3 mm and a long 10 minute acquisition time was required [4]. More recently, Yamauchi *et al*. have reported the first demonstration of spin-polarized MEEM [5] which has potential applications for imaging, for example, the surface spin polarization of spintronic materials [6].

3. IMAGING OPTICS

The electron imaging optics necessary to perform MEEM are identical to those used in PEEM systems. Electrons emitted due to He 2^3S de-excitation are typically accelerated to high energies (10 keV) to form an image using a cathode objective lens. Using an array of finely focused He (2^3S) probes, rather than this 'flood and image' approach, will result in the ejection of electrons from an area defined by the probe size. Modifying the electron optics of conventional MEEM apparatus will allow these individual signals to be combined to produce an image without the need for an aperture. Coupled with the high intensity associated with the focused helium nanoprobes, parallel acquisition will reduce the minutes long exposure times currently required to produce MEEM images.

4. STANDING WAVE LENS ARRAY

One promising approach to producing an array of helium nanoprobes is to use a standing wave lens array (SWLA) such as that generated by counter-propagating laser beams in 2D (Fig. 1(a)). A dipole force is created that causes atoms to be attracted to the antinodes of the array by using laser light with a frequency detuned to the blue side of the He 2^3S_1—2^3P_2 transition (1083 nm). Using parameters typical for our experiment (longitudinal velocity of 1000 ms^{-1}), simulations show it is possible to tighly focus helium atoms as each antinode acts as a thick immersion lens (Fig. 1(b)). Even when broadening effects such as beam divergence and chromatic and spherical aberrations are considered, focal spot sizes in the nanometer range may be obtained.

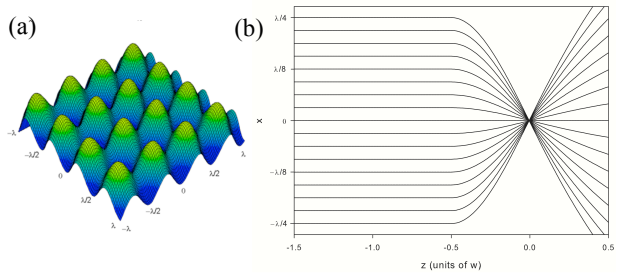

Figure 1: (a) Intensity profile for a 2D SWLA proposed for use in generating an array of He 2^3S nanoprobes. (b) Simulated trajectories of He 2^3S atoms through a single antinode of a standing wave lens array under the paraxial approximation.

5. REFERENCES

[1] A. Pratt, A. Roskoss, H. Ménard, and M. Jacka, Rev. Sci. Instrum. **76**, 053102 (2005).
[2] A. Pratt and M. Jacka, J Phys. D: Appl. Phys. **42**, 055308 (2009).
[3] Y. Harada, S. Yamamoto, M. Aoki, S. Masuda, T. Ichinokawa, M. Kato, and Y. Sakai, Nature **372**, 657 (1994).
[4] S. Yamamoto, S. Masuda, H. Yasufuku, N. Ueno, Y. Harada, T. Ichinokawa, M. Kato, and Y. Sakai, J. Appl. Phys. **82**, 2954 (1997).
[5] Y. Yamauchi, *private communication*.
[6] A. Pratt, M. Kurahashi, X. Sun, D. Gilks, and Y. Yamauchi, Phys. Rev. B 85, 180409(R) (2012).

* Corresponding author e-mail address: andrew.pratt @york.ac.uk

FEMTOSECOND LASER PULSE INDUCED DESORPTION: A MOLECULAR DYNAMICS SIMULATION

Ivor Lončarić[1,*], *M. Alducin*[1,2], *P. Saalfrank*[2,3] *and J. I. Juaristi*[1,2,4]

[1] Centro de Física de Materiales CFM/MPC (CSIC-UPV/EHU), San Sebastián, Spain
[2] Donostia International Physics Center DIPC, San Sebastián, Spain
[3] Institut für Chemie, Universität Potsdam, Potsdam, Germany
[4] Departamento de Física de Materiales, Facultad de Químicas, Universidad del País Vasco (UPV/EHU), San Sebastián, Spain

1. INTRODUCTION

Hot electrons created on a metal surface by a femtosecond laser pulse can be used to promote chemical reactions on the surfaces and even open new reaction channels not accessible by thermal activation or continuous light excitation. One of the simplest laser induced reactions on surfaces is the desorption of an adsorbed molecule from a surface. Recently, we have extended previously used models to theoretically simulate the dynamics of such reactions [1]. Our model consists in preforming molecular dynamics on the ground state potential energy surface (PES) with electronic degrees of freedom included via friction and associated fluctuation forces. The ground state PES is obtained by fitting to a large set of energy values calculated by density functional theory (DFT) for different configurations of the molecule. We use the two temperature model (2TM) to describe the heating of electrons and phonons upon excitation by the laser pulse. Surface (phonon) temperature is included in the dynamics using the Generalized Langevin Oscillator model. The effect of heated electrons on the molecule is modelled by random forces which are linked to the friction forces via the second fluctuation-dissipation theorem. Friction forces are calculated in the basis of the local density friction approximation.

2. DESORPTION OF O_2 FROM Ag(110)

The oxygen molecule is known to adsorb on the Ag(110) in several states: physisorption state, molecular chemisorption state and dissociative chemisorption state. This makes it an interesting study system. Recently, we have constructed a six dimensional PES showing that the system has four molecular adsorption wells with different adsorption energies and with the molecule at different distances from the surface [2]. We simulate the desorption from these four adsorption wells using the model described above. Interestingly, the results of the dynamics show that desorption from the wells at hollow sites is principally induced by hot electrons while desorption from the wells at bridge sites is primarily phonon induced. The reason is that the hollow wells are relatively close to the surface with the molecule embedded in high electronic density regions which results in large fluctuation forces. On the other hand in the wells at the bridge sites the molecule lies further from the surface in regions of lower electronic density. In this work, we explore ways of controlling desorption from the different adsorption wells by modifying the laser pulse parameters (pulse width, wavelength...) or the initial surface temperature in order to achieve selectivity in desorption between electron and phonon induced processes. In Fig. 1 we show results

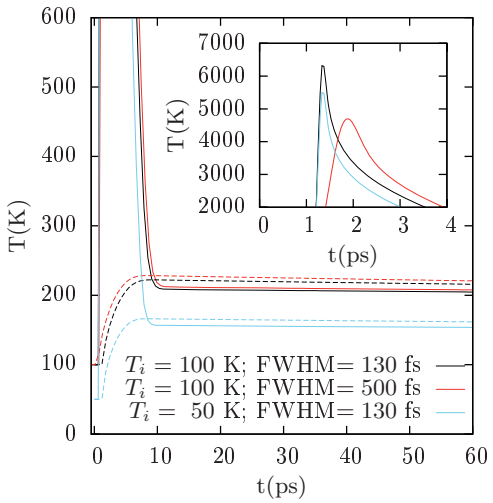

Figure 1: Electron (solid line) and phonon (dashed line) temperatures as a function of time, calculated from the 2TM for different pulse widths FWHM and initial surface temperatures T_i.

of the 2TM for different laser widths and surface temperatures. As shown, wider laser pulses result in somewhat larger phonon temperatures on equilibration. Lower initial surface temperatures reduce both electron and phonon temperatures at longer times considerably. We investigate the consequences of these differences on the desorption yields.

3. REFERENCES

[1] Ivor Lončarić, M. Alducin, P. Saalfrank and J.I. Juaristi, to be submitted.

[2] Ivor Lončarić, M. Alducin and J.I. Juaristi, Phys. Chem. Chem. Phys. **17**, 9436 (2015).

*Corresponding author e-mail address: ivor.loncaric@gmail.com

ELECTRONIC STOPPING OF SLOW LIGHT IONS IN VANADIUM DIOXIDE

D.Roth[*,1], *B. Bruckner*[1], *Ch. L. McGahan*[2], *R.F. Haglund, Jr.*[2], *and P. Bauer*[1]

[1]Institute for Experimental Physics, Johannes Kepler University Linz, A-4040 Linz, Austria
[2]Dept. of Physics and Astronomy and Interdisciplinary Materials Science Program, Vanderbilt University, TN 37235-1807, USA

1. INTRODUCTION

The investigation of electronic energy loss of ions propagating in a solid yields valuable insights into the fundamentals of ion-solid interactions. Furthermore, it provides useful knowledge for ion beam analysis techniques, material science or medical applications.
The mean energy loss per monolayer due to electronic interactions is given by the electronic stopping cross section (SCS)

$$-\frac{dE}{dx} = n\,S_e \qquad (1)$$

where n represents the atomic density of the target. Open questions about prevailing mechanisms of energy dissipation still persist in the regime of low ion velocities as used in Low Energy Ion Scattering (LEIS).

Recently, it has been reported that for very slow H ions (v < 0.2 a.u., corresponding to proton energies < 1 keV) electronic stopping in metals is dominated by excitation of electrons at the Fermi level [1,2]. For insulators, e.g. LiF, a distinct velocity threshold v_{th} was observed, below which no electronic stopping occurs. However, a comparison to TD-DFT calculations [3] suggests that different energy loss mechanisms may be important, e.g. charge-exchange cycles, by which the formation of H^- ions in grazing surface scattering has been explained [4].

For semiconductors, knowledge about dominant energy loss processes at low ion velocities is rather limited. Experimental data are available for proton stopping in Si and Ge [5, 6]: while Ge exhibits a finite velocity threshold, such an excitation threshold was not observed for Si. Furthermore, it is not clear whether in semiconductors electronic energy loss processes are similar as in metals or as in insulators. Therefore, vanadium dioxide (VO_2) represents a key material to investigate the possibly different stopping mechanisms in metals and in semiconductors, since VO_2 exhibits a phase transition from a monoclinic semiconductor (band gap ~ 0.6 eV) to a rutile metal at T = 340 K, which has been discovered over 50 years ago [7].

In this contribution, we present data on the low-velocity electronic stopping cross section of H and He ions in VO_2 at room temperature (below T_C, semiconducting phase) and T = 400 K (above T_C, metallic phase).

2. RESULTS

In Fig. 1, preliminary results of the electronic stopping cross section of H and D ions in VO_2 are shown as function of the ion velocity in atomic units between 0.3-0.63 a.u., corresponding to stopping of protons with primary energies between 2.25 keV and 10 keV, respectively. The full symbols refer to data acquired at room temperature (semiconducting phase), the open symbols to data measured at T = 400 K (metallic phase).

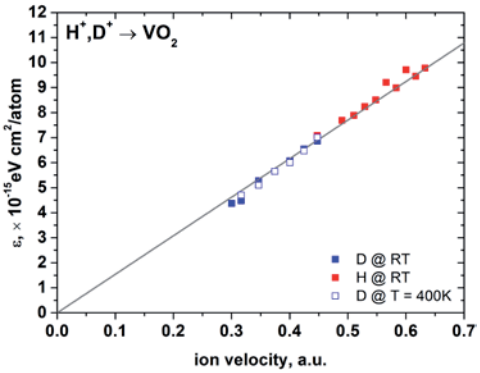

Figure 1: Electronic SCS of H, D ions in VO_2 as a function of the ion velocity in atomic units for both, semiconducting and metallic phase.

For v > 0.3 a.u., the electronic energy loss of hydrogen ions in VO_2 is proportional to the ion velocity for both, semiconducting and metallic phase. Furthermore, data acquired in both phases are concordant within experimental uncertainty.

3. REFERENCES

[1] D. Goebl, W. Roessler, D. Roth, and P. Bauer, Phys. Rev. A **90,** 042706 (2014).
[2] P.M. Echenique, R.M. Nieminen, J.C. Ashley, and R.H. Ritchie, Phys. Rev. A **33**, 897 (1986).
[3] M.A. Zeb, J. Kohanoff, D. Sanchez-Portal, E. Artacho, Nucl. Instr. Meth. B. **303**, 59-61 (2013).
[4] C. Auth, A.G. Borisov, H. Winter, Phys. Rev. Lett. **75**, 12, 2292-2295 (1995).
[5] H.O. Funsten, S.M. Ritzau, R.W. Harper, J.E. Borovsky, and R.E. Johnson, Phys. Rev. Lett. **92**, 213201 (2004).
[6] D. Roth, D. Goebl, D. Primetzhofer, P. Bauer, Nucl. Instr. Meth. B **317**, 61-65 (2013).
[7] F.J. Morin, Phys. Rev. Lett. **3**, No.1, 34-36 (1959).

* Corresponding author e-mail address: dietmar.roth@jku.at

TDDFT CALCULATIONS OF THE VICINAGE EFFECT IN THE ENERGY LOSS OF A HYDROGEN DIMER

Natalia Koval[1,2,*], *D. Sánchez-Portal*[1,2], *A. G. Borisov*[3] *and R. Díez Muiño*[1,2]

[1] Centro de Física de Materiales, CFM (CSIC-UPV/EHU), San Sebastián, Spain
[2] Donostia International Physics Center, DIPC, San Sebastián, Spain
[3] Institut des Sciences Moléculaires d'Orsay, ISMO, CNRS-Université Paris-Sud UMR 8214, Orsay Cedex, France

1. INTRODUCTION

In this work we present an *ab initio* study of the vicinage effect in the interaction of a hydrogen dimer, H_2, with a spherical free electron (jellium) nanocluster. The nanocluster is characterized by the Wigner-Seitz parameter $r_s = 1.56$ a.u. which represents an effective electron density of SiO_2. This allows to compare results of the present calculations with experimental data of Ref. [1]. The vicinage effect is analysed using the so called stopping power ratio,

$$R = \frac{S_{H_2}}{2S_H}, \tag{1}$$

where S_{H_2} is the stopping power (or energy loss per unit trajectory length) of the H_2 dimer and $2S_H$ is the sum of the stopping powers of two independent hydrogen projectiles. The time dependent density functional theory (TDDFT) used here allows us an exact (within chosen model system) assessment of the vicinage effect at low, intermediate, and high velocities. Our work thus provides an *ab initio* strategy for the calculations of the vicinage effect and sets a benchmark for comparison with simplified and/or perturbative treatments.

2. METHODOLOGY

We represent the nanocluster using the spherical Jellium Model (JM). The nanocluster comprises 338 electrons. The ground state electronic density of the nanocluster is calculated using the Kohn-Sham (KS) scheme of the density functional theory (DFT). The ground state KS wave functions of the nanocluster are expanded in the spherical harmonics basis set. The ground state wave functions of the hydrogen dimer (and of the H atom) are calculated solving KS equations in cylindrical coordinates.
Once the ground state configuration of our system is obtained, we allow the projectile to move with a constant velocity v along the straight line trajectory passing through the geometrical center of the cluster. The axis of the dimer is collinear with trajectory. The time evolution of the electronic density is then calculated using TDDFT as detailed in Ref. [2]. As a result we obtain the time-dependent electronic density $n(t)$, from which we calculate the force, $F(t)$, acting on the moving projectiles and the energy loss

$$E_{loss} = -v \int F(t)dt. \tag{2}$$

The stopping power is the mean energy loss per unit path length:

$$S = E_{loss}/D, \tag{3}$$

where D is the diameter of the nanocluster. For this large enough cluster size the surface effects on the stopping can be neglected [3], and S given by Eq. 3 corresponds to the bulk stopping power in the free electron gas.

3. RESULTS

In Figure 1 we show the stopping power ratio R for the hydrogen dimer. Calculated and experimental data are presented as a function of the kinetic energy of the projectile. Our results are in a good agreement with the experiment.

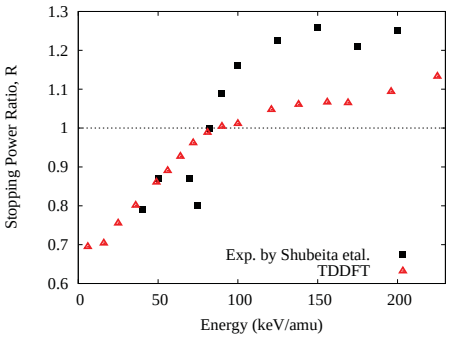

Figure 1: Stopping power ratio as a function of the projectile kinetic energy. Experimental points are taken from Ref.[1]

The change from the "negative" ($R < 1$) to the "positive" ($R > 1$) stopping ratio is observed at the energy about 80-90 keV/amu, both in the experiment and in calculations. We provide a detailed analysis of the stopping power of H_2 dimer and of each projectile in order to explain this behaviour.

4. REFERENCES

[1] S. M. Shubeita et al, Phys. Rev. B **77**, 115327 (2008).

[2] N. E. Koval et al, Nanoscale Res. Lett. **7**, 447 (2012).

[3] M. Quijada et al, Phys. Rev. A **75**, 042902 (2007).

*Corresponding author e-mail address: natalia_koval@ehu.eus

INFLUENCE OF THE INTERACTION POTENTIAL ON THE SCATTERING CROSS SECTION AND THE ENERGY SPECTRA IN LEIS

K.Khalal-Kouache[*], *S.Hafidi and A.Soukhal*

Université des Sciences et de la Technologie Houari Boumediene (USTHB), Faculté de Physique, Laboratoire SNIRM, Bab-Ezzouar, 16111 Algiers, Algeria

At low energy $(0.5-10\,\mathrm{keV})$, the interaction between a projectile and an atom (in a solid target) is described by a screened Coulomb potential $V(r)$:

$$V(r)=\frac{Z_1 Z_2 e^2}{r}\Phi\left(\frac{r}{a}\right) \quad (1)$$

Z_1 and Z_2 are the atomic numbers of projectile and target atom respectively, e is the electron charge, r is the distance between the colliding atoms, $\Phi\left(\frac{r}{a}\right)$ is a screening function and a is the screening length. The mostly used potentials are the Ziegler-Biersack-Littmark (ZBL) [1] potential and the Thomas-Fermi-Molière (TFM) [2] potential. The corresponding screening lengths are respectively a_U and a_F.

In this contribution, we consider the scattering of low energy He^+ ions from different solid surfaces where the Binary Collision Approximation (BCA) is assumed.

In this study, ZBL and TFM potentials are considered.

The scattering angle ψ of the projectile (in a collision) is calculated for different values of the impact parameter. The ratio R(TFM/ZBL) is defined as:

$$R(TFM/ZBL)=\frac{\psi(TFM)}{\psi(ZBL)} \quad (2)$$

$\psi(TFM)$ and $\psi(ZBL)$ are the scattering angles calculated with TFM and ZBL potentials respectively for the same impact parameter. The variation of R(TFM/ZBL) with the impact parameter is given for the collision He/Cu (figure 1).

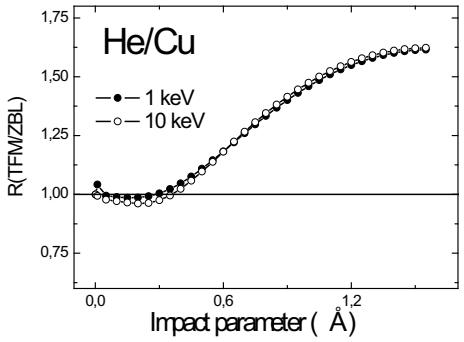

Figure 1: Variation of the ratio R(TFM/ZBL) with the impact parameter for He/Cu.

The scattering cross section values are then deduced and the effect of the interaction potential on these values is studied. Monte Carlo simulation [3] is used to calculate energy spectra of the scattered particles. Different values of the incident (α) and scattering (θ) angles are considered. The precedent results are used to discuss the influence of the potential on the energy spectra.

Keywords: Low energy ion scattering, Scattering cross section, Interaction potential, Monte Carlo simulation, Energy spectra.

REFERENCES

[1] J.F. Ziegler, J.P. Biersack and U. Littmark, The stopping and Ranges of Ions in Solids, Pergamon, New York, 1985.

[2] G. Molière, Z.Naturforsch. **2a** (1947) 133.

[3] K. Khalal-Kouache, A.C. Chami, M. Boudjema, Y. Boudouma, P. Benoit-Cattin and C. Benazeth, Alg. J. Adv. Mater. **3** (1999) 1.

[*] Corresponding author e-mail address: kkouache@yahoo.fr

AUTHOR INDEX

Author index

List of Participants

Åhlgren, Harriet	Finland
Alducin , Maite	Spain
Aliaga Gosalvez, Maria José	Spain
Allegrini, Frederic	USA
Andersson, Gunther	Australia
Arnau, Andres	Spain
Atkinson, Paola	France
Aumayr, Friedrich	Austria
Ban d'Etat, Brigitte	France
Bannister, Mark	USA
Barlow, Anders	UK
Bauer, Peter	Austria
Berger, Bernhard	Austria
Blanco-Rey, Maria	Spain
Borissov, Andrey	France
Böttger, Roman	Germany
Bourin, Charles	France
Bruckner, Barbara	Austria
Bundesmann, Carsten	Germany
Cervera, Sophie	France
Costa, Catia	UK
Deuzeman, Mart Johan	The Netherlands
Díaz, Cristina	Spain
Díez Muiño, Ricardo	Spain
Echenique, Pedro Miguel	Spain
El-Said, Ayman	Saudi Arabia
Engler, Martin	Germany
Facskc, Stefan	Germany
Feldman, Leonard	USA
Fuchs-Fuchs, Alexander	Austria
García Carrasco, Alvaro	Sweden
Gnaser, Hubert	Germany
Gravielle, Maria Silvia	Argentina
Gruber, Elisabeth	Austria
Grygiel, Clara	France
Gustafsson, Torgny	USA
Heller, Rene	Germany
Hellsing, Bo	Sweden
Herbig, Charlotte	Germany
Hijazi, Hussein	USA
Hoekstra, Ronnie	The Netherlands
Juaristi, Iñaki	Spain

Khalal-Kouache, Karima	Algeria
Kimura, Kenji	Japan
Kolodney, Eli	Israel
Koshikawa, Takanori	Japan
Koslowski, Hans Rudolf	Germany
Koval, Natalia	Spain
Kozubek, Roland	Germany
Lebius, Henning	France
Linsmeier, Christian	Germany
Loncaric, Ivor	Spain
Marenkov, Evgeny	Russia
Martinez, Rafael	Brazil
Marumo, Tomoya	Japan
Matsuo, Jiro	Japan
Monreal, Rosa C.	Spain
Nakagawa, Sachiko	Japan
Nakajima, Kaoru	Japan
Nienhaus, Hermann	Germany
Nosir, Mohamed Ahmen	Spain
Novko, Dino	Spain
Pratt, Andrew	UK
Riccardi, Pierfrancesco	Italy
Roncin, Philippe	France
Roth, Dietmar	Austria
Ryabtsev, Sergey	Russia
Saavedra Agüera, Rafael	Spain
Sánchez-Portal, Daniel	Spain
Schwarz-Selinger, Thomas	Germany
Schwestka, Janine	Austria
Shigin, Pavel	France
Sigmund, Peter	Denmark
Sosolik, Chad	USA
Suzuki, Taku	Japan
Tanis, John	USA
Terry, William	UK
Tolk, Norman	USA
Trassinelli, Martino	France
van Kampen, Maarten	The Netherlands
Wang, Yuyu	China
Weidtmann, Boris	Germany
Wilhelm, Richard	Germany
Winter, Helmut	Germany
Yamauchi, Yasushi	Japan
Zugarramurdi, Asier	Finland

Institutional support and funding

DONOSTIA INTERNATIONAL PHYSICS CENTER

21st International Workshop on
Inelastic Ion-Surface Collisions (IISC-21)
Donostia-San Sebastián, Spain

Organized by Donostia International Physics Center (DIPC)
Iñaki Juaristi (Chair)

Sunday 18th October	Monday 19th October	Tuesday 20th October	Wednesday 21st October	Thursday 22nd October	Friday 23rd October
	9:00 **Opening** 9:10 **PL1** Andersson 9:55 **I1** Nakajima 10:25 **O1** Barlow	9:00 **PL2** Nienhaus 9:45 **I8** Wilhelm 10:15 **O8** Novko	9:00 **I13** Echenique 9:30 **I14** Borissov 10:00 **PL3** Winter	9:00 **PL4** Schwarz-Selinger 9:45 **I17** Bannister 10:15 **O15** Marenkov	9:00 **PL5** Gustafsson 9:45 **I24** Yamauchi 10:15 **O22** Pratt
	10:45 COFFE BREAK	**10:35 COFFE BREAK**	**10:45 COFFE BREAK**	**10:35 COFFE BREAK**	**10:35 COFFE BREAK**
	11:15 **I2** Ban-d'Etat 11:45 **I3** Grygiel 12:15 **O2** Kimura 12:35 **O3** Terry	11:05 **I9** Bauer 11:35 **I10** Sigmund 12:05 **O9** Riccardi 12:25 **O10** Sánchez Portal	11:15 **I15** van Kampen 11:45 **I16** Costa 12:15 **O13** Tolk 12:35 **O14** Trassinelli	11:05 **I18** Berger 11:35 **I19** Allegrini 12:05 **O16** García Carrasco 12:25 **O17** Ryabtsev	11:05 **O23** Loncaric 11:25 **O24** Roth 11:45 **O25** Koval 12:05 **O26** Khalal-Kouache 12:25 **CLOSING REMARKS**
	13:00 LUNCH	**13:00 LUNCH**	**13:00 LUNCH**	**13:00 LUNCH**	**13:00 LUNCH**
	15:00 **I4** Bottger 15:30 **I5** Herbig 16:00 **O4** Facsko 16:20 **O5** Gnaser	15:00 **I11** Suzuki 15:30 **I12** Monreal 16:00 **O11** Hellsing 16:20 **O12** Nakagawa	**OUTING**	15:00 **I20** Roncin 15:30 **I21** Atkinson 16:00 **O18** Gravielle 16:20 **O19** Díaz	**PL: Plenary talk (40+5 min.)** **I: Invited talk (25+5 min.)** **O: Oral Contribution (15+5 min.)**
	16:40 COFFE BREAK	**16:40 COFFE BREAK**		**16:40 COFFE BREAK**	
17:30 REGISTRATION	17:10 **I6** Ahlgren 17:40 **I7** Kozubek 18:10 **O6** Engler 18:30 **O7** Bourin	17: 10 POSTER INTRO 18: 10 POSTER SESSION		17:10 **I22** Hijazi 17:40 **I23** Martinez 18:10 **O20** Kolodney 18:30 **O21** Bundesmann	
19:30 RECEPTION **20:00 DINNER**	**20:00 DINNER**	**20:00 DINNER**	**20:00 DINNER**	**20:00 REFRESHMENTS** **20:30 CONFERENCE DINNER**	
	21:00 Committee Meeting				